Studies on Kinetic Analysis and Modeling of Biochar Gasification

ザイダ ファイザ ザハラ

Studies on Kinetic Analysis and Modeling of Biochar Gasification

by

Zayda Faizah Zahara

Department of Applied Sciences for Electronics and Materials

Interdisciplinary Graduate School of Engineering Sciences

Kyushu University

2018

ACKNOWLEDGEMENTS

First of all, I would like to express my sincere gratitude to my supervisor Professor Jun-ichiro Hayashi, for his kindness, guidance, support, fruitful discussion, patience, and motivation continuously during my study. It would have been impossible for me to complete this work without his mentoring and moral support.

I would also like to express my sincere gratitude to the committee members, Associate Professor Shinji Kudo and Professor Hisahiro Einaga for their invaluable comments, suggestions, and supports during my study.

My special appreciation is due for Professor Arief Budiman of Gadjah Mada University, Dr. Daniyanto, and Dr. Karnowo, for their support on my research, discussions, and collaborative studies. They have provided a lot of technical suggestions, personal encouragements, emotional and moral supports.

Special thanks for all of the member of Hayashi laboratory, especially Ms. Asuka Mori, Ms. Yasuyo Hachiyama, Mr. Kentaro Shima, Dr. U.P.M. Ashik, Ms. Phatchada Santawaja, Mr. Nurulhuda Halim, Ms. Ni'mah Ayu Lestari, and Mr. Aditya Wibawa for their kind assistance and creating a joyful environment in the laboratory.

My deep gratitude should be addressed to my parents and my sister for their endless love, support, and prayer. Also special thanks for my beloved husband for always supporting me in all my hard times.

Finally, I would like to thank to the Kyushu University Advanced Leading Graduate Program for the financial support. I also would like to express my gratitude for all of Green Asia professors and staffs for their continuous supports.

Finally, I would like to thank to the Kyushu University Advanced Leading Graduate Program for the financial support. I also would like to express my gratitude for all of Green Asia professors and staff for their continuous supports.

CONTENTS

NOMENCLATURE

k_{sp}	specific rate of gasification with respect to mass of carbonaceous part of char. k_{sp} is a function of char conversion X	[min^{-1}]
$k_{sp,0}$	initial specific rate ($k_{sp,0}$ at $t = 0$)	[min^{-1}]
$k_{sp,f}$	fictitious ultimate specific rate	[min^{-1}]
α	coefficient for rapidity of change of k_{sp}	[–]
k_{cg}	the rate of catalytic gasification	[min^{-1}]
k_{cn}	the individual rate of gasification catalyzed by n catalyst	[min^{-1}]
$k_{\text{loss-}n}$	rate constant for loss of n catalyst	[min^{-1}]
t	time from the commencement of gasification	[min]
X	conversion of chars based on the mass of chars	[–]
0	time at commencement of gasification (at $t = 0$)	[–]
C_{Cn}	Concentration of catalyst Cn	[–]
C_{C1prec}	Concentration of precursor of catalyst C1	[–]
k'_{C}	The rate of catalytic gasification per amount of catalyst	[min^{-1}]
k_{Cn}	Rate of catalytic gasification defined by $k'_{C}m_{Cn}$	[min^{-1}]
k_{C1prec}	Rate constant for transformation of C1 precursor to C1	[min^{-1}]
$k_{\text{loss-}n}$	Rate constant for loss of Cn	[min^{-1}]
k_{nc}	Rate constant for non-catalytic gasification	[min^{-1}]

m_{Cn}	Amount of catalyst C*n*	[–]
m_{C1prec}	Amount of precursor of catalyst C1	[–]

Chapter 1

General Introduction

1.1 Background

The world's energy demand has been increasing since the 1990 and estimated will continue to increase with a growth rate of 1.3% in average per annum (p.a.). This energy demand has been supported by different kinds of sources, mostly from fossil fuel such as oil, natural gas, and coal with a growth rate of 0.5% p.a. and 1.6% p.a. respectively. On the other hand, the demand for coal is expected to decrease. The continuous increase in energy demand will create massive emission of CO_2 to the atmosphere which has been accused of causing the pressing issue of global warming. It has been revealed that the CO_2 concentration in the atmosphere has exponentially increased since 1750 to potentially dangerous levels mainly due to the continuous exploitation of fossil fuels, especially that from coal. [1]

To minimize the emission of CO_2, the developed and the developing countries are making join efforts in a global program with COP21 agreement. The agreement focused on the following(s); (a) to rapidly decrease the carbon emissions, (b) to reduce the rate of the concentration rise in CO_2 to 0.0% per year, (c) to suppress the temperature rise to approximately 1.5 °C by 2100 (d) to encourage selected countries to adopt a climate change mitigation program and annually contribute to it as much as $100 while providing an appropriate technology as well as to do capacity-building by 2020 and (e) to reevaluate the progress every five years. [2]

One of the approach to reduce the CO_2 emission is to promote the renewable energy in the energy mix strongly. Renewable energy is the energy which derived from renewable sources including wind, water, sun, thermal, and biomass. The energy derived from biomass or so-called as bioenergy is the largest source of renewable energy that can provide heat, electricity, as well as transport fuel. Bioenergy could contribute 10% of the global primary energy supply. Therefore it becomes crucial energy sources, especially in the developing countries. Moreover, it is expected that by 2050 bioenergy could provide 3100 Terawatt-hours (TWh) of electricity, i.e., 7.5% of world electricity generation. [3,4]

1.2 Biomass potential

Biomass is organic material derived from plants and animals. The potential biomass feedstock such as that from forestry, agricultural crops, and industrial waste including forestry, straw, and bagasse are commonly referred to as lignocellulosic biomass. Other than the above, prospective feedstock of biomass also can be derived from sewage, municipal solid waste, animal residues, such as manure and liquid manure. [5,6] Lignocellulosic biomass is traditionally used in low-income household for cooking and heating. However, these activities were supported by insufficient technology with a low efficiency which caused air pollution. The continuous use of these traditional technologies in a long run may cause a severe health problem which can lead to premature death. In order to promote the more sustainable use of solid biomass resources and reduce the associated health and social impacts from their traditional, it was suggested to take initiatives to ensure universal access to clean energy. The transition away from traditional use of solid biomass to more modern and efficient heating and cooking solutions can be achieved through the utilization of liquefied petroleum gas (LPG), as well as renewable energy solutions. The latter solution is more desirable, and more advanced biomass stoves (e.g., micro gasifiers) including the biogas systems are currently available to offer improved efficiency and lower pollutant emissions, reducing health impacts and biomass resource demand. [3]

Beside as source of bioenergy, biomass also an excellent source of chemicals, which usually called as biochemical or renewable chemical. Many researchers believe that future chemical will be switched to the biomass-based. It has proven that lignocellulosic biomass can be synthesized into some valuable chemicals such as levoglucosenone, levulinic acid, phenol and its derivative compounds. [7–10] Due to its significant advantages for both energy and chemicals sources, research and development on this issue are necessary to be carried out. Especially, utilization of local specialty biomass such as rice husk, rice hull, wood chips, bamboo, sugarcane, etc. is important.

1.3 Thermochemical conversion of biomass

There have been different thermochemical conversion methods which are known as convenient routes to convert biomass into energy. This includes combustion, pyrolysis, gasification, and hydrothermal treatment.

1.3.1 Combustion

The traditional technology of biomass conversion is through combustion. In the combustion process, fuel (biomass) reacts rapidly with oxygen and gives off heat. The resulting heat can be utilized directly for cooking or heating, or in the modern technology, it is used to generate steam which further drives a generator to produce electricity. However, the drawback of this process is the low efficiency and relatively high heat loss. Moreover, due to the nature of biomasses which have a variety of minor constituents, such as chlorine, sulfur, phosphorus, nitrogen, and a variety of ash-forming metals, biomass fuels cause several challenges. In addition, to achieve high-efficiency conversion, the moisture of biomass should be lower than 50%. [11–13]

1.3.2 Pyrolysis

Pyrolysis is defined as a thermochemical decomposition process in which organic material is converted into a carbon-rich solid and volatile matter by heating in the absence of oxygen. The black-colored solid will remain after the process and it variously termed as char, charcoal, coke or biochar (commonly used for char from biomass). The char is commonly having high carbon contain around more than half the total carbon of the original organic matter, typically ranging 60–90%. The characteristic of char is the small content of inorganic material, particularly that of Na, K, Ca, Fe, Si, which is termed as ash. Aside from the solid product, the volatiles produced during the process can be partly condensed to give a liquid fraction, frequently termed as bio-oil. This liquid is generally hydrophilic containing many oxygenated compounds and is present, sometimes as a single aqueous phase, sometimes phase-separated, together with water produced in the pyrolysis reaction or remaining from the feedstock. The mixture of the non-condensable volatiles is the gas product which is termed as synthesis gas, shortened to syn-gas. It is generally composed of carbon dioxide, carbon monoxide, methane, hydrogen and two-carbon hydrocarbons in varying proportions. [14–16]

1.3.3 Hydrothermal treatment

Hydrothermal carbonization (HTC), also known as hydrothermal pretreatment or wet torrefaction, is a thermo-chemical conversion technique which uses liquid subcritical water as a reaction medium for conversion of wet biomass and waste streams. It is usually performed at temperatures higher than 180 °C, at pressures high enough to ensure liquid water, and under an inert atmosphere. During hydrothermal pretreatment, hemicelluloses and cellulose are

hydrolyzed to oligomers and monomers, while lignin is mostly unaffected. The solid product from treatment, known as char, can be further pelletized and fed to gasifier or power plant. The liquid products usually contain organic acids and can be further fractionated by means of extraction with a polar organic solvent. [17–19]

1.3.4 Gasification

Gasification is one of the efficient way to produce syn-gas from carbonaceous fuel. It is continuous to get an increase of interest, proven by the escalating number of the publication and patent in this subject. [20] Especially with the utilization of biomass as the feedstock, it can provide high efficiency and environmental friendly method to get bioenergy as electricity.

Bioenergy through gasification technology currently has undergone the early market development. One of the advanced technology is the use of combustion turbines and steam turbines in biomass integrated gasification/combined-cycle (BIGCC) which offers an option for producing electricity with higher efficiency. The BIGCC consists of four major subsystems; fuel handling and feeding system, the gasifier, the gas clean-up unit (GCU), and the combined power system. In an BIGCC system, biomass is converted into a gaseous fuel, which is comparable to natural gas. The gas is further cleaned by an advanced cleanup process before being burned in the gas turbine to generate electricity. Exhaust heat from the gas turbine is used to produce steam for a conventional steam turbine, resulting in the two cycles of electric power generation.

The BIGCC systems have demonstrated exceptional environmental performance shown by they ability to remove sulfur dioxide (SO_2), nitrogen oxides (NOx) reduction, and particulate removal. In fact, the emission of SO_2 and NOx from this systems are less than one-tenth of that allowed by New Source Performance Standards limits. At the same time, BIGCC efficiency levels at 40 percent which is higher than the conventional coal-fired plant that has an efficiency of 34 percent at its best. [21]

In gasification, biomass is reacted with the gasifying agent (*i.e.* steam, CO_2) and converted to combustible gas or known as synthetic-gas (syngas) such as H_2, CO, CO_2, H_2O, and CH_4. It involves partial combustion of biomass in a gas flow containing a controlled level of oxygen at relatively high temperatures (500–900°C). When biomass is heated in the absence of oxidizing agent, it undergoes pyrolysis producing char, tar, and combustible gasses. As the reaction progress, the char, tar, and gas are further converted to syn-gas leaving the remaining ashes. The gasification is usually catalyzed by alkali and alkaline earth metallic species

(AAEM) in biomass. Due to this inherent catalytic species, it is believed that the gasification can be performed at a lower temperature. [22–24]

1.4 Kinetics and mechanism of char gasification

For designing high-efficiency reactors or processes, kinetics investigation and study of the char gasification mechanism are necessary. In char gasification or combustion, there is a strong interaction between chemical and physical processes. It includes the conversion of char, diffusion to the surface of the char, and the external chemical interaction. Thus, it is not easy to compose the general unified law. Majority of the kinetic analysis employs the global reaction, using the state-of-art Langmuir-Hinshelwood kinetic model while others considers deeper to the structural models of the char gasification through shrinking core model (SCM), the random pore model (RPM), the random capillary model (RCM), volumetric model (VM), etc. However, only the VM, SCM, and RPM are exclusively applied in the biochar gasification

1.4.1 Shrinking core model

Shrinking core model or shrinking un-reacted core model (SCM) also known as grain model (GM) is the model that has been commonly used for char gasification and the chemical reaction involving solid state reactant. This model assumes the coal or char particle to be grain-shaped. The diameter of the particle thus decreases as the matter reacts with the gasifying agent. The outer layer becomes products and ashes, leaving the inner core, or the un-reacted core remains at the equilibrium state. Assuming the surface reaction to be elementary, having the rate constant of k_{SCM}. The differential expression of this model is written by equation below;

$$\frac{dX}{dt} = 3k_{SCM}(1-X)^{2/3} \quad (1)$$

Hajaligol, M.R. and Yi, S.C. [25] utilized this concept to approximate the coal pyrolysis, while Maa and Bailie [26] are believed to be the first researchers who attempted using the SCM model to describe the pyrolysis of cellulose. Both studies modeled pyrolysis as a single spherical particle which pyrolyzed via the first-order reaction with Arrhenius kinetics.

Many researchers studied the application of SCM for describing the gasification of biochar. [27–31] Fermoso *et al.* [27] used non-isothermal TGA methods to study the steam gasification behavior and to obtain the kinetic parameters of chestnut wastes, olive stones and their blends with a bituminous coal from room temperature to 1100 °C at heating rates of 5, 10

and 15 °C min^{-1}. From the study, the SCM was applied for describing the reactivity of the gasification.

Zhai *et al.* [28] studied the kinetic behavior of rice-husk char steam gasification, and they concluded that the surface reaction controlled GM model best described the steam gasification reaction of rice-husk char at temperatures lower than 850 °C and that gas diffusion controlled the overall reaction at temperatures higher than 850 °C.

González-Vázquez *et al.* [29] evaluated the steam gasification of twelve different biomass including samples of hard (wood, almond, olive and pine kernel wastes) and soft (miscanthus, switchgrass, coffee, cocoa and grape wastes) biomass. The fitting of the gasification profiles suggested that SCM were not applicable for every type of biomass and it failed to describe the gasification at a temperature lower than 950°C as seen in **Figure 1.1.**

Wang *et al.* [30] evaluated the CO_2 gasification of four kinds of herbaceous residues and two types of wooden by the method of isotherm-gravimetric analysis. Similar to the study by González-Vázquez *et al.*, [29] the SCM model was unable to describe the gasification behavior of most of the biomass chars. The study by Lahijani P. *et al.* [31] also suggested the inapplicability of SCM to explain the entire range of conversion of CO_2 gasification of 5% Na-added char from pistachio nutshell (PNS) at reaction temperature ranged from 800–875°C.

1.4.2 Volumetric model

In the volumetric model (VM), the structural changes of the sample during the reaction is not considered. Instead, it assumes that the gasifying agents react with the particles of char at all active sites, which are uniformly distributed on both the outside and inside the particle. The overall reaction rate is expressed by:

$$\frac{\mathrm{d}X}{\mathrm{d}t} = k_{VM}(1 - X) \tag{2}$$

The application of this type of model was evaluated in different studies on gasification of biomass. [27–31] It was suggested that the VM was the poorest model to describe the gasification profiles. Kasaoka, S. *et al.* [32] developed the modified volumetric model (MVM) which modifies the equation of the homogeneous model by adding a new parameter, the time power *B*. Whereas *A*, and *B*, which are determined from the conversion versus time data by the least-squares method, are empirical constants and have no any physical and chemical significance.

$$\frac{dX}{dt} = (1 - X)A^{1/B}B[-ln(1 - X)]^{(B-1)/B} \tag{3}$$

This model was applied to the study on the gasification of char from wheat straw in CO_2 at 700–1000°C to obtain the activation energy. [33]

1.4.3 Random pore model

Random pore model (RPM) defines the reaction occurs on the surface of the particle`s pores. The model assumes that the pore shaped like cylindrical capillary which is located randomly and oriented with any distribution of pore radii. [34,35] As the reaction progressed, the product will be formed around each pore, which distinguishes the growing of the surface of solid in the pores. Therefore, the physical structure of particle changes through the reaction.

In the char gasification, the surface area of chars may increase due to the surface reaction of carbon. The relation of the conversion of char with the structural parameters could be expressed in this equation where k_{RPM} is the reaction rate constant and ψ is the pore structural parameter, obtained from the morphology of solid particle (L_0: pore length, S_0: pore surface area, ε_0: solid porosity):

$$\frac{dX}{dt} = k_{RPM}(1 - X)\sqrt{1 - \psi ln(1 - X)} \quad (4)$$

$$\Psi = \frac{4\pi L_0(1-\varepsilon_0)}{S_0^2} \quad (5)$$

Application of this model for describing the gasification of biomass was evaluated in different studies where it was acclaimed to be able to explain the conversion profile better than the other model like SCM or VM. [27–31]

1.4.4 The consideration of the importance of AAEM species in the kinetic model

Despite the wide application of the three models which described in the previous section, in many cases, these models cannot represent well the biomass char gasification profiles, especially in high-temperature regime (as seen in **Figure 1.2**). These models (SCM and RPM) are also known to be highly dependent only on the structure or the morphology of chars. It is also important to consider that these models were mostly applicable for the char from coal or the carbon material which have highly ordered structure. Biomass, which has a highly heterogeneous and disordered structure, can be prone to changes during the course of char oxidation or gasification. [36]

When series of chars are prepared and gasified under identical conditions, the differences of reactivity may only be attributed to differences of morphological structure and

inorganic elements content. As highlighted in Di Blasi's review, surface area, and consequently morphological structure, seems to be less influential on steam gasification reactivity than content in inorganic elements, and particularly soluble minerals. [37] The latter parameter appears to be the most critical parameter to consider for understanding the differences in the gasification behavior of chars from different types of biomasses.

Kudo, S. *et al.* [38] investigated the non-catalytic steam gasification of char from biomass and lignite which concluded that the gasifying agent permeated to the entire part of char without any discrepancy of the physical structure and participated in the reaction. The latter conclusion is that the surface area of char would not be the main influence of the kinetic of gasification.

Considering this AAEM influence on the gasification of char from biomass, Zhang, Y. *et al.* proposed the modification of the random pore model with two additional dimensionless constants that correlate with biomass properties. The developed model can describe the conversion of fourteen different types of biomasses. However, this model is still highly dependent on the structure of biomass char for using RPM as the basic model. [39]

Wu, H. et al. [36] studied the evolution of the carbon structure of char from biomass in steam gasification. The structure change between raw char (catalytic) and acid-treated char (non-catalytic) was very similar (**Figure 1.3**) although the specific reactivity of raw char was distinctly higher (**Figure 1.4**), which indicated that the catalytic species effect was significant for the raw char gasification. Therefore, it was suggested that the gasification of char could not be modeled by an oversimplified equation such as the homogeneous model, shrinking core model, random capillary model, and random pore model which predict the char reactivity based on the pore surface area. A reasonable representation of kinetics of gasification of char from biomass would need to consider both catalytic and non-catalytic reactions in parallel.

1.4.5 The application of the parallel kinetic model for describing the profile of catalytic gasification

Parallel kinetic model is a model which assumes the progress of non-catalytic and catalytic gasification in parallel. Equation expresses the overall gasification rate are given by:

$$\frac{dX}{dt} = \left(\frac{dX}{dt}\right)_{non-cat.} + \left(\frac{dX}{dt}\right)_{cat.} \quad (6)$$

$$\frac{dX}{dt} = k_{nc}(1 - X) + k_{cg} \quad (7)$$

k_{nc} defines the rate constant of the non-catalytic gasification while k_{cg} describes the rate

constant of the catalytic gasification. Equation 7 assumes that the non-catalytic gasification follows the first-order reaction, while catalytic gasification is a zero-order reaction with respect to the unconverted fraction of char. The application of this parallel kinetic model for gasification of biomass, lignite, and coal was carried out by several researchers. [40–44]

Bazardorj, B. *et al.* [40] proposed the parallel kinetic model to describe the steam gasification of nascent char from slow and rapid pyrolysis of brown coal. It was found that the gasification of raw char at the conversion of X>0.8 similar to that from the acid-washed coal which obeys first-order kinetics over the entire range of X. Thus, the char conversion can be described by

$$\frac{dX}{dt} = k_{nc}(1 - X) \tag{8}$$

It was confirmed in this study [40] that the involvement of AAEM species in the raw coal enhanced the gasification rate. The AAEM species were highly dispersed in char matrix. Therefore it can be assumed that the rate of the catalytic gasification would be a function of the amount of the active AAEM species as well as their activities, independent of the amount of char as the matrix. The rate of the catalytic gasification can thus be expressed by

$$\frac{dX}{dt} = k_{cg} \tag{9}$$

k_{cg} is assumed to be proportional to the amount of active AAEM species remaining in/on the gasifying char, i.e.

$$k_{cg} = k'_{cg} C_{AAEM} \tag{10}$$

where k'_{cg} and C_{AAEM} are the rate constant for catalytic gasification per unit amount of active AAEM species and the amount of active AAEM species, respectively. It is further assumed that C_{AAEM} decreases obeying first-order kinetics, i.e

$$C_{AAEM} = C_{AAEM,0} \exp(-k_{loss} t) \tag{11}$$

$C_{AAEM,0}$ and k_{loss} are C_{AAEM} at t=0 and overall rate constant for the loss of active AAEM species due to volatilization and intra-particle deactivation, respectively. Application of the first-order kinetics for the loss of catalysis is just for simplifying the model. k_{cg} is then given from Equations 10 and 11 by

$$k_{cg} = k'_{cg} C_{AAEM,0} \exp(-k_{loss} t) \tag{12}$$

Therefore, overall rate gasification can be expressed by

$$\frac{dX}{dt} = k_{nc}(1 - X) + k_{cg,0} \exp(-k_{loss} t) \tag{13}$$

The Equation 13 could describe the steam gasification of nascent char in the study [40]. The initial catalytic activity of AAEM species and the rate of activity loss strongly was found to depend on the operating variables such as the heating rate for the pyrolysis, total pressure and partial pressure of steam. However, this study did not consider the relation of the initial catalytic activity and deactivation with the amount of the AAEM in the chars.

Kitsuka, T. *et al.* [41] analyzed the steam gasification of four pairs of raw and acid-washed brown coals in a fixed bed reactor. The chars from the acid-washed coals were gasified obeying the first-order kinetics with respect to the fraction of unconverted char regardless of the presence/absence of forced gas flow. The catalytic gasification, in which AAEM species play the role of catalyst, is recognized as a zero-order reaction with the initial rate constant $k_{cg,0}$. The overall rate of gasification described by the Equation 13.

The group [41] also scrutinized the behavior of the inherent metallic species in the steam gasification of char from pyrolyzed coal. It was found in the study that AAEM species did not volatilize from the char in the steam gasification carried out in the fixed bed reactor. Instead, the metallic species seemed to mobilize throughout the particle, underwent repeated adsorption and desorption while catalyzing the gasification.

In the study carried out by Kajita, M. *et al.* [42], chars from the pyrolysis of a Japanese bamboo and cedar were gasified by steam under different partial pressure of steam, P_{H2O}. Describing the gasification profile, the overall rate of gasification was following the parallel kinetic model represented by Equation 7. However, since there were variations on the concentration of H_2O and H_2, Langmuir-Hinshelwood (L-H) was applied to analyze the non-catalytic gasification rate constant, k_{nc}. Thus the k_{nc} mechanism was following the equation below

$$k_{nc} = \frac{k_{nc,a}P_{H2O}}{1+k_{nc,b}P_{H2O}+k_{nc,c}P_{H2}} \quad (14)$$

The rate constant of the catalytic gasification, k_{cg} were evaluated with the L-H mechanism as

$$k_{cg} = \frac{k_{cg,a}P_{H2O}}{1+k_{cg,b}P_{H2O}+k_{cg,c}P_{H2}} \quad (15)$$

It is shown in the study that the catalytic activity of K was dominant, and the activity could change to its maximum depending on its critical concentration. Moreover, K activity could fluctuate throughout the conversion due to the formation of active clusters of K from that dispersed at an atomic scale and growth of such clusters together with their reactions with Si- and/or Al-containing species, respectively.

The study by Kim, H.S. *et al.* [43], pointed out the relationship of the catalytic gasification rate constant, k_{cg} with the concentration of catalytic species of Ca. The activity of the catalyst will be improved as the concentration of catalyst increased to the maximum or saturated level. From the kinetic model analyses (Equation 13), catalysts were necessary to be divided into two types, which is type 1 and type 2. Thus, the overall rate constant of the catalytic gasification was determined with the following equation

$$k_{cg} = k_{cg1,0}\exp(-k_{loss1}t) + k_{cg2,0}\exp(-k_{loss2}t) \quad (16)$$

The type-1 catalyst was mainly contributed to the early stage of gasification, and it had a much higher initial activity ($k_{cg1,0}$) than that of type-2 ($k_{cg2,0}$). However, its rate of activity lost (k_{loss1}) was also higher, resulting in quicker deactivation.

On the other hand, Byambajav, E. *et al.* [44] proposed a kinetic model with the assumption of the progression of catalytic and non-catalytic gasification in parallel for describing the CO_2 gasification of eleven Mongolian lignites at 900°C. The overall rate of char gasification was expressed as the total rates of non-catalytic gasification and catalytic gasification.

$$\frac{dX}{dt} = k_{nc}(1-X) + \sum_n k_{Cn} \quad (17)$$

k_{nc} and k_{Cn} are the first-order rate constants for the non-catalytic gasification and zero-th-order rate constant for the catalytic gasification, respectively. *n* denotes the catalytic component C*n* (*n* = 1–4). k_{cn} is given as the product of the effective amount of catalyst (m_{Cn}) and rate constant (k'_C).

$$k_{Cn} = k'_C m_{Cn} \quad (18)$$

$$k_{Cn,0} = k'_C m_{Cn,0} \text{ (at } t = 0) \quad (19)$$

Equation 18 is based on the fact that the rate of catalytic gasification is determined by the amount of catalyst retained in each char particle. k_{Cn} represents the activity of C*n* catalyst, while k'_C is common among the catalytic components with different *n*.

k_{Cn} changes along the char conversion and with m_{Cn}. It decreases while the catalyst undergoes deactivation. Volatilization of catalyst, which often takes place for alkali and alkaline earth metallic species, is another process to decrease m_{cn}, but it was not important under the present gasification, which was performed with no gas flow forced to pass through the fixed bed of char particles. [40–42] When the catalyst is dispersed in the char matrix on an atomic scale or in the form of nanosized particles, it is deactivated, obeying a general

coalescence/growth mechanism (i.e., self-deactivation mechanism). Increasing particle size decreases the catalyst activity per amount, and then m_{Cn} accordingly. The other important mechanism of deactivation is the reaction of the catalyst with mineral matters such as silica, alumina, and aluminosilicates. [45–47] For both mechanisms, the rate of deactivation is a function of the catalyst concentration in the char, rather than the amount. The catalyst concentration increases as X increases as a result of the loss of the carbonaceous matrix.

There is no need to either know or determine the absolute value of catalyst concentration, but it is necessary to express dependency of the concentration upon X. The catalyst concentration is simply given by a simple equation for the gasification-induced enrichment of catalyst.

$$C_{Cn} = \frac{m_{Cn}}{1 - X} \tag{20}$$

Then the kinetics of catalyst deactivation is expressed by

$$\frac{dm_{Cn}}{dt} = -k_{loss\text{-}n} C_{Cn} = -k_{loss\text{-}n} \frac{m_{Cn}}{1 - X} \tag{21}$$

under an assumption that the deactivation obeys first-order kinetics with respect to the catalyst concentration. Some previous studies reported the effectiveness of this assumption, although the concentration and amount of catalyst were not distinguished clearly from each other. [40–43]

m_{Cn} increases by transformation of the catalyst precursor. The model assumes for expedience that a type of precursor (C1prec) is transformed exclusively into the catalyst C1. Equation 21 is here revised to the following equations:

$$\frac{dm_{C1}}{dt} = k_{C1prec} C_{C1prec} - k_{loss\text{-}1} C_{C1} \quad n = 1 \tag{22}$$

$$\frac{dm_{Cn}}{dt} = -k_{loss\text{-}n} C_{Cn} \quad n \geq 2 \tag{23}$$

The concentration of C1prec is defined in the same way as C_{Cn}.

$$C_{C1prec} = \frac{m_{C1prec}}{1 - X} \tag{24}$$

The kinetics of the transformation of C1prec is expressed by

$$\frac{dm_{C1prec}}{dt} = -k_{C1prec} C_{C1prec} \tag{25}$$

The model defines that the total amounts of the catalysts and the catalyst precursor is unity at the beginning of gasification.

$$\sum_{n=1} m_{\mathrm{C}n,0} + m_{\mathrm{C1prec},0} = 1 \tag{26}$$

The rate of catalytic gasification at $t = 0$ is defined as ICA-1

$$\text{ICA-1} = \sum_{n=1} k_{\mathrm{C}n,0} = \sum_{n=1} k_{\mathrm{C}}^{\phi} m_{\mathrm{C}n,0} \tag{27}$$

ICA-1 represents the initial catalytic activity. When the catalyst precursor, C1prec, is involved in the char, it is also reasonable to define an initial and potential catalytic activity, considering C1prec. This type of the initial activity is presented by

$$\text{ICA-2} = k_{\mathrm{C}}^{\phi} m_{\mathrm{C1prec},0} + \sum_{n=1} k_{\mathrm{C}n,0} = k_{\mathrm{C}}^{\phi} \left(m_{\mathrm{C1prec},0} + \sum_{n=1} m_{\mathrm{C}n,0} \right) = k_{\mathrm{C}}^{\phi} \tag{28}$$

It was suggested that in the study by Byambajav et al. [44] the initial catalytic activity, ICA-2, was well correlated to the initial concentration of the AAEM species, especially that of Ca, K, and Na. The activity of several chars was decreased due to the Si formation during pyrolysis. Hence, the deactivation of the catalyst during gasification was not strongly affected by the abundance amount of Si. Instead, it was suggested that the deactivation may be triggered by their self-deactivation through agglomeration or growth of size.

1.5 The objective of this study

The significant use of biomass in energy and chemical is an essential topic to discuss, especially considering its market potential (as fuel/feedstock), its advantage as one of the CO_2 emission mitigation method, and as one of the alternatives for replacing the fossil fuel. Some technologies have been developed to make an efficient process, and some kinetic models on char gasification have been constructed for the purpose. However, the commonly used kinetic models are depending on the char structure which involving active surface area and adsorption-desorption mechanism of gasifying agent and product. These models were applied based on the gasification study on coal, or carbon material which has ordered structure. The models could not describe the biomass due to its heterogeneous and disordered structure. Also, recent studies suggested the important involvement of inherent AAEM species in biomass gasification. This inherent metallic species is believed to be the crucial players in the biomass char gasification than the physical structure of chars. However, the carbon structure of char still plays important role in the overall reactivity through interaction with catalytic species.

Therefore, the application of kinetic model assuming the progress of catalytic and non-catalytic gasification is more appropriate to describe the biomass gasification. It is also noted from the review that very few studies attempted to correlate the catalyst activity with the concentration of the catalytic species and to explain the catalyst deactivation mechanism. Moreover, currently there is no study that explain the differences of catalytic behavior between catalytic steam gasification and CO_2 gasification of biochar. Therefore, this thesis makes a particular focus on the kinetics and mechanism of gasification of char from sugarcane bagasse under the catalysis of inherent metallic species using the parallel kinetic model, aiming at quantitative description of the kinetics over the entire range of the char conversion into syn-gas with oxidizing agents, i.e., carbon dioxide (**Chapter 2**) and steam (**Chapter 3**). This thesis also aimed to explain the mechanism of catalyst activation and deactivation throughout the gasification, and to compare the differences between the catalytic steam and CO_2 gasification (**Chapter 3**). Finally, this thesis discusses hydrothermal pretreatment of biomass, which is expected to upgrade it as a solid fuel with a strong focal point of fates and behaviors of the inherent metallic species (**Chapter 4**).

1.6 Summary of the dissertation

Chapter 1 of this thesis comprehensively reviews the potential of biomass as an energy resource and chemical feedstock as well as the thermochemical technologies for the biomass conversion. A particular focus is made on gasification of char with a consideration of mechanism, kinetics, and process. It is believed that, in the presence of catalytic species, the structural-based kinetic model is not plausible to describe the char conversion. Therefore, a construction of an advanced model with the consideration of the catalytic species is essential.

Chapter 2 discussed the results of the gasification of eighteen chars from the pyrolysis of six trios of sugarcane bagasses (SCBs; original, water-washed, and acid-washed) with CO_2 at 900°C. This study aimed at the quantitative description of the rate of gasification catalyzed by inherent metallic species and correlation of the catalytic activity and its change during the gasification with the metallic species composition. The measured kinetics was described quantitatively over a range of char conversion, 0–0.999, by a model that assumed progress in parallel of the catalytic gasification and non-catalytic one, together with the presence of a catalytic precursor and 3–4 types of catalysts having different activities and deactivation characteristics. A series of regression analyses was scrutinized and reached expression of initial catalytic activity as a linear function of Na, K, Ca, Fe and Si concentrations in the char with a

correlation factor (r^2) > 0.98. The catalyst precursor was contributed fully by the water-soluble Na, K and Ca. Si was responsible for the catalyst deactivation during the pyrolysis, but not during the gasification. The chars produced from original SCBs followed a linear relationship between the initial catalytic deactivation rate and initial activity (r^2 > 0.99), while such a linear relationship was not valid for those formed from the water-washed SCBs. This was explained mainly by more rapid deactivation of Fe catalyst in the chars from water-washed SCBs than that in the chars formed from the original SCBs. Na and K in char from the original SCBs, originating from the water-soluble ones SCBs, chemically interacted with Fe catalyst slowing down its deactivation.

Chapter 3 discussed the results of the steam gasification of chars from the pyrolysis of sugarcane bagasse (SCBs) prepared in the different types of preparation techniques; no-pretreatment, water-washed treatment, and acid-washed treatment. The steam gasification process was carried out in the thermogravimetric analyzer at 850°C with the concentration of gasifying agent being 20 vol. % steam/N_2. The conversion profile of chars was following a first-order kinetic which indicated more rapid catalyst precursor to catalyst transformation compared to the study in CO_2 gasification. Thus, the assumption of the catalytic precursor was unnecessary in the kinetic models of steam gasification. The parallel kinetic model used in this study was able to describe the measured profiles of the catalytic gasification with an assumption of one to two types of catalysts which has different activation and deactivation characteristics. The initial catalytic activity of individual chars was measured against the total concentration of AAEM species. Following a series of regression analysis, it was suggested that Na, K, and Ca was actively and equally involved in the catalytic activity. Similar to the CO_2 gasification, there was no evidence of the effect of SiO_2 on the catalyst deactivation during gasification. The catalytic species experienced self-deactivation and volatilized during gasification. In steam gasification, the interaction between Na/K with Fe was suppressed. Thus, Fe played as a single catalyst and deactivated faster during the gasification.

Chapter 4 described the results of the investigation of heat treatment of Japanese Cedar in hot-compressed water (hydrothermal treatment) at 250 °C. The process was able to upgrade the woody biomass to solid with particular features by converting a major portion of carbohydrate (cellulose and hemicellulose) into the water-soluble matter and solvent-soluble lignin-like material, removing more than 90% of the alkali and alkaline earth metallic (AAEM) species. The upgraded biomass is available in the production of metallurgical coke that has mechanical strength higher by more than six times than that of conventional one from coals, and activated carbon with specific surface area well above 2,000 m^2 g^{-1} without any

additives/chemicals. Repeated use of product water maximizes the yield of upgraded biomass, maintaining its ability of leaching of AAEM species. It is well described here that with the absence of AAEM species, the char conversion rate in steam decreased significantly compared to the reactivity of the char from non-treated biomass. Further leaching by HCl resulted in a near-identical trend with that of char from upgraded biomass, indicating that although not fully eliminated the AAEM species, the HT eradicated the catalytic AAEM species. It is noted from this chapter that specific surface area might not be the critical factor in the biomass char reactivity, but the catalysis of AAEM species was the compelling circumstances in gasification.

Finally, **Chapter 5** summarized the findings described in the preceding chapters.

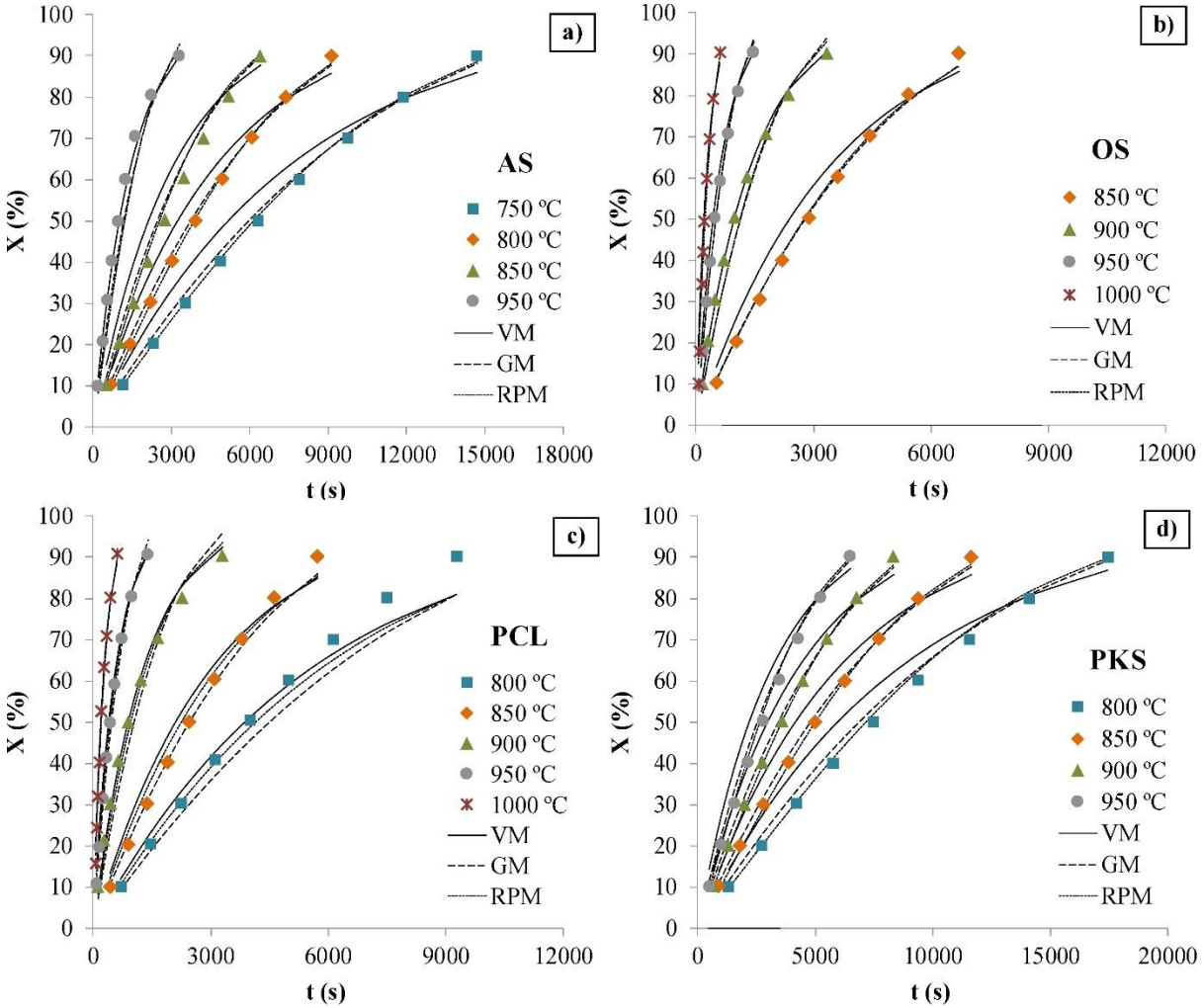

Figure 1.1. The SCM for describing the gasification profile of 5% Na loaded PNS char. [28]

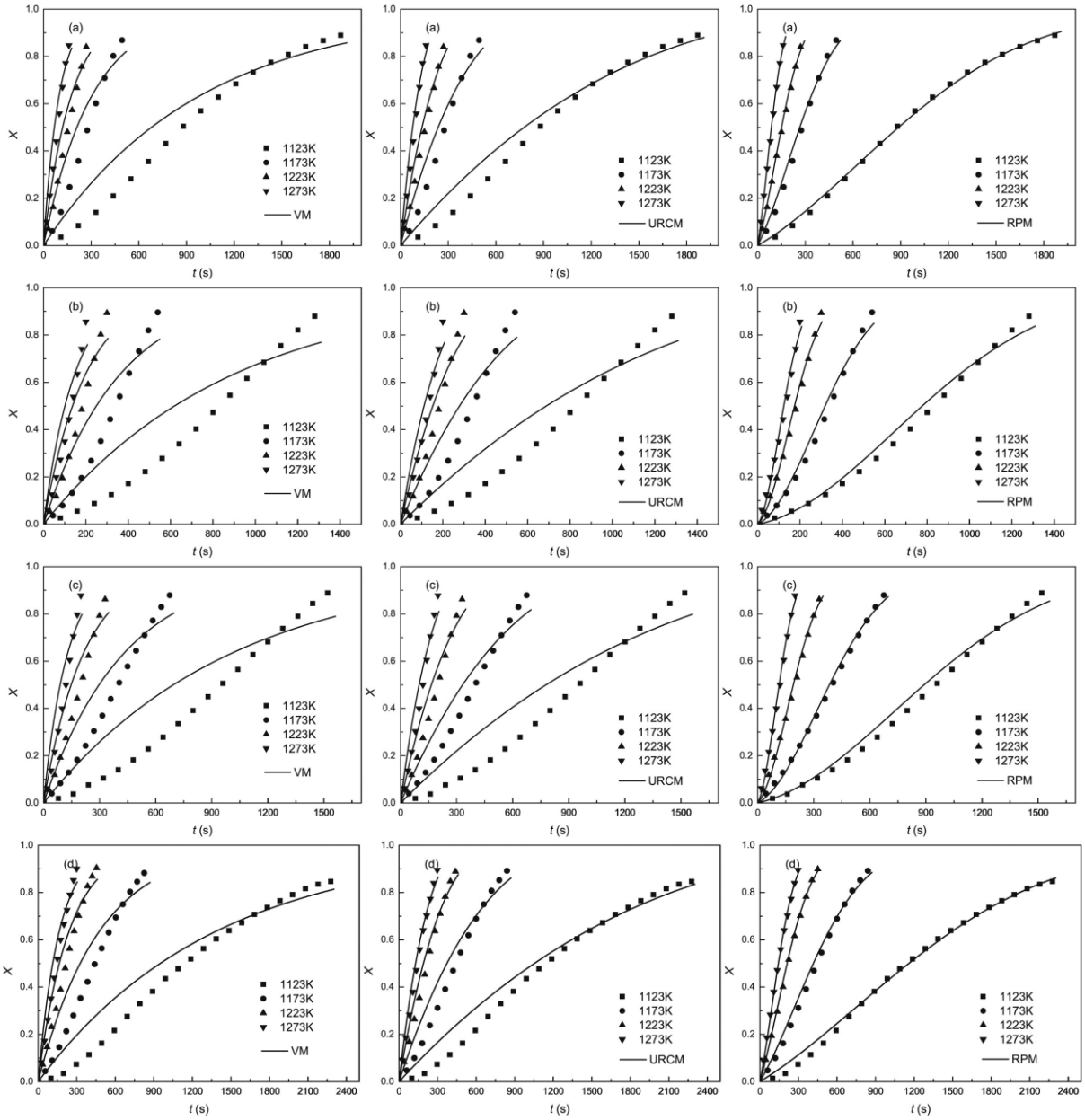

Figure 1.2. VM, GM, and RPM for describing the CO_2 gasification of different char from: (a) peanut shell, (b) maize cob, (c) wheat straw, and (d) rice lemma. [29]

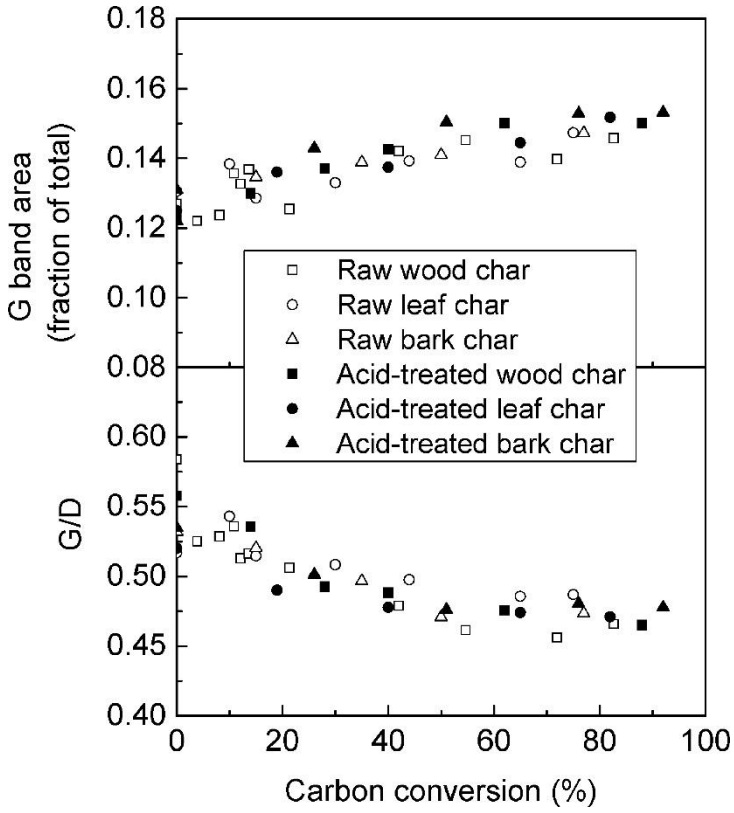

Figure 1.3. Peak area of G band, and the ratio of G/D as a function of carbon conversion. [36]

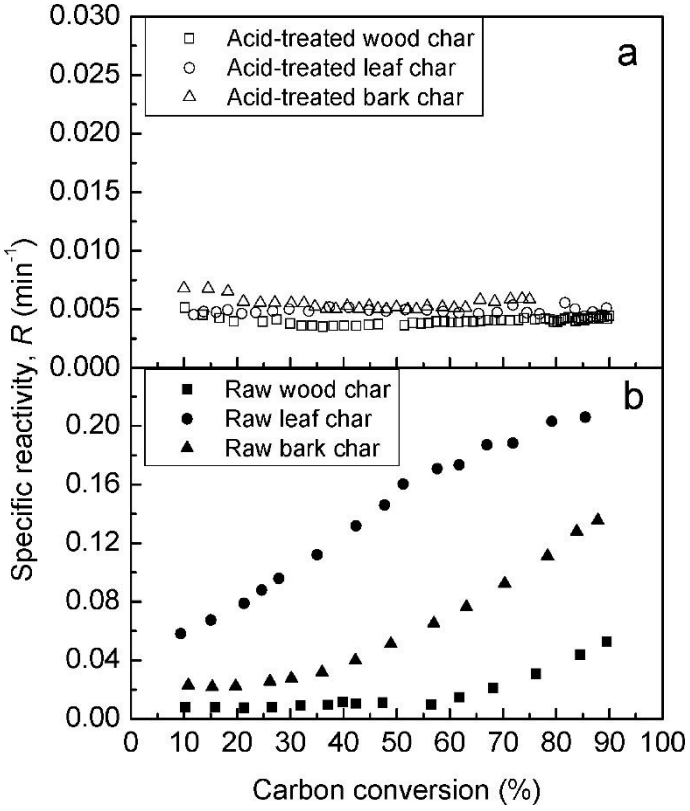

Figure 1.4. Specific gasification reactivity as a function of carbon conversion for various biochars, gasification at 750 °C with an intended steam concentration of 8.2 vol %: (a) acid-treated biochars; (b) raw biochars. [36]

1.7 References

1. BP Energy Economics. *BP Energy Outlook*, **125** (2018). [Retrieved from https://www.bp.com/]
2. L, F.C.P: Adoption of the Paris Agreement Proposal by the President, (2015).
3. IEA: Technology Roadmap: Delivering Sustainable Bioenergy, **94** (2017).
4. IEA: Technology Roadmap: Bioenergy for Heat and Power, (2012).
5. H. Yamamoto, J. Fujino, K. Yamaji: *Biomass and Bioenergy*, **21** (2001), 135–203.
6. A. Brosowski, D. Thrän, U. Mantau, B. Mahro, G. Erdmann, P. Adler, W. Stinner, G. Reinhold, T. Hering, C. Blanke: *Biomass and Bioenergy*, **95** (2016), 257–272.
7. Statistics Indonesia, (2015). [Retrieved from http://www.bps.go.id/].
8. Ministry of industry, [Retrieved from http://www.kemen-perin.go.id/].
9. D. Restuti, A. Michaelowa: *Energy Policy*, **35** (2007), 3952-3966.
10. Japan Institute of Energy: *Asian Biomass Handbook*, (2008).
11. M. J. Wornat, R. H. Hurt, N. Y. C. Yang, T. J. Headley: *Combustion and Flame*, **100**, **1–2** (1995), 131–143.
12. A.J. Saraber: *Fuel Processing Technology*, **128** (2014**)**, 68–82.
13. P. McKendry: *Bioresource Technology*, **83**, **1** (2002), 37–46.
14. A. Demirbas, G. Arin: *Energy Sources*, **24** (2002), 471–482.
15. A.V. Bridgwater: *Fuel*, **74**, **5** (1995), 631–653.
16. A.V. Bridgwater: *Applied Catalysis A: General*, **116** (1994) 5–47.
17. M.T. Reza, J.G. Lynam, M.H. Uddin, C.J. Coronella: *Biomass and Bioenergy*, **49** (2013), 86–94.
18. J. Stemann, A. Putschew, F. Ziegler: *Bioresource Technology*, **143** (2013), 139–146.
19. X.J. Ma, S.L. Cao, L. Lin, X.L. Luo, H.C. Hu, L.H. Chen, L.L. Huang: *Bioresource Technology*, **148** (2013), 408–413.
20. Li, C.-Z: *Process Safety and Environmental Protection*, **84** (2006), 407–408.
21. M. Carpentieri, A. Corti, L. Lombardi: *Energy Conversion and Management*, **46**, **11–12** (2005), 1790–1808.
22. J.-i, Hayashi, S. Kudo, H.-S. Kim, K. Norinaga, K. Matsuoka, S. Hosokai: *Energy Fuels*, **28** (2014), 4−21.
23. Brown, R. (2009). Biochar Production Technology. Chapter 8 in J. Lehmann and S. Joseph (eds) Biochar for Environmental Management. Earthscan, London.

24. E.G. Pereira, J.N. da Silva, J.L. de Oliveira, C.S. Machado: *Renewable and Sustainable Energy Reviews*, **16** (2012), 4753–4762.
25. M.R. Hajaligol, S.C. Yi: Preprint, American Chemical Society, Division of Fuel Chemistry, **34**, **4** (1989), 1300–1307.
26. P.S. Maa, R.C. Bailie: *Combustion Science Technology*, **7** (1973), 257–269.
27. J. Fermoso, M.V. Gil, A.G. Borrego, C. Pevida, J.J. Pis, F. Rubiera: *Energy Fuels*, **24** (2010), 5586–5595.
28. M. Zhai, Y. Zhang, P. Dong, P. Liu: *Fuel*, **158** (2015), 42–49.
29. M.P. González-Vázquez, R. García, M.V. Gil, C. Pevida, F. Rubiera: *Energy*, **155** (2018), 426–437.
30. G. Wang, J. Zhang, J. Shao, Z. Liu, H. Wang, X. Li, P. Zhang, W. Geng, G. Zhang: *Energy*, **114** (2016), 143−154.
31. P. Lahijani, Z.A. Zainal, A.R. Mohamed, M. Mohammadi: *Bioresources Technology*, **144** (2013), 288−295.
32. S. Kasaoka: *International Chemical Engineering*, **25** (1985), 160–175.
33. Y. Li, Y.Q. Wu, J. Gu, S.Y. Wu, J.S. Gao: *ACTA Energiae Solaris Sin*, **30** (2009), 1258–1262.
34. S. K. Bhatia, D. D. A Perlmutter: *AIChE Journal*, **26**, **3** (1980), 379–386.
35. S. K. Bhatia, D. D. A Perlmutter: *AIChE Journal*, **27**, **2** (1981), 247–254.
36. H. Wu, K. Yip, F. Tian, Z. Xie, C.-Z. Li: *Industrial and Engineering Chemistry Research*, **48** (2009), 10431–10438.
37. C. Di Blasi: *Progress in Energy and Combustion Science*, **35** (2009), 121–140.
38. S. Kudo, Y. Hachiyama, H-S. Kim, K. Norinaga, J.-i. Hayashi: *Energy Fuels*, **28** (2014), 5902−5908.
39. Y. Zhang, M. Ashizawa, S. Kajitani, K. Miura: *Fuel*, **87** (2008), 475−481.
40. B. Bayarsaikhan, J.-i. Hayashi, T. Shimada, C. Sathe, C.-Z. Li, A. Tsutsumi, T. Chiba: *Fuel*, **84** (2005), 1612−1621.
41. T. Kitsuka, B. Bayarsaikhan, N. Sonoyama, S. Hosokai, C.-Z. Li, K. Norinaga, J.-i Hayashi: *Energy Fuels* **21** (2007), 387−394.
42. M. Kajita, T. Kimura, K. Norinaga, C.-Z. Li, J.-i. Hayashi: *Energy Fuels*, **24** (2010)**,** 108−116.
43. H-S. Kim, S. Kudo, K. Tahara, Y. Hachiyama, H. Yang, K. Norinaga, J.-i. Hayashi: *Energy Fuels*, **27** (2013), 6617−6631.

44. E. Byambajav, Y. Hachiyama, S. Kudo, K. Norinaga, J-i. Hayashi: *Energy Fuels*, **30** (2016), 1636−1646.
45. H. Risnes, J. Fjellerup, U. Henriksen, A. Moilanen, P. Norby, K. Papadakis, D. Posselt, L.H. Sørensen: *Fuel*, **82** (2003), 641−651.
46. G. Bruno, M. Buroni, L. Carvani, G. D. Piero, G. Passoni: *Fuel*, **67** (1988), 67−72.
47. L. Kühn, H. Plogmann: *Fuel*, **62** (1983), 205−208.

Chapter 2

CO_2 Gasification of Sugarcane Bagasse: Quantitative Understanding of Kinetics and Catalytic Roles of Inherent Metallic Species

2.1 Introduction

Gasification employing carbon dioxide as gasifying agent, which is hereafter termed CO_2 gasification, has been drawing attention in academic and industrial fields of thermochemical processing of biomass. This is because the CO_2 gasification offers potential advantages over conventional processes in reducing carbon emission. [1] The CO_2 gasification with subsequent water-gas shift conversion and further conversion into organic compounds leads to carbon-negative conversion of biomass depending on the net conversion of CO_2. This feature is further promoted by increasing the efficiency of the gasification (i.e., cold gas efficiency) by maximizing the contribution of the endothermic reaction (i.e., CO_2 conversion) to the overall solid-to-gas conversion of biomass. [2] Steam is a more popular gasifying agent, of that reaction with biomass is endothermic, while its generation requires a large latent heat. There is no such requirement for CO_2. It is, however, known that CO_2 is generally less reactive than steam [3,4], and that effective use of inherent catalyst (exactly saying, catalyst precursor) or even application of extraneous catalyst is mandatory for fast and complete char conversion [5,6]. Alkali, alkaline earth, and also transition metals are the most commonly used catalysts, and their effective use has been reported in literature. [7-10] Fortunately, not all but many types of biomass inherently contain metallic species such as sodium (Na), potassium (K), calcium (Ca) and transition metals. [2]

Sugar cane is one of the most abundant biomass in Indonesia and the annual production reaches 34 million tons. [11] Sugar production is associated with byproducts, such as bagasse, leaves/trash, filter cake (sugar juice residue), and molasses. The bagasse is the most important byproduct in terms of mass, of which production is about a half of the sugar cane, [12] and is expected as a major feedstock for the gasification-based production of power and chemicals. As mentioned later, Indonesian sugar cane bagasses, hereafter referred to as SCBs, are relatively rich in Na, K, Ca, magnesium (Mg), and also in iron (Fe). SCBs are thus attractive for studying the catalysis of inherent metallic species in the gasification.

It is well agreed that overall rate of solid-to-gas conversion of biomass is determined by that of char gasification, and quantitative understanding and prediction of its characteristics is therefore essential for designing gasifier and optimization of operating conditions. [13] Many previous studies employed existing kinetic models such as random-pore models, shrinking core models and homogeneous reactions models with *n*-th order kinetics for the kinetic analysis, but it seemed to be difficult for any of those models to describe the kinetics over the entire range of char conversion. [14-19] This is, in the view of the present authors, primarily due to the above-described models originally considered non-catalytic gasification but not catalytic gasification. A most reasonable way to analyze the kinetics may be to distinguish the catalytic gasification from the non-catalytic gasification and then relate the former kinetics with the behavior of metallic species.

Some recent studies on the gasification of lignite chars or catalyst-loaded chars applied kinetic models that assumed progress in parallel of non-catalytic gasification and catalytic gasification together with generation and loss of catalysis and described the kinetics well and over ranges of char conversion up to 0.99 or even higher. [5,20-22] A quantitative description of the char conversion kinetics over its entire range is definitely useful for understanding of the mechanism of catalytic gasification, in particular, catalytic roles of the metallic species and their behavior in the gasification if catalyst-related kinetic parameters are correlated with total or individual abundances of the metallic species.

The present authors have been studying the CO_2 gasification of chars from Indonesian SCBs that were collected at different sugar factories, and also those from acid-washed SCBs and water-washed SCBs. This paper reports successful application of a catalytic/non-catalytic parallel reaction model and draws the catalytic behaviors and roles of inherent metallic species through systematic correlations of the kinetic parameters with the abundances of the metallic species, K, Na, Ca, Mg, Fe and silicon (Si).

2.2 Experimental

2.2.1 SCB samples.

Six different types of SCBs (GB, KB, KR, MK, PJ and SR) were pulverized to sizes smaller than 150 mesh and dried, leaving residual moisture (< 10 wt%). The SCBs were also washed with 1 N HCl aqueous solution at 60°C for 24 h, or with deionized water at 60°C for 24 h according to a procedure reported previously. [23] A sufficiently large liquid/solid ratio (100 ml/5 g) was applied to the acid washing to avoid change in the pH of the aqueous solution

due to exchange between proton and metallic cation. The water washing was performed with the same liquid/solid as in the acid. The acid-washed and water-washed SCBs will be referred to as AW-SCBs and WW-SCBs, respectively.

2.2.2 Char preparation and analyses.

SCBs, AW-SCBs and WW-SCBs were pyrolyzed individually in a fixed bed reactor under the following conditions: heating rate of 30 °C min^{-1}, peak temperature of 600°C, holding time at the peak temperature of 15 min, pressure of 0.1 MPa, N_2 carrier gas (purity > 99.9995 vol.%). The contents of the metallic species in the chars were determined according to procedures reported previously. [24,25] The alkali and alkaline earth metallic species (i.e., Na, K, Mg and Ca) were quantified by a sequence of dissolution of ash with an aqueous solution of HNO_3/HF, evaporation to dryness, re-dissolution into an aqueous solution of CH_3SO_3H and its analysis by ion chromatography, while X-ray fluorescence spectroscopy was employed to quantify Fe, Si, Al and other minor species in the ash. **Table 2.1** shows the ash contents and elemental compositions of the SCBs, AW-SCBs and WW-SCBs. The individual char samples indicated by X, X-AW or X-WW in **Table 2.1** denote the chars from the original, acid-washed or water-washed X (= GB, KB, KR, MK, PJ or SR), respectively. **Table 2.1** also exhibits the elemental compositions and ash contents of the char samples. While, those for the chars from WW-SCBs and AW-SCBs are available in **Appendix 2**.

2.2.3 Gasification of chars.

All of the 18 char samples were subjected individually to CO_2 gasification in a type of thermogravimetric analyzer (TGA model STA7200, Hitachi Hi-Tech Science,). The char sample was heated in atmospheric N_2 flowing at 700 mL standard temperature and pressure (STP)/min up to 900°C, which was held for 60 min. The atmosphere was then switched to 50:50 (in volume) mixed gases of N_2 and CO_2 without changing the total flow rate. A sufficiently small initial mass of the char (< 2 mg) and gas flow rate as high as above allowed for the monitorization of the kinetics of gasification without effects of mass transport. Details of the procedure were reported previously. [22]

2.3 Kinetic model

The overall rate of char gasification is expressed as the total rates of non-catalytic gasification and catalytic gasification.

$$\frac{dX}{dt} = k_{nc}(1 - X) + \sum_{n} k_{Cn} \quad (1)$$

k_{nc} and k_{Cn} are the first-order rate constants for the non-catalytic gasification and zero-th-order rate constant for the catalytic gasification, respectively. n denotes the catalytic component Cn (n = 1–4). k_{cn} is given as the product of the effective amount of catalyst (m_{Cn}) and rate constant (k'_C).

$$k_{Cn} = k'_C m_{Cn} \quad (2)$$

$$k_{Cn,0} = k'_C m_{Cn,0} \text{ (at } t = 0) \quad (3)$$

Equation 2 is based on the fact that the rate of catalytic gasification is determined by the amount of catalyst retained in each char particle. k_{Cn} represents the activity of Cn catalyst, while k'_C is common among the catalytic components with different n.

k_{Cn} changes along the char conversion and with m_{Cn}. It decreases while the catalyst undergoes deactivation. Volatilization of catalyst, which often takes place for alkali and alkaline earth metallic species, is another process to decrease m_{cn}, but it was not important under the present gasification, which was performed with no gas flow forced to pass through the fixed bed of char particles. [5,20,26] When the catalyst is dispersed in the char matrix on an atomic scale or in form of nanosized particles, it is deactivated, obeying a general coalescence/growth mechanism (i.e., self-deactivation mechanism). Increasing particle size decreases the catalyst activity per amount, and then m_{Cn} accordingly. The other important mechanism of deactivation is the reaction of catalyst with mineral matters such as silica, alumina and aluminosilicates. [10,27,28] For both mechanisms, the rate of deactivation is a function of the catalyst concentration in the char, rather than the amount. The catalyst concentration increases as X increases as a result of the loss of carbonaceous matrix. The pathways of catalyst transformation are illustrated in **Figure 2.1**.

There is no need to either know or determine the absolute value of catalyst concentration, but it is necessary to express dependency of the concentration upon X. The catalyst concentration is simply given by a simple equation for the gasification-induced enrichment of catalyst.

$$C_{Cn} = \frac{m_{Cn}}{1 - X} \quad (4)$$

Then the kinetics of catalyst deactivation is expressed by

$$\frac{\mathrm{d}m_{\mathrm{C}n}}{\mathrm{d}t} = - k_{\text{loss-}n} C_{\mathrm{C}n} = - k_{\text{loss-}n} \frac{m_{\mathrm{C}n}}{1 - X} \tag{5}$$

under an assumption that the deactivation obeys first-order kinetics with respect to the catalyst concentration. Some previous studies reported effectiveness of this assumption, although the concentration and amount of catalyst were not distinguished clearly from each other. [5,20,21,26]

$m_{\mathrm{C}n}$ increases by transformation of the catalyst precursor. Preliminary kinetic analyses showed necessity of assuming the presence of at least a type of catalyst precursor for the chars from the original SCBs and a char from WW-SCB. Previous studies on gasification of chars from Na-loaded lignite or K-loaded biomass [30,31] showed that occurrence of catalytic activity requires certain (critical) concentration of Na or K. Such metallic species, if dispersed in the char matrix at an atomic or similar scale as a result of its sufficiently low concentrations, can transform into a catalyst when its concentration exceeds a critical concentration. The assumption of a catalyst precursor in the char from SCBs and also WW-SCBs is thus reasonable. The model assumes for expedience that a type of precursor (C1prec) is transformed exclusively into the catalyst C1. Equation 5 is here revised to the following equations:

$$\frac{\mathrm{d}m_{\mathrm{C1}}}{\mathrm{d}t} = k_{\mathrm{C1prec}} C_{\mathrm{C1prec}} - k_{\text{loss-1}} C_{\mathrm{C1}} \quad n = 1 \tag{6}$$

$$\frac{\mathrm{d}m_{\mathrm{C}n}}{\mathrm{d}t} = - k_{\text{loss-}n} C_{\mathrm{C}n} \quad n \geq 2 \tag{7}$$

The concentration of C1prec is defined in the same way as $C_{\mathrm{C}n}$.

$$C_{\mathrm{C1prec}} = \frac{m_{\mathrm{C1prec}}}{1 - X} \tag{8}$$

The kinetics of the transformation of C1prec is expressed by

$$\frac{\mathrm{d}m_{\mathrm{C1prec}}}{\mathrm{d}t} = - k_{\mathrm{C1prec}} C_{\mathrm{C1prec}} \tag{9}$$

The model defines that the total amounts of the catalysts and the catalyst precursor is unity at the beginning of gasification.

$$\sum_{n=1} m_{\mathrm{C}n,0} + m_{\mathrm{C1prec},0} = 1 \tag{10}$$

The rate of catalytic gasification at $t = 0$ is defined as ICA-1

$$\text{ICA-1} = \sum_{n=1} k_{\mathrm{C}n,0} = \sum_{n=1} k_{\mathrm{C}n} m_{\mathrm{C}n,0} \tag{11}$$

ICA-1 represents the initial catalytic activity. When the catalyst precursor, C1prec, is involved in the char, it is also reasonable to define an initial and potential catalytic activity, considering C1prec. This type of the initial activity is presented by

$$\text{ICA-2} = k_C m_{\text{C1prec},0} + \sum_{n=1} k_{Cn,0} = k_C \left(m_{\text{C1prec},0} + \sum_{n=1} m_{Cn,0} \right) = k_C \tag{12}$$

ICA-1 and ICA-2 are identical to each other in the absence of C1prec. ICA-2 would be a better measure in discussing the relationship between the catalytic activity and the composition of metallic species in the char. In a way similar to this, the initial and overall rate of catalyst deactivation can be defined as ICD.

$$\text{ICD-1} = \sum_{n=1} k_{\text{loss-}n} C_{Cn,0} \tag{13}$$

$$\text{ICD-2} = k_{\text{loss-1}} \left(C_{Cn,0} + C_{\text{C1prec},0} \right) + \sum_{n=2} k_{\text{loss-}n} C_{Cn,0} \tag{14}$$

2.4 Results and discussion

2.4.1 Char yield and composition of metallic species.

Figure 2.2 shows the char yields from the original SCBs, WW-SCBs and AW-SCBs. The decreases in the char yield by water washing and acid washing are not significant but systematic. This trend is in broad agreement with previous reports. [6,22,29]

2.4.2 Determination of non-catalytic reactivity of char.

Figure 2.3 shows change in the unconverted fraction of char, 1–*X*, with *t* for the chars from AW-SCBs. The gasification of GB-AW, KR-AW, MK-AW and PJ-AW chars obeys first-order kinetics with respected to 1–*X* over the ranges of *X* up to 0.98 or 0.99. It is also seen that the specific rate, (d*X*/d*t*)/(1–*X*) = r_{sp}, seems to increase at higher *X*. This is explained by either or both of the following mechanisms.

2.4.2.1 Mechanism I

The acid-washing removed a major portion of the metallic species from SCB while leaving a minor portion in the AW-SCB and then in the resulting char (see **Appendix 2**). The metallic species left in the char had no significant catalysis until its concentration became high enough in the late stage of gasification. In the absence of catalysis, the char underwent the CO_2 gasification obeying first-order kinetics. It was believed that the specific surface area of char,

though not measured in the present study, increased along with its conversion. [6,21,29] The r_{sp} was, nonetheless, steady until X reached 0.98–0.99. This suggested that the specific surface was not a factor determining the rate of gasification of the chars from the acid-washed SCB (the same references as above). In the gasification of the chars from KB-AW and SR-AW, 1–X decreases in a linear manner with t but within a limited range of X up to ca. 0.93. This is probably due to that more effective amounts of catalytic species being left in KB-AW and SR-AW than those for the other AW-SCBs, and therefore the catalysis appeared earlier.

2.4.2.2 Mechanism II

The present authors have been studying CO_2 gasification of chars from synthetic polymers that contain no metallic species and those from demineralized coals and lignites, the latter of which were prepared by repeated washing with aqueous solutions of HF and HCl. It has been confirmed a remarkable increase in r_{sp} of chars at $X > 0.8$–0.9. For example, 1–X vs t profiles for demineralized lignites were very similar to those shown in **Figure 2.3**. The increase in r_{sp} in the late-stage gasification was not necessarily attributed to the catalysis of metallic species remaining in AW-SCBs. Structural changes of the char causing such rapid increase in r_{sp} in the late stage gasification is not clear at present. Some results are shown in **Appendix 1**, but details will be reported in the future**.**

On the basis of the results shown in **Figure 2.3**, the non-catalytic (intrinsic) reactivity of the char from each SCB was represented by the following kinetics. The rate constant (k_{nc}) was determined from the slope of the broken line drawn in **Figure 2.3**.

$$\frac{dX}{dt} = k_{nc}\left(1 - X\right) \tag{15}$$

The kinetic analysis for the chars from the original SCBs and WW-SCBs were performed by assuming that the non-catalytic gasification obeyed the above first-order kinetics over the entire range of X. The validity of this assumption is discussed in detail in **Appendix 4**.

Table 2.2 lists k_{nc} values for the individual AW-SCB chars. k_{nc} values are within a range of 4.5×10^{-3} to 6.4×10^{-3} min^{-1}. The maximum k_{nc} to minimum ratio was as small as 1.4. There was not a significant but certain variety of the intrinsic reactivity.

2.4.3 Kinetic analysis of gasification of char from original SCBs and WW-SCB.

Figure 2.4 presents the measured changes with t of 1–X for the gasification of the chars from the original SCBs and WW-SCBs and compares those with the calculation by the kinetic model with optimized kinetic parameters. It is seen that the model describes the kinetics of

gasification quantitatively over the range of X up to 0.999. The assumption of progress in parallel of the non-catalytic gasification and catalytic gasification with multi-catalytic components was thus applied successfully to the kinetic analysis. **Figure 2.5** compares the measured and calculated changes in dX/dt with X. For all of the chars from the original SCBs, dX/dt changes through a maximum, and this is due to a maximum of the rate of catalytic gasification and recognized by the model that the transformation of the catalyst precursor (C1prec) into the C1 catalyst. Details will be discussed later.

Table 2.3 summarizes the optimized kinetic parameters. For the entire-range description of the char conversion kinetics, assumption of three catalytic components (C1–C3) was sufficient for the five chars from the original SCBs and two chars from WW-SCB, while four components (C1–C4) were necessary for the other chars. It was also found for every char from the original SCBs that an assumption of the C1 catalyst precursor was necessary. On the other hand, such an assumption was not needed for the chars from WW-SCBs, except KR-WW. This difference is indicative of that the catalyst precursor was largely contributed by the water-soluble metallic species. This will be discussed in detail later.

As shown in **Figure 2.6**, the kinetic contributions of the individual components are reasonably evaluated by $C_{Cn,0}$ and also $C_{C1prec,0}$. $C_{C1,0}$ and $C_{C1prec,0}$ account for 77–91% and 62–87% of ICA-2 for the chars from the original SCBs and WW-SCBs, respectively. In addition to this, $C_{C1,0}$, $C_{C1prec,0}$ and $C_{C2,0}$ hold 96–99% or even more. Thus, the two components, C1 and C2, were responsible for the major part of the catalytic gasification. However, as shown in **Figure 2.7,** in the late stage gasification where the catalysis of C1 and C2 as well as C1prec have diminished, C3 or C3/C4 play essential roles toward completion of char conversion. Their initial activities are insignificant, compared with those of C1 and C2, but deactivation is very slow. C3 or C3/C4 then survives in the very late stage of gasification. Great contribution of the catalytic gasification to the overall rate of gasification is clearly shown in **Figure 2.8**. The fractional rate of catalytic gasification to the total rate, i.e., dX/dt, fairly depends on the type of char at lower X, but it is more than 95% at $X > 0.9$ regardless of the char type. The catalytic gasification thus became more important along the progress of gasification, regardless of deactivation.

2.4.4 Understanding of variety of ICA-2 by composition of metallic species.

ICA-2 has a meaning of potential of catalytic activity, in other words, the total amount of metallic species that have catalysis. It was therefore believed that ICA-2 was explained by

the effective concentration of catalytic species, i.e., Na, K, Ca, Mg and/or Fe, and then presented as a function of the composition of such metallic species. ICA-2 for every char was correlated with the following metallic species concentrations in the char: Na, K, Ca, Mg, Fe, or sum of one or more species. Hereafter, the concentration of the metallic species is defined at $t = 0$ and denoted by $C_{M,0}$ (M: Na, K, Ca, Mg and/or Fe) in the unit of mol/kg-dry-char.

Under the assumption that ICA-2 is a function of the concentration of one or more metallic species in the char at $t = 0$ [i.e., ICA-2 = $F(C_{M,0})$], many functions were examined with a criterion of linearity between ICA-2 and $F(C_{M,0})$. In the first step (Step 1.1), the relationship of ICA-2 was examined with $C_{M,0}$ (M = Na, K, Ca, Mg or Fe), ($C_{Na,0}$+ $C_{K,0}$+ $C_{Ca,0}$), ($C_{Na,0}$+ $C_{K,0}$+ $C_{Ca,0}$+ $C_{Mg,0}$), ($C_{Na,0}$+ $C_{K,0}$+ $C_{Ca,0}$+ $C_{Fe,0}$) and ($C_{Na,0}$+ $C_{K,0}$+ $C_{Ca,0}$+ $C_{Mg,0}$+ $C_{Fe,0}$). As shown in **Table 2.4**, the correlation factors (r^2) with $C_{M,0}$ values for M = Na, Fe, Ca, Mg or Fe were clearly lower than the other concentrations and therefore eliminated without further consideration. For the other concentrations, it was found that their correlations with ICA-2 were improved by modifying ICA-2 into ICA-2/k_{nc} (Step 1.2). This ratio was reasonable if the rate of catalytic gasification was influenced by the intrinsic reactivity of char as well as the catalyst activity.

It is well known that alkali and alkaline earth metallic species react with SiO_2 and also Al_2O_3 during the pyrolysis, thereby losing catalysis [32]. In Step 2.1, the five candidates were modified by multiplying $C_{M,0}$ by ($C_{M,0}$/$C_{Si,0}$) on the basis of that abundance of SiO_2 caused loss of the effective concentration of catalytic species. As a result, the correlations with the two candidates; ($C_{Na,0}$+ $C_{K,0}$+ $C_{Ca,0}$+ $C_{Fe,0}$) and ($C_{Na,0}$+ $C_{K,0}$+ $C_{Ca,0}$+ $C_{Mg,0}$+ $C_{Fe,0}$) were further improved. Step 2.2 employed {$C_{M,0}$/($C_{Si,0}$+ $C_{Ai,0}$)} instead of ($C_{M,0}$/ $C_{Si,0}$), but r^2 remained unchanged.

Further improvement of the correlation factor was aimed by considering that the fractions of active species and inactive (or deactivated) one depended on the metallic species, in other words, different metallic species had different fractions of active species. In Step 3.1, an effective concentration, $C'_{M,0}$, was introduced, expecting a linear relationship as presented by Equation 16.

$C'_{M,0} = a_1C_{Na,0} + a_2C_{K,0} + a_3C_{Ca,0} + a_4C_{Mg,0} + a_5C_{Fe,0}$ [conditions: $a_1 = a_2$, $a_3 = 1$ (fixed)]

$$\frac{\text{ICA-2}}{k_{nc}} = a\left(\frac{C'_{M,0}}{C_{Si,0}}\right) + pC'_{M,0} \qquad (16)$$

The constant of the above equation, p, was introduced so that ICA-2/k_{nc} was proportional to $F(C'_{M,0})$. The coefficients were optimized on a Microsoft Excel™ with a Solver™. In the

optimization, various sets of the initial values for a_1–a_5 were applied for confirming the uniqueness of the optimized set. As expected, the correlation factor was improved to 0.981 with $a_1 = a_2 = 0.60$, $a_3 = 1$ (*fixed*); $a_4 = 0$, $a_5 = 0.96$, and $p = 0.050$. It is noted that the coefficients a_1 and a_2 (for Na/K) were smaller than a_3 (Ca) and also a_5 (Fe). This is reasonable because Na and K are more reactive with SiO_2 than Ca and Fe from a thermodynamic point of view. At temperature up to that for the gasification, reactions of Na and K with SiO_2 have lower Gibbs free energies than those of Ca. Reactions of Fe with SiO_2 is unlikely to occur under the present experimental conditions, considering the positive Gibbs free energies, as shown in **Appendix 10**. Mobility of Na and K in the char matrix higher than Ca and Fe is favored in the sense of kinetics. It is also noted that a_4 was optimized at zero. This is a very interesting indication of no or little catalysis of Mg under the present conditions for the pyrolysis and gasification. It was suspected in previous studies [15,33] that the catalytic effect of Mg in biomass char was, if any, very low compared with K, Na, Ca and Fe.

In Step 3.2, optimization of the individual coefficients (a_1, a_2, a_4 and a_5) was done while a_3 was fixed at 1 in the same manner as in Step 3.1. As shown in the table, the correlation factor was slightly but further improved. The optimized coefficients and constant were $a_1 = 0.48$; $a_2 = 0.62$; $a_4 = 0$; $a_5 = 0.95$ and $p = 0.050$, respectively. The result from Step 3.2 is very similar to that from 3.1 in terms of $a_1 \approx a_2 < a_3 \approx a_5$ and $a_4 \approx 0$. The results of correlation in Step 1.1 to 3.2 are summarized in **Figure 2.9** for M = Na+K+Ca+Fe.

2.4.5 Discussion on catalyst precursor.

$k'_C \cdot C_{C1prec}$ represents the abundance of the C1 catalyst precursor (C1prec). It is plotted against ($C_{Na,0} + C_{K,0} + C_{Ca,0}$) at $t = 0$ in **Figure 2.10(a)**. $k'_C \cdot C_{C1prec}$ seems to be correlated relatively well with $C_{M,0}$ (M = Na+K+Ca or Na+K+Ca+Fe). This is consistent with disappearance of C1prec by the water washing that removed Na, K and Ca substantially (see **Figure 2.11**). The C1prec concentration seems to be zero for the chars from WW-SCBs or very low (KR-WW). This demonstrates that the water-soluble Na, K and/or Ca were responsible for C1prec. On the other hand, for the chars from the original SCBs, $C_{Na,0}+C_{K,0}+C_{Ca,0}$ seems to be above a threshold concentration around 0.15 mol/kg of char. $k'_C \cdot C_{C1prec}$ seems to increase with {($C_{Na,0}+C_{K,0}+C_{Ca,0}$) – *ca.* 0.15}. This trend was further analyzed by considering the concentration of the water-insoluble Na, K and Ca. As shown in **Figure 2.10(b)**, $k'_C \cdot C_{C1prec}$ is roughly correlated in a linear manner with the total concentration of the water-soluble Na, K and Ca, which are denoted by $C_{Na\text{-}ws,0}$, $C_{K\text{-}ws,0}$, $C_{Ca\text{-}ws,0}$, respectively.

A most general mechanism of the catalyst transformation is precipitation of nanosized particles of metallic species from those "dissolved" in the carbonaceous matrix of char. The precipitation is normally induced by supersaturation, and driven by its degree. Once the precipitation starts, the degree decreases and becomes steady (at a level slightly higher than that of saturation) while the precipitation continues. It was believed that the chemical properties (including the holding capacity of precursor) of the chars from the SCBs were similar or very similar to one another. If the precursors had been saturated or supersaturated at the beginning of gasification, $k'_{C} \cdot C_{C1prec}$ could be independent on $\sum C_{M,0}$ or dependent much less than that seen in **Figure 2.11**. It was thus suggested that the precursor in the SCB chars had not been either saturated or supersaturated yet at the beginning of the gasification. Kim *et al.*. [21] investigated kinetics of steam gasification of Ca-loaded lignite chars with a variety of Ca concentrations (1.0–13.2 wt% char). Results of their kinetic analysis revealed that the concentration of highly dispersed Ca was saturated and therefore steady over a range of 2.0–13.2 wt%-char. The $C_{Ca,0}$ of the chars from the original SCBs was 0.21–0.52 wt%, which was not so high as to cause supersaturation or saturation of Ca. Wu *et al.*.[30] investigated variation in the catalytic activity of Na (derived from extraneous NaCl) with its concentration for the gasification of lignite char and demonstrated that the activity of the Na catalyst occurred when its concentration became higher than a critical one. Yang *et al.*. [31] reported on K-catalyzed gasification of lignite char and investigated variation in the catalytic activity of K based on dX/dt with its concentration in the gasifying char. It was then strongly suggested that the catalytic activity occurred at a certain critical concentration of K. The kinetic data shown in **Figure 2.10** are thus strongly supported by the above-described knowledge.

A possible explanation of the trends shown in **Figure 2.10** is that the water-soluble Na, K, and/or Ca were different from the water-insoluble ones. The water-insoluble species in the WW-SCB had already transformed into catalysts, or otherwise, experienced deactivation (probably and mainly due to reactions with SiO_2). On the other hand, substantial portions of the water-soluble species were highly dispersed in the carbonaceous matrix of the char until the commencement of gasification. Thus, $k'_{C1}C_{C1prec}$ was determined by the concentration of Na, K and/or Ca species that had been arisen from the water-soluble species. If the water-soluble and water-insoluble species were undistinguishable from each other (in other words, if the Na, K and Ca concentration were simply a factor determining $k'_{C} \cdot C_{C1prec}$), there would be no "threshold" that is seen in **Figure 2.10(a)**. Rather, even saturation of $k'_{C} \cdot C_{C1prec}$ could occur at a certain $C_{Na,0}+C_{K,0}+C_{Ca,0}$. However, it was not the case.

The kinetics of the C1prec transformation into C1 catalyst is discussed briefly. The gasification takes place, eliminating carbon as the support or matrix of metallic species, thereby increasing their concentration. It was hence expected that the rate of transformation was closely related with that of the gasification. In **Figure 2.12,** k'_{C1prec} is plotted against $\mathrm{d}X/\mathrm{d}t$ at $t = 0$. As expected, k'_{C1prec} increases as the $\mathrm{d}X/\mathrm{d}t$ does. It is reasonably said that the C1 precursor transformation occurred being driven by the loss of the carbonaceous matrix that caused saturation and then precipitation of the precursor.

2.4.6 Kinetic and mechanism of catalyst deactivation.

Understanding the kinetics of catalyst deactivation is essential to that of its mechanism and then the catalytic gasification, but efforts were made on quantification of the kinetics in few of the previous studies. [9,34] **Figure 2.13** shows the relationship of either the initial rates of catalyst deactivation, ICD-1 or ICD-2 with four different parameters from the composition of metallic species or initial catalytic activity. **Figure 2.13(a)** shows that ICD-2, the potential rate of catalyst deactivation, as a function of the total concentration of Na, K, Ca and Fe, expecting a correlation between ICD-2 and the initial catalytic activity. The correlation seems to be good for the chars from the original SCBs but not for those from WW-SCB. **Figure 2.13(b)** plots ICD-2 with $C_{\mathrm{Si},0}/\sum C_{\mathrm{M},0}$. This figure was prepared to examine the importance of reactions between SiO_2 and catalytic species (silicate formation) for the catalyst deactivation. However, a very poor correlation indicates that the silicate formation provided no important pathways to the deactivation during the gasification. This is supported by the Gibbs free energies for conversion of Na, K and Ca species into carbonates in the presence of CO_2, which are as negative as or even more negative than those for the silicate formation. This trend is graphically shown in **Appendix 10**. The carbonates of Na, K and Ca have no catalysis, but their formation from oxides (reaction R1, forward) and decomposition into the oxides (reaction R1, backward) effectively avoided silicate formation, helping well-known oxide-metal cycles (see reactions R2 and R3) that were essential for the catalytic gasification.

$M_2O + CO_2 \leftrightarrow M_2CO_3$ or $MO + CO_2 \leftrightarrow MCO_3$ (R1)

$M_2O + C \rightarrow CO + 2M$ or $MO + C \rightarrow CO + M$ (R2)

$2M + CO_2 \rightarrow M_2O + CO$ or $M + CO_2 \rightarrow MO + CO$ (R3)

On the other hand, neither silicate nor carbonate formation from Fe species is thermodynamically favored. This supports unimportance of the silicate formation for the Fe catalyst deactivation.

Figure 2.13(c) examines the relationship between the overall rate of catalyst deactivation and that of gasification at the beginning of gasification. These are correlated linearly and well for the chars from the original SCBs. This suggests a special relationship between the rates of catalyst deactivation and gasification (i.e., loss of carbonaceous matrix). However, such a good linear correlation cannot be applied to the chars from WW-SCBs, in which the catalyst seemed to undergo deactivation more rapidly than in those from the original SCBs. **Figure 2.13(d)** employs ICD-2 and ICA-2/k_{nc}, both of which consider the C1prec. It is seen that ICD-2 for the chars from the original SCBs is proportional to their ICA-2 with a correlation factor as high as 0.993. On the other hand, the ICD-2 *vs* ICA-2/k_{nc} relationship for the chars from WW-SCB is clearly different from that for those from the original SCBs. The present authors [20–22,26] previously studied steam or CO_2 gasification of chars from lignites and reported linear or semi-linear relationship between the activity of the catalyst and rate (or rate constant) of its loss.

An important mechanism of the catalyst deactivation was suggested from the correlations in panels c and d of **Figures 2.13**. The deactivation was induced by the loss of the carbonaceous matrix by the gasification. The loss caused coarsening of the catalyst particles, unless the catalyst is highly mobile in the matrix. The gasification was, as mentioned previously, contributed mainly by the catalytic one in terms of the rate. In other words, more active catalyst brought about more rapid loss of carbon, inducing faster deactivation.

2.4.7 Detailed discussion on the mechanism of the catalyst deactivation.

The very good linear correlation of ICD-2 with ICA-2/k_{nc} for the chars from the original SCBs encouraged the present authors to consider this more in detail. The linearity, $\text{ICD-2} \mu \frac{\text{ICA-2}}{k_{nc}}$, is expressed by

$$k_{\text{loss-1}}\left(C_{\text{C1prec}}+C_{\text{C1,0}}\right)+k_{\text{loss-2}}C_{\text{C2,0}}+k_{\text{loss-3}}C_{\text{C3,0}}+\cdots \propto \frac{k_{\text{C}}^{'}\left(C_{\text{C1prec}}+C_{\text{C1,0}}\right)+k_{\text{C}}^{'}C_{\text{C2,0}}+k_{\text{C}}^{'}C_{\text{C3,0}}+\cdots}{k_{nc}}$$

$$=\frac{k_{\text{C}}^{'}\left(C_{\text{C1prec}}+C_{\text{C1,0}}+C_{\text{C2,0}}+C_{\text{C3,0}}+\cdots\right)}{k_{nc}}=\frac{k_{\text{C}}^{'}}{k_{nc}}=\frac{\text{ICA-2}}{k_{nc}}$$

The above equation draws most reasonable and unique relationships, i.e.,

$$k_{\text{loss-1}} \propto \frac{\text{ICA-2}}{k_{nc}}, \quad k_{\text{loss-2}} \propto \frac{\text{ICA-2}}{k_{nc}}, \quad k_{\text{loss-3}} \propto \frac{\text{ICA-2}}{k_{nc}}, \cdots \tag{17}$$

Figure 2.14 shows the relationship between $k_{\text{loss-}n}$ and ICA-2/k_{nc} for the chars from the original SCBs. As mentioned previously, C1 and C2 catalysts accounted for 97–99% of the total catalytic activity. It is seen that $k_{\text{loss-1}}$ and $k_{\text{loss-2}}$ are both correlated in linear manners with ICA-2/k_{nc}. Though not shown, the same trend was confirmed for n = 3. (see **Appendix 7**). Thus, the linear relationship between the rapidity of catalyst loss and catalyst activity was valid not only overall but also for the individual catalytic components.

2.4.8 Consideration of difference in ICD-2 *vs* ICA-2/k_{nc} relationship between chars from original SCBs and WW-SCBs.

For the chars from the original SCBs, ICA-2/k_{nc} and ICD-2 were correlated linearly and very well with each other, but this correlation could not be applied to those from WW-SCBs, except SR-WW. It was believed that such difference arose from that in the composition of the catalytic species.

A numerical analysis was performed on relative molar abundances of metallic species, which were represented by $C_{\text{Na,0}}$ $C_{\text{K,0}}$, $C_{\text{Ca,0}}$ and $C_{\text{Fe,0}}$. By trial and error, it was found that the $(C_{\text{Ca,0}}+C_{\text{Fe,0}})/(C_{\text{Na,0}}+C_{\text{K,0}})$ ratios for the chars from WW-SCBs (except SR-WW) were lower than any of those for the chars from the original SCBs. A threshold was thus found for distinguishing the chars from WW-SCBs from those from the original SCBs. **Figure 2.15** displays $(C_{\text{Na,0}}+C_{\text{K,0}})/(C_{\text{Ca,0}}+C_{\text{Fe,0}})$ ratios for the chars. The ratios for the WW-SCBs chars (except SR-WW) are lower than 0.95 while over 1.1 for those from the original SCBs and SR-WW. Such lower ratios occurred mainly as a result of the removal of Na and K by the water washing.

The five chars from WW-SCBs, i.e., GB-WW, KB-WW, KR-WW, MK-WW and PJ-WW, are here categorized into Group B while the others into Group A. For Group B chars, ICA-2/k_{nc} was modified to ICA-2/k_{nc}·B.

$$B = \frac{b_{\text{Na,B}}C_{\text{Na,0}}+b_{\text{K,B}}C_{\text{K,0}}+b_{\text{Ca,B}}C_{Ca,0}+b_{\text{Fe,B}}C_{Fe,0}}{C_{\text{Na,0}}+C_{\text{K,0}}+C_{\text{Ca,0}}+C_{\text{Fe,0}}}$$

On the other hand, for Group A chars, the coefficient B was fixed at 1, i.e., so that the high linearity (shown in **Figure 2.13(d)**) was maintained.

$b_{\text{Na,A}} = b_{\text{Na,A}} = b_{\text{Ca,A}} = b_{\text{Fe,A}} = 1$, i.e., $B = 1$

The coefficients, $b_{\text{M,B}}$'s, for Group B chars were assumed as follows.

Case I: $b_{\text{Na,B}} = b_{\text{K,B}} = b_{\text{Ca,B}} = 1\ (fixed),\ f_{\text{Fe,B}} \neq 1$

Case II: $b_{\text{Na,B}} = b_{\text{K,B}} = b_{\text{Ca,B}} \neq 1,\ b_{\text{Fe,B}} \neq 1$

Case III: $b_{\mathrm{Na,B}} = b_{\mathrm{K,B}} \neq 1, b_{\mathrm{Ca,B}} \neq 1,\ b_{\mathrm{Fe,B}} \neq 1$

Unless a coefficient was assumed to be 1, it was optimized, so that the linearity between ICD-2 and ICA-2/k_{nc} was maximized in terms of the correlation factor, r^2. The optimization was done on a Microsoft Excel™ with Solver™. The coefficients were then optimized as

Case I: $b_{\mathrm{Na,B}} = b_{\mathrm{Na,B}} = b_{\mathrm{Ca},B} = 1,\ b_{\mathrm{Fe,B}} = 5.1$

Case II: $b_{\mathrm{Na,B}} = b_{\mathrm{K,B}} = b_{\mathrm{Ca,B}} = 0.17,\ b_{\mathrm{Fe,B}} = 6.5$

Case III: $b_{\mathrm{Na,B}} = b_{\mathrm{K,B}} = 0.40, b_{\mathrm{Ca,B}} = 0,\ b_{\mathrm{Fe,B}} = 6.4$

Figure 2.16 plots ICD-2 against (ICA-2/k_{nc})·*B*. r^2 for cases I, II and III were 0.964, 0.982_6 and 0.983_1, respectively. The correlation factors optimized for cases II and III are better than those for case I. A common feature among the three cases is $b_{\mathrm{Fe,B}}$ much greater than 1. This strongly suggests either or both of the following: mechanism A, Fe catalysts of Group B chars are deactivated much more rapidly than those of group A chars; mechanism B, Fe catalysts greatly accelerate deactivation of others (i.e., Na, K, and/or Ca).

It is also noted for cases II and III that all of $b_{\mathrm{Na,B}}$, $b_{\mathrm{K,B}}$ and $b_{\mathrm{Ca,B}}$ are clearly smaller than unity. This feature suggests slower deactivation of Na, K and Ca catalysts of group B chars than those of Group A chars. With this suggestion taken into consideration, mechanism A is more reasonable than mechanism B.

2.4.9 Estimation of the mechanism of catalyst deactivation.

The result from the optimization of coefficients $b_{\mathrm{M,B}}$'s, which is summarized by $b_{\mathrm{Fe,B}}$ >>1 and $b_{\mathrm{Na,B}}$, $b_{\mathrm{K,B}}$ and $b_{\mathrm{Ca,B}}$ < 1 or << 1, leads to the following estimation of catalyst behaviors:

- During the gasification of Group A char, the Fe catalyst had more or less chemical interaction with other species (Na and K or, otherwise, these two and Ca). This chemical interaction decelerates the deactivation of the Fe catalyst, while accelerates that of Na, K and Ca catalysts.
- In the gasification of group B char, due to lack of Na/K catalysts, the Fe catalyst tended to play a catalytic role as a single catalyst, which underwent fast deactivation. Previous studies showed fast coarsening and deactivation of Fe catalysts within the gasifying char matrix. [35-37] On the other hand, Na/K catalysts behaved mainly as single catalysts that were deactivated slowly.

- Chemical interaction was also important between Ca and Na/K. Along the conversion of Group A chars, such an interaction promoted their deactivation to a more or less degree probably as a result of faster agglomeration and coarsening. On the other hand, the lack of Na and K resulted in slower deactivation of the Ca catalyst.

From the above estimations, the followings can be derived:

- Deactivation rate of Ca catalyst < that of Ca-Na/K mixed catalysts
- Deactivation rate of Na/K catalysts < that of Ca-Na/K mixed catalysts
- Deactivation rate of Fe catalyst >> that of Fe-Na/K mixed catalysts (or plus Fe/Ca mixed ones)
- Deactivation rate of Na/K catalysts < that of Fe-Na/K mixed catalysts

It was difficult to explain the difference in the ICD-2 versus ICA-2/k_{nc} relationship between group A and group B chars without the above assumptions. It was also believed that the loss of chemical interactions between or among different catalytic species was primarily due to removal of Na and K to significant extents (and Ca but less extensively), and secondarily selective removal of water-soluble Na, K and Ca that could easily interact with Fe in the gasifying Groups A char.

Regardless of the mechanisms proposed above, it is said that the Fe catalyst is an important catalytic species that influenced the catalytic gasification of the chars. It seems that the inherent Fe catalyst has been out of focus in the previous studies on the gasification of biomass chars. However, it is difficult to explain the experimental results and those of the kinetic modeling without considering importance of the Fe catalyst in the initial catalytic activity and kinetics of the catalysis loss. It is also necessary to know chemical interaction among the co-existing catalytic species for deeper and full understanding the kinetics of the catalytic gasification.

2.5 Conclusion

The following conclusions have been drawn from results of this study within the ranges of conditions employed for the six trios of SCBs.

1. The kinetic model, which assumes the progress of non-catalytic gasification and catalytic gasification in parallel, the presence of catalytic components with different activity and

deactivation characteristics, and that of a catalyst precursor, successfully describes time-dependent changes in the char conversion over its range up to 0.999.

2. The catalyst activity (in terms of the rate of catalytic gasification) and the rate of catalyst deactivation distribute over 3 and 5 orders of magnitudes.
3. The inherent catalysts are contributed by Na, K, Ca, and Fe but not by Mg. Their activities are lost partly by reactions with SiO_2 (or SiO_2 and Al_2O_3) during the pyrolysis, i.e., prior to gasification. However, this mechanism is not important during the gasification.
4. Water-soluble Na, K, and Ca are fully responsible for the catalyst precursor.
5. The catalyst deactivation occurs during the gasification following the self-deactivation mechanism. The rate of catalyst deactivation is correlated linearly and very well with the initial activity for the chars from the original SCBs. Such a correlation was, however, not the case of the chars from WW-SCBs. The removal of the water-soluble Na, K, and Ca accelerates the Fe catalyst deactivation but decelerates that of themselves.

Table 2.1. Elemental composition, ash contents, and those of AAEM species of chars from original SCBs.

District	ID	C	H	N	ash	Na	K	Mg	Ca	Fe	Al	Si
		wt%-daf			wt%-dry	mol/kg-char						
Gondang Baru	GB	76.7	1.96	0.61	3.68	0.071	0.21	0.057	0.13	0.059	0.1	1.9
Krebet Baru	KB	78.1	1.83	0.6	3.26	0.065	0.19	0.05	0.079	0.038	0.077	1.8
Kremboong	KR	78.2	1.74	0.57	2.57	0.061	0.17	0.059	0.086	0.026	0.069	1.8
Madukismo	MK	74.8	2.04	0.52	3.87	0.058	0.089	0.026	0.055	0.064	0.19	2
Panji	PJ	73.8	1.95	0.39	6.16	0.08	0.12	0.011	0.051	0.12	0.23	3.5
Sragi	SR	76.7	2.04	0.53	2.95	0.062	0.21	0.06	0.11	0.022	0.049	1.8

Table 2.2. k_{nc} for chars from AW-SCBs.

ID	$10^3 \cdot k_{nc}$, min^{-1}
GB-AW	5.5
KB-AW	5.4
KR-AW	6.1
MK-AW	6.4
PJ-AW	6.1
SR-AW	4.5

Table 2.3. Optimized kinetic parameters for catalytic gasification.

(a) Chars from the original SCBs

	ICA-2, min^{-1}	ICA-1, min^{-1}	$k_{C1,0}$, min^{-1}	$k_{C2,0}$, min^{-1}	$k_{C3,0}$, min^{-1}	$k_{C4,0}$, min^{-1}
MK	4.10E-02	3.49E-02	3.11E-02	3.49E-03	2.91E-04	
KR	4.90E-02	3.28E-02	2.69E-02	4.66E-03	1.32E-03	
KB	5.00E-02	2.90E-02	1.76E-02	1.02E-02	1.18E-03	
GB	8.20E-02	5.08E-02	4.11E-02	8.82E-03	7.95E-04	9.84E-05
PJ	3.80E-02	1.48E-02	6.75E-03	7.33E-03	7.41E-04	
SR	5.20E-02	2.42E-02	1.51E-02	8.22E-03	8.58E-04	

	k'_{C1prec}, min^{-1}	$C_{C1prec,0}$, -	$C_{C1,0}$, -	$C_{C2,0}$, -	$C_{C3,0}$, -	$C_{C4,0}$, -
MK	1.50E-01	1.50E-01	7.58E-01	8.50E-02	7.10E-03	
KR	1.00E-01	3.30E-01	5.48E-01	9.50E-02	2.69E-02	
KB	9.50E-02	4.20E-01	3.52E-01	2.05E-01	2.35E-02	
GB	2.00E-01	3.80E-01	5.02E-01	1.08E-01	9.70E-03	1.20E-03
PJ	3.80E-02	6.10E-01	1.78E-01	1.93E-01	1.95E-02	
SR	5.50E-02	5.35E-01	2.91E-01	1.58E-01	1.65E-02	

	ICD, min^{-1}	k_{loss-1}, min^{-1}	k_{loss-2}, min^{-1}	k_{loss-3}, min^{-1}	k_{loss-4}, min^{-1}
MK	1.34E-02	1.46E-02	1.25E-03	3.00E-05	
KR	1.57E-02	1.76E-02	2.20E-03	2.70E-04	
KB	1.97E-02	2.45E-02	4.02E-03	3.20E-04	
GB	3.13E-02	3.50E-02	3.95E-03	4.90E-04	2.00E-05
PJ	1.46E-02	1.78E-02	3.15E-03	1.50E-04	
SR	2.44E-02	2.90E-02	3.10E-03	1.47E-04	

(b) Chars from WW-SCBs

	ICA-2, min^{-1}	ICA-1, min^{-1}	$k_{C1,0}$, min^{-1}	$k_{C2,0}$, min^{-1}	$k_{C3,0}$, min^{-1}	$k_{C4,0}$, min^{-1}
MK-WW	2.75E-02	2.75E-02	2.17E-02	5.39E-03	3.85E-04	6.33E-05
KR-WW	2.00E-02	1.50E-02	1.11E-02	3.62E-03	2.16E-04	4.40E-05
KB-WW	1.45E-02	1.45E-02	1.14E-02	2.86E-03	2.10E-04	
GB-WW	1.93E-02	1.93E-02	1.24E-02	6.37E-03	5.02E-04	3.76E-05
PJ-WW	2.20E-02	2.20E-02	1.37E-02	7.48E-03	7.04E-04	1.33E-04
SR-WW	1.16E-02	1.16E-02	1.01E-02	1.42E-03	7.30E-05	

	k'_{C1prec}, min^{-1}	$C_{C1prec,0}$, -	$C_{C1,0}$, -	$C_{C2,0}$, -	$C_{C3,0}$, -	$C_{C4,0}$, -
MK-WW			7.88E-01	1.96E-01	1.40E-02	2.30E-03
KR-WW	8.00E-02	2.50E-01	5.56E-01	1.81E-01	1.08E-02	2.20E-03
KB-WW			7.89E-01	1.97E-01	1.45E-02	
GB-WW			6.42E-01	3.30E-01	2.60E-02	1.95E-03
PJ-WW			6.22E-01	3.40E-01	3.20E-02	6.05E-03
SR-WW			8.72E-01	1.22E-01	6.30E-03	

	ICD, min^{-1}	k_{loss-1}, min^{-1}	k_{loss-2}, min^{-1}	k_{loss-3}, min^{-1}	k_{loss-4}, min^{-1}
MK-WW	2.09E-02	2.57E-02	3.49E-03	2.68E-04	
KR-WW	1.12E-02	1.35E-02	1.80E-03	1.75E-04	
B-WW	6.90E-03	8.48E-03	1.08E-03	5.00E-05	
B-WW	1.52E-02	2.21E-02	3.04E-03	2.60E-04	1.20E-05
-WW	2.60E-02	3.85E-02	6.10E-03	5.40E-04	
-WW	3.74E-03	4.22E-03	5.30E-04	4.00E-06	

Table 2.4. Correlation factors (r^2) for functions ($y = ax + b$ or $y = ax$) employed in the process for numerical expression of initial catalytic activity.

Step ID	1.1	1.2	2.1	2.2
Parameter for catalytic activity (y)	ICA-2	(ICA2)/k_{nc}	(ICA-2)/k_{nc}	(ICA-2)/k_{nc}
Parameter for composition of metallic species (x)	$C_{M,0}$	$C_{M,0}$	$(C_{M,0})(C_{M,0}/C_{Si,0})$	$(C_{M,0})\{C_{M,0}/(C_{Si,0}+C_{Al,0})\}$
Fe	0.005	0.026	eliminated	eliminated
Na	0.396	0.358	eliminated	eliminated
Mg	0.685	0.759	eliminated	eliminated
Ca	0.634	0.715	eliminated	eliminated
K	0.806	0.866	0.855	0.848
Na+K+Ca	0.851	0.912	0.910	0.902
Na+K+Ca+Mg	0.841	0.906	0.892	0.885
Na+K+Ca+Fe	0.851	0.856	0.966	0.961
Na+K+Ca+Mg+Fe	0.872	0.891	0.950	0.944
Type of function for correlation	$y = ax + b$	$y = ax + b$	$y = ax + b$	$y = ax + b$

Step ID	3.1	3.2
Parameter for catalytic activity (y)	(ICA-2)/k_{nc}	(ICA-2)/k_{nc}
Parameter for composition of metallic species (x)	$(C'_{M,0})(C'_{M,0}/C_{Si,0} + p)$	$(C'_{M,0})(C'_{M,0}/C_{Si,0} + p)$
Fe	eliminated	eliminated
Na	eliminated	eliminated
Mg	eliminated	eliminated
Ca	eliminated	eliminated
K	eliminated	eliminated
Na+K+Ca	eliminated	eliminated
Na+K+Ca+Mg	eliminated	eliminated
Na+K+Ca+Fe	0.9808	0.9811
Na+K+Ca+Mg+Fe	0.9808	0.9811
Type of function for correlation	y = ax	y = ax

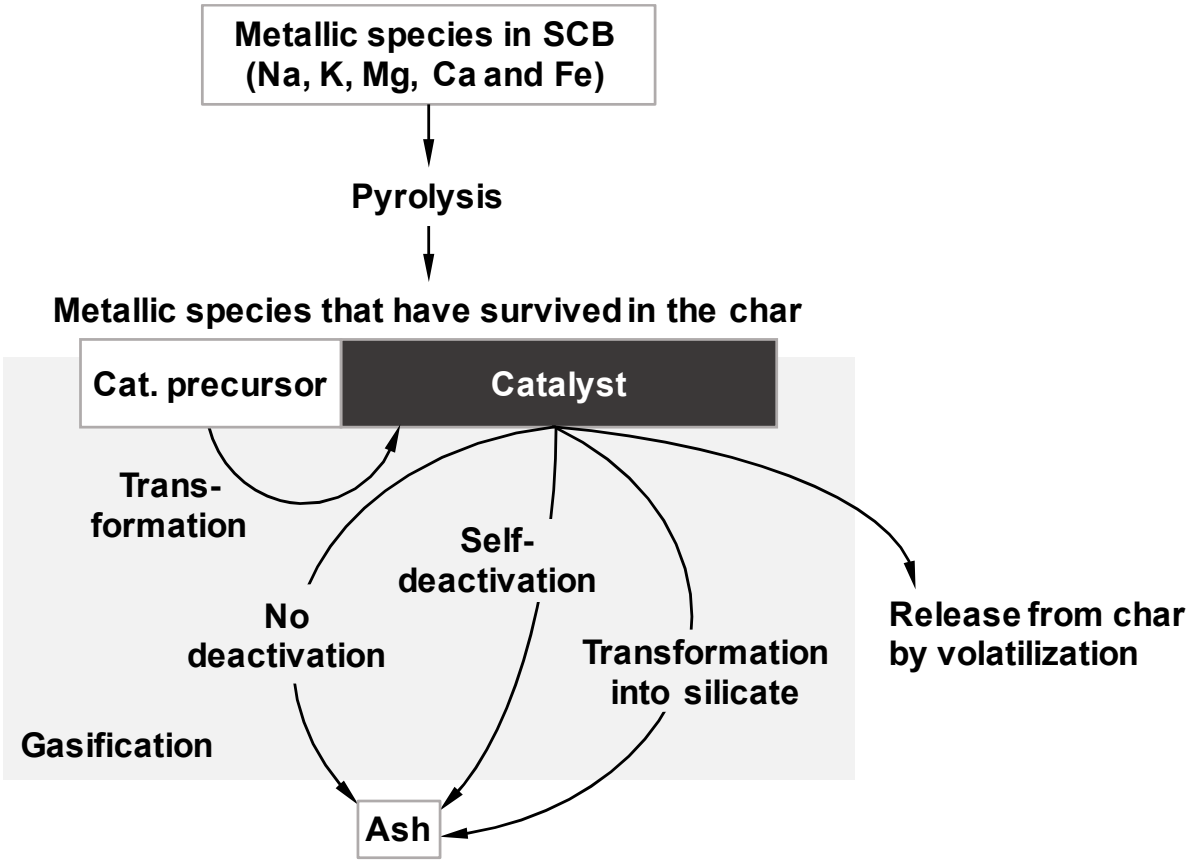

Figure 2.1. Pathways of catalyst formation from inherent metallic species and deactivation.

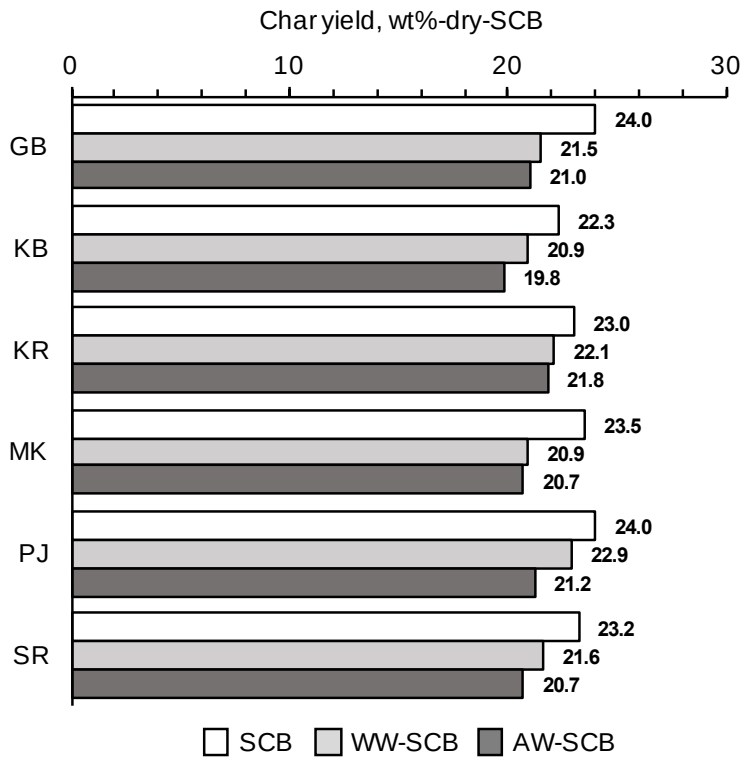

Figure 2.2. Char yields from original SCBs, WW-SCBs and AW-SCBs.

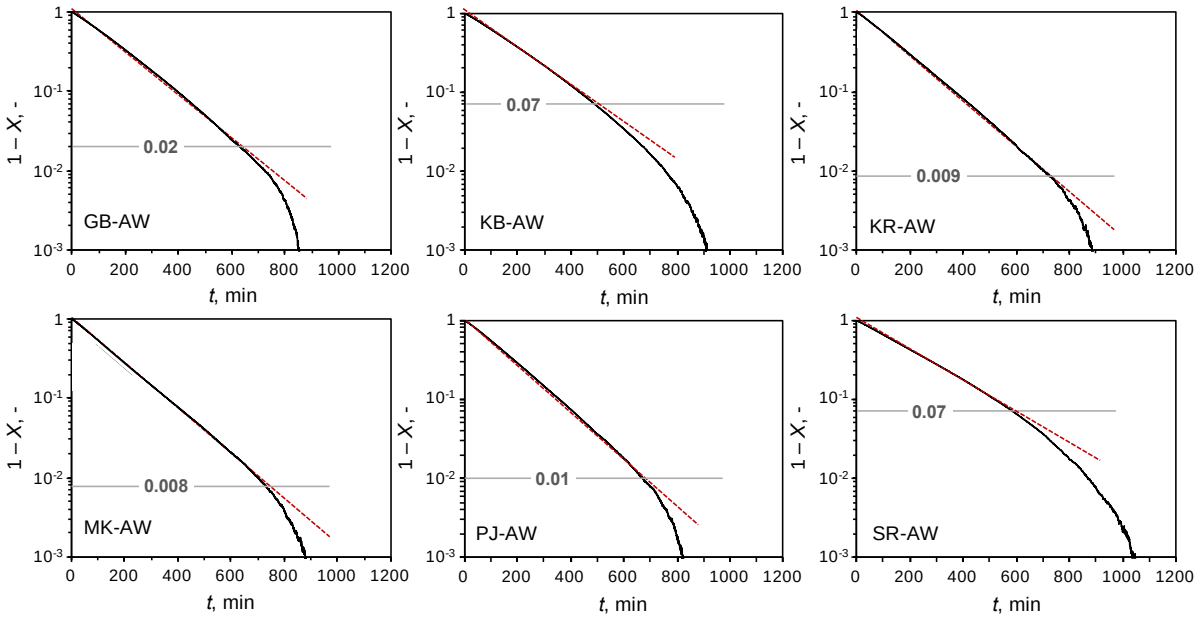

Figure 2.3. 1–*X* vs *t* profiles for gasification of chars from AW-SCBs. Each red-colored broken line is drawn for showing decrease in 1–*X* in a linear manner with *t*, which are indicative of first-order kinetics with respect to 1–*X*.

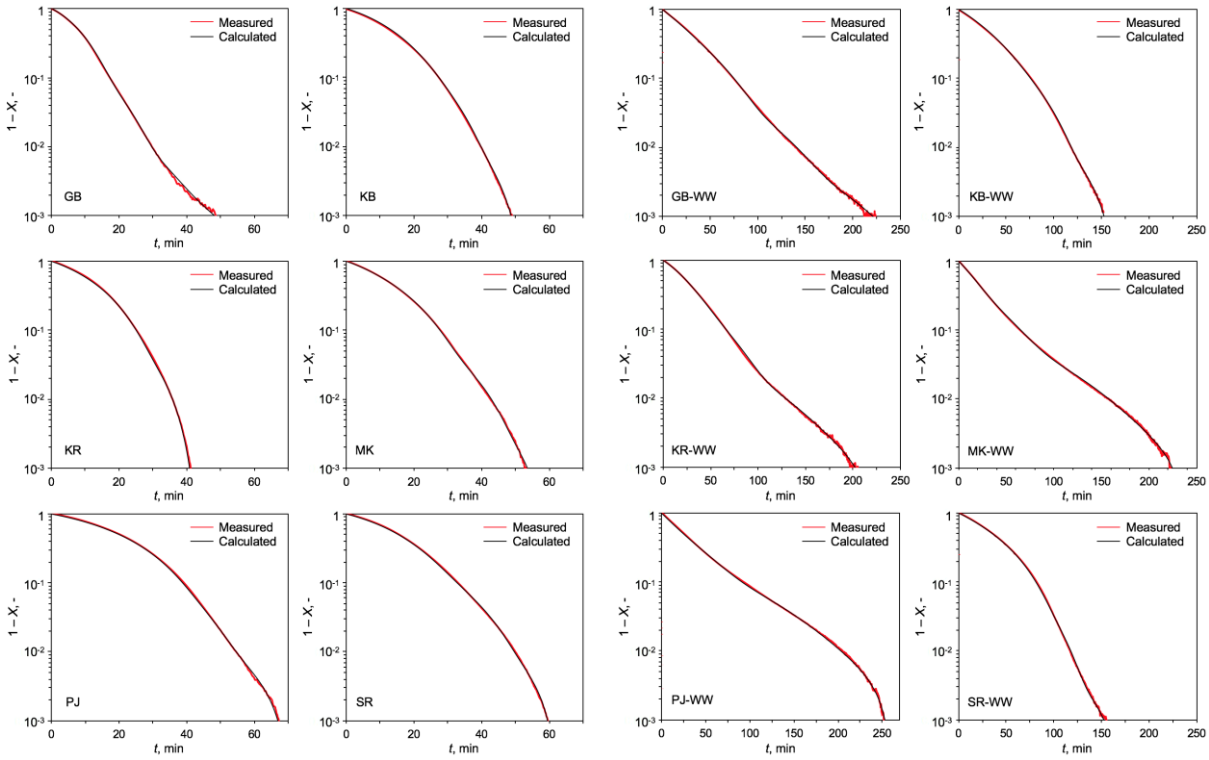

Figure 2.4. Measured and calculated 1–*X* vs *t* profiles for the gasification of chars from the original SCBs and those from WW-SCBs.

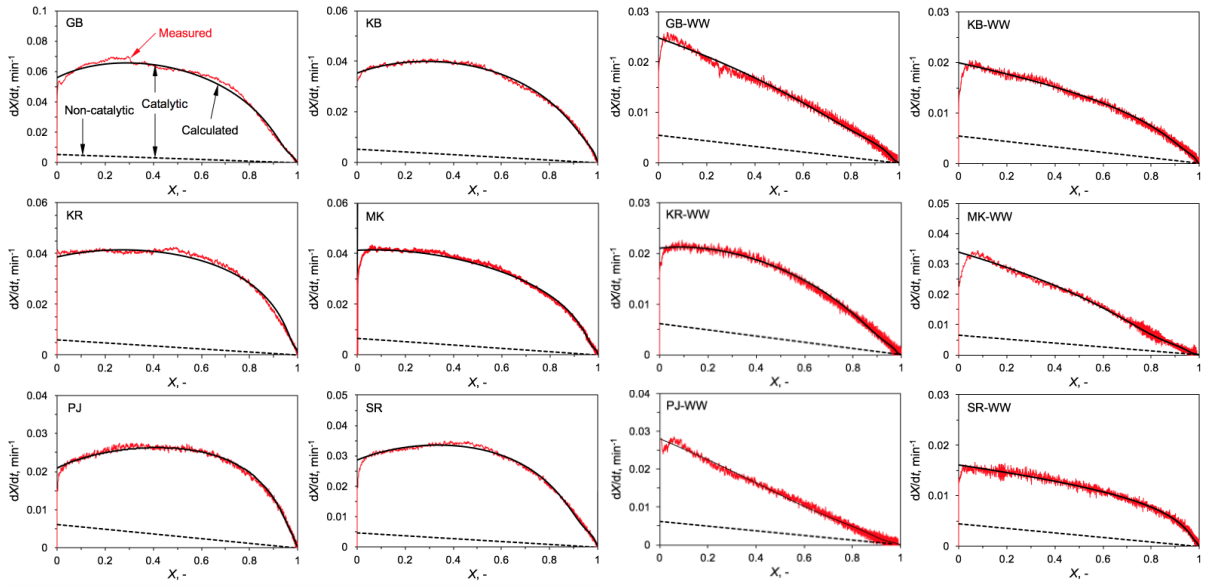

Figure 2.5. Measured and calculated changes in d*X*/d*t* with *X* for the gasification of chars from the original SCBs and those from WW-SCBs.

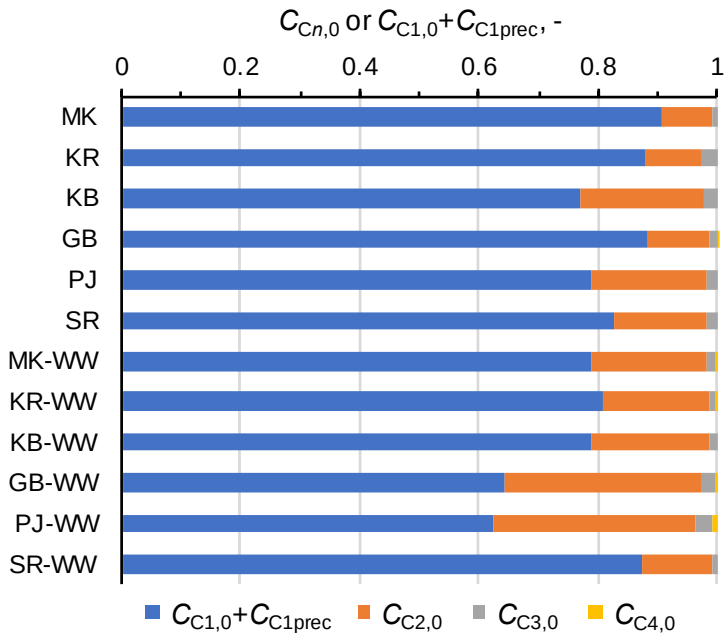

Figure 2.6. Catalyst composition given from the optimized kinetic parameters.

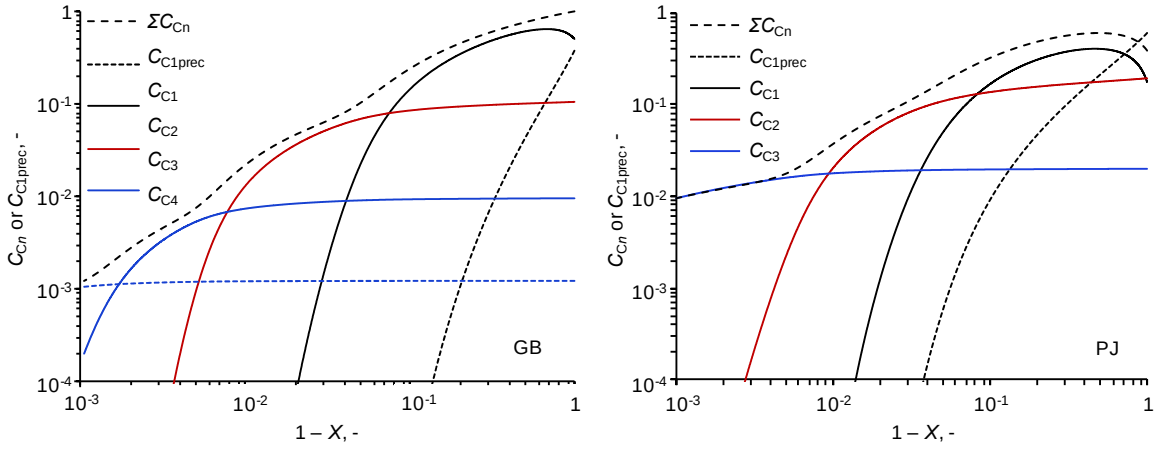

Figure 2.7. Examples of change in the catalyst concentration as a function of 1–*X* (GB and PJ chars) presented by the model with optimized kinetic parameters.

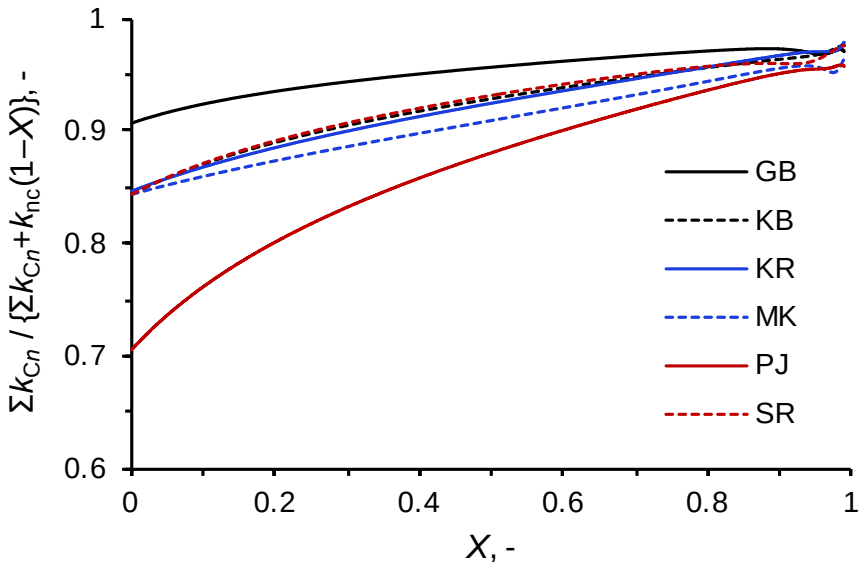

Figure 2.8. Contribution of catalytic gasification to the overall rate of gasification (dX/dt) as a function of X for the chars from the original SCBs. The meaning of the vertical axis is (rate of catalytic gasification)/(overall rate of gasification).

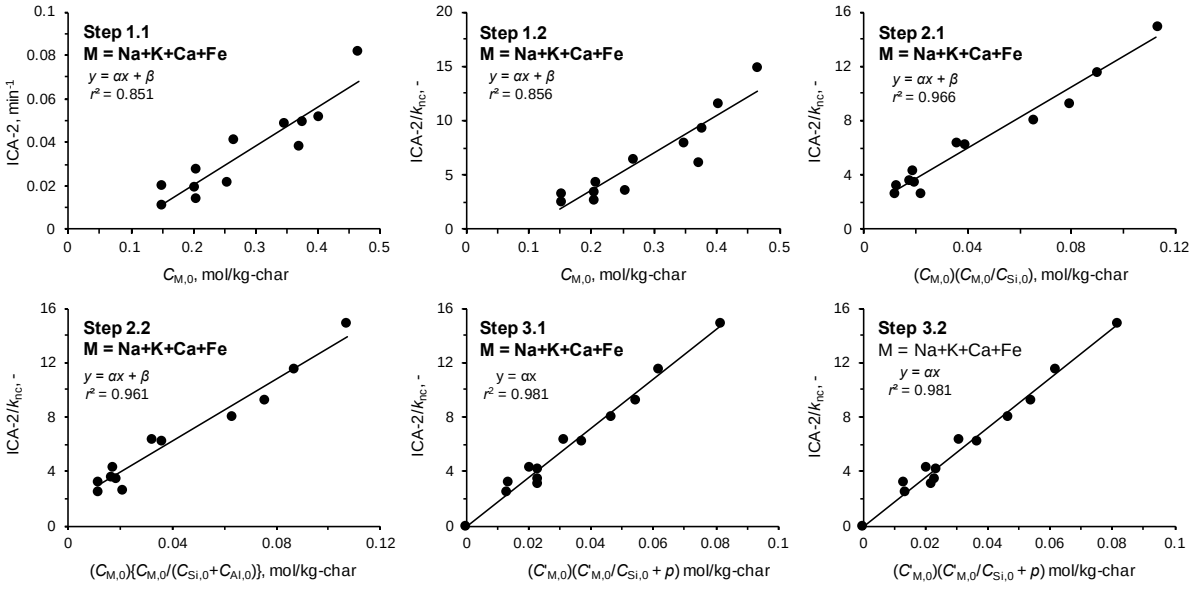

Figure 2.9. Correlation of ICA-2 or ICA-2/k_{nc} with total concentration of Na, K, Ca and Mg (Step 1.1–2.2) or effective concentration (Step 3.1–3.2).

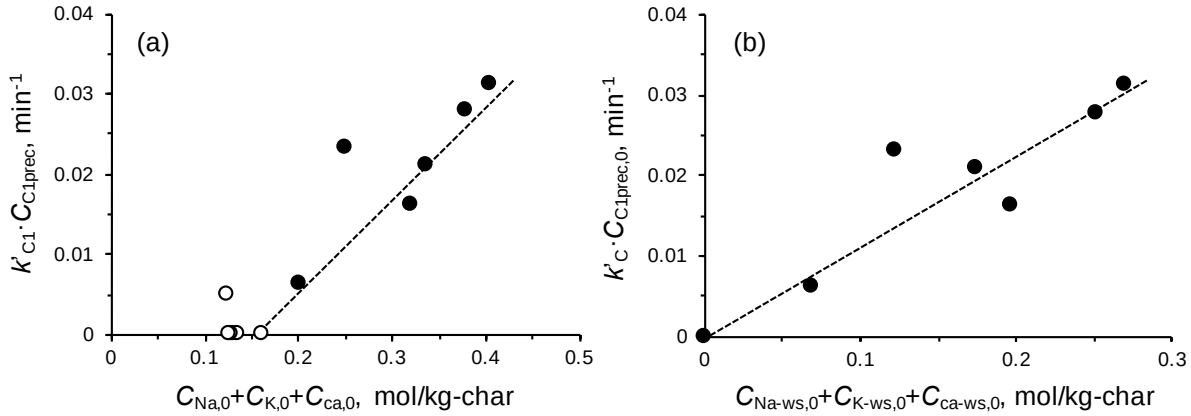

Figure 2.10. Plot of $k'_C C_{C1prec}$ against (a) the total concentration of Na, K and Ca in the char at $t = 0$ and (b) that of water-soluble Na, K and Ca at $t = 0$. Symbols: solid; chars from the original SCBs, open: those from WW-SCBs.

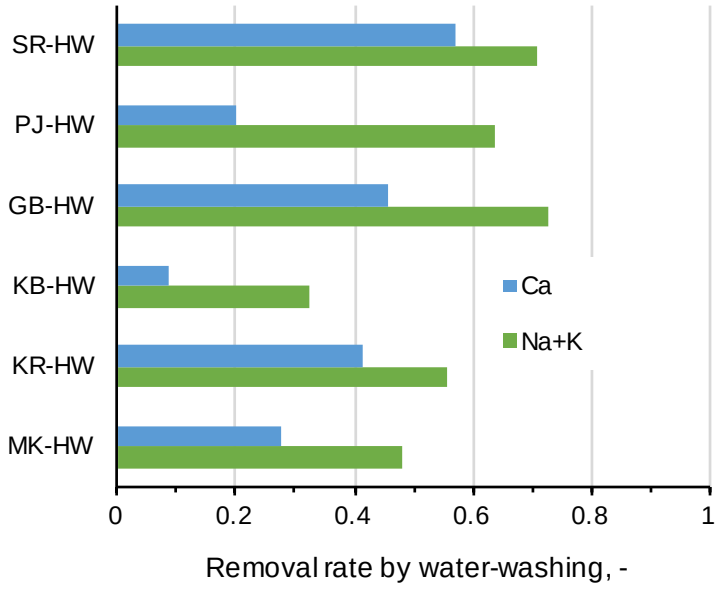

Figure 2.11. Removal rate of Na/K and Ca by water washing. The rate was defined as $C_{M,0}$ (WW-SCB char)/$C_{M,0}$ (original SCB char).

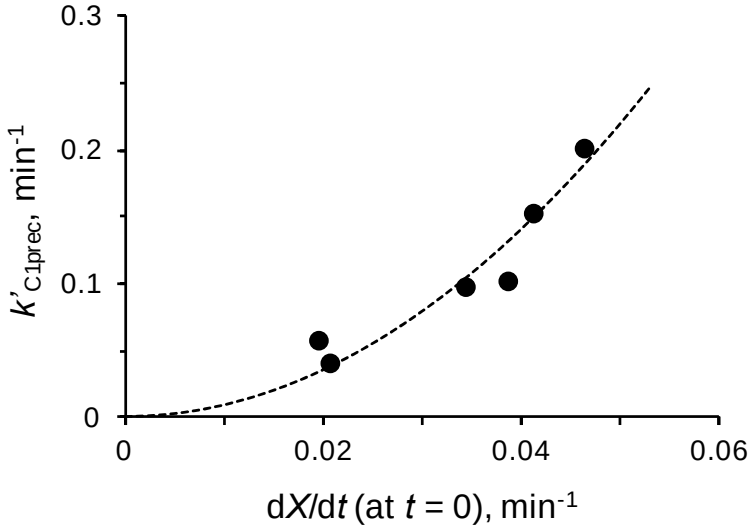

Figure 2.12. Correlation of k'_{C1prec} with (a) $\sum C_{M,0}$ (M = Na, K and Ca) and (b) the initial rate of gasification for the chars that contain C1 catalyst precursors (all of the chars from the original SCBs and KW-WW).

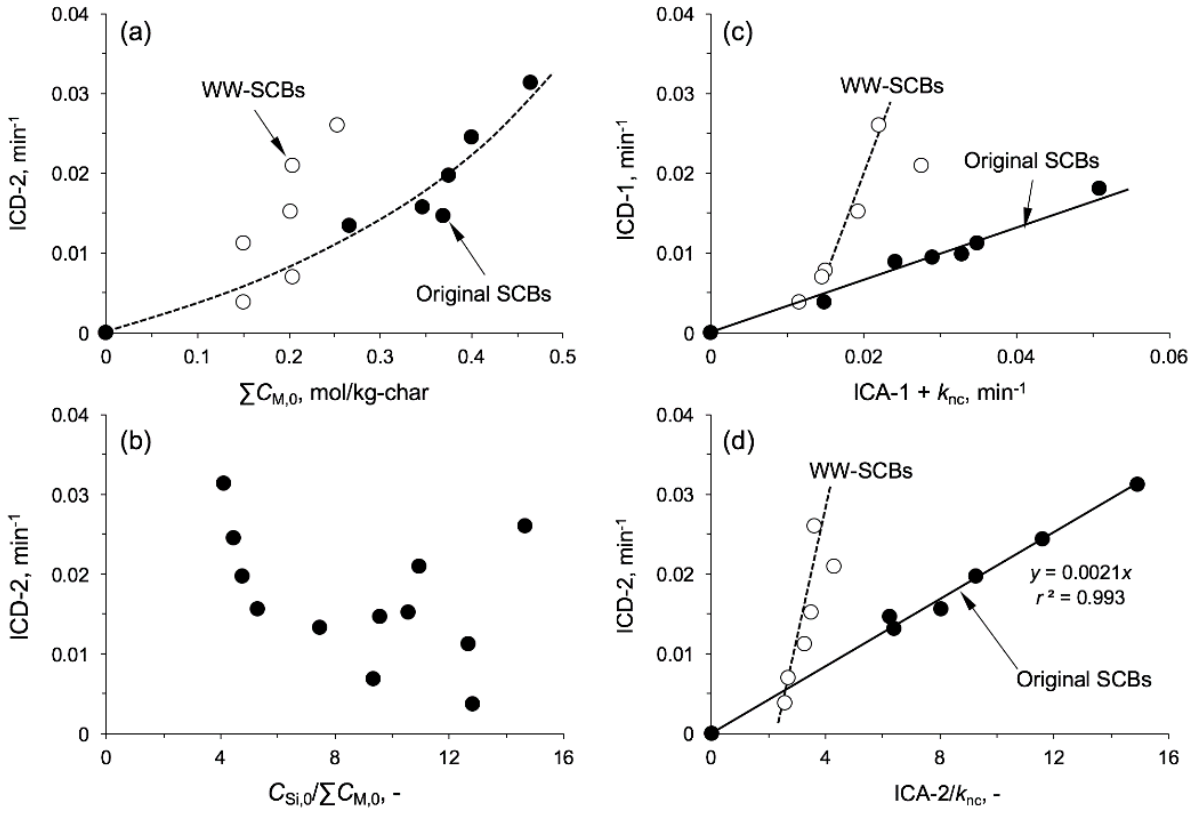

Figure 2.13. Correlation of ICD-1 or ICD-2 with (a) total concentration of Na, K, Ca and Fe ($\sum C_{M,0}$), (b) $C_{Si,0}/\sum C_{M,0}$, (c) ICD-1+k_{nc}, which represents dX/dt at t = 0, and (d) ICA-2/k_{nc}. Though not shown in this figure, ICD-2 was also correlated with ICA-2/k_{nc}·($C_{Si,0}/\sum C_{M,0}$). The result is available in **Appendix 6**.

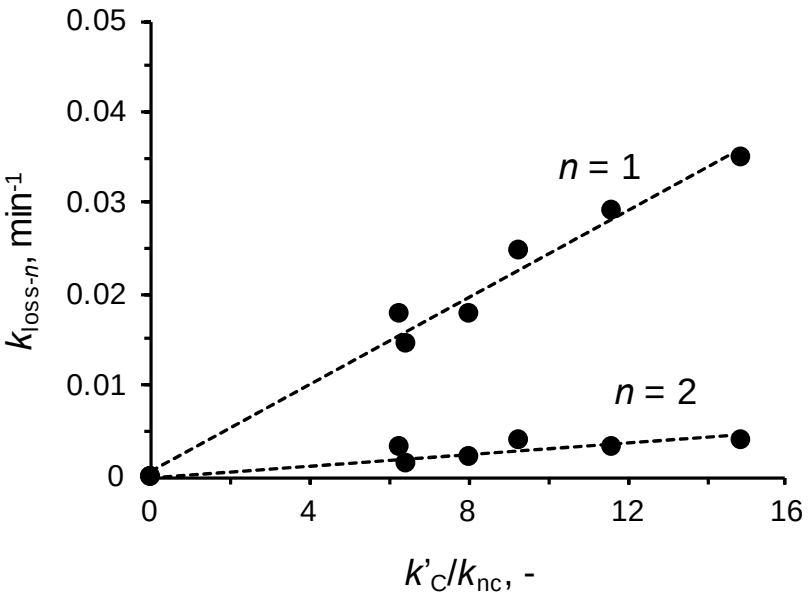

Figure 2.14. Relationship between $k_{loss\text{-}n}$ and k'_C/k_{nc} (n = 1 and 2) for the chars from original SCBs. Note that k'_C = ICA-2.

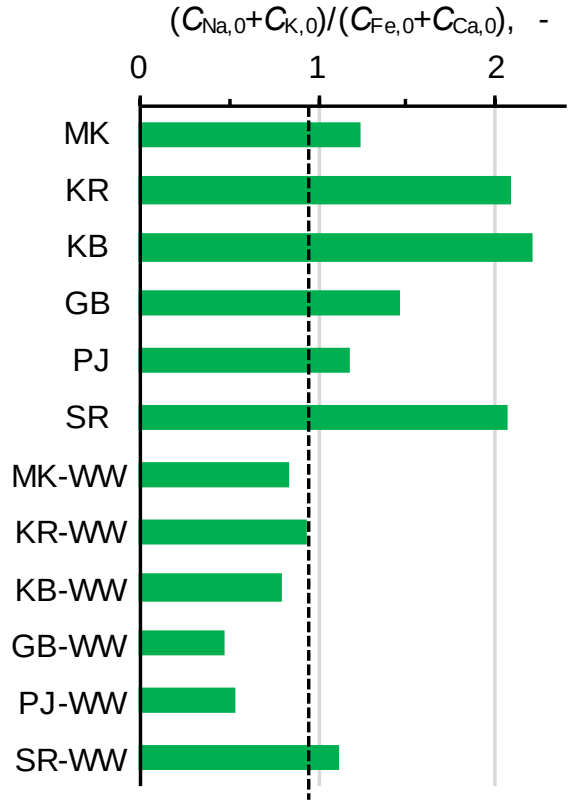

Figure 2.15. $(C_{Ca,0}+C_{Fe,0})/(C_{Na,0}+C_{K,0})$ ratios for the chars.

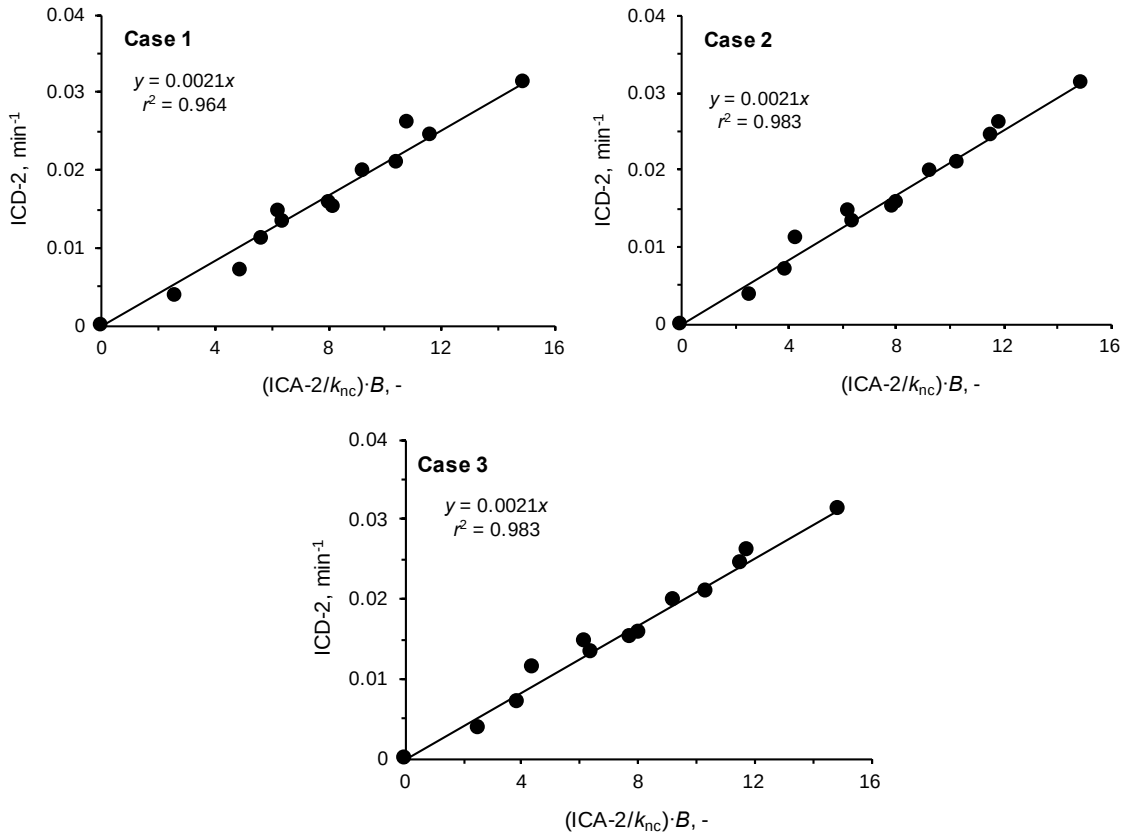

Figure 2.16. Optimized correlation of ICD-2 with (ICA-2/k_{nc})·B.

2.6 References

1. H. C. Butterman, M.J. Castaldi: *Environmental Science and Technology*, **43** (2009), 9030−9037.
2. J.-i. Hayashi, S. Kudo, H.-S. H.-S. Kim, K. Norinaga, K. Matsuoka, S. Hosokai: *Energy Fuels*, **28** (2014), 4−21.
3. S. Takeda, K. Kitano, J. Kubota, J. Kawabata, S. Sato, J.W. Shih, T.J. Chiba: *Journal of the Japan Institute of Energy*, **64** (1985), 409–418.
4. S. Takeda, S. Honma, Y. Tazaki, M. Yumiyama, K. Kitano, J. Kawabata, T. Chiba, N. Takezawa: *Journal of the Japan Institute of Energy*, **67** (1988), 764–769.
5. M. Kajita, T. Kimura, K. Norinaga, C.-Z. Li, J.-i. Hayashi: *Energy Fuels*, **24** (2010), 108−116.
6. L. Bai, Karnowo, S. Kudo, K. Norinaga, Y.-g. Wang, J.-i. Hayashi: *Energy Fuels*, **28** (2014), 7133−7139.
7. K. Mitsuoka, S. Hayashi, H. Amano, K. Kayahara, E. Sasaoka, A. Uddin: *Fuel Processing Technology*, **92** (2011), 26−31.
8. R.P.W.J. Struis, C.V. Scala, S. Stucki, R. Prins: *Chemical Engineering Science*, **57** (2002), 3593−3602.
9. J. Kramb, N. DeMartini, M. Perander, A. Moilanen, J. Konttinen: *Fuel Processing Technology*, **148** (2016), 50−59.
10. H. Risnes, J. Fjellerup, U. Henriksen, A. Moilanen, P. Norby, K. Papadakis, D. Posselt, L.H. Sørensen: *Fuel*, **82** (2003), 641−651.
11. D. Restuti, A. Michaelowa: *Energy Policy*, **35** (2007), 3952−3966.
12. Daniyanto, Sutidjan, Deendarlianto, A. Budiman: *Energy Procedia*, **68** (2015), 157−166.
13. C. Dupont, T. Nocquet, J.A. Da Costa, C. Verne-Tournon: *Bioresources Technology*, **102** (2001), 9743−9748.
14. N. Sadhwani, S. Adhikari, M.R. Eden, Z. Wang, R. Baker: *Fuel Processing Technology*, **150** (2016), 64−70.
15. P. Lahijani, Z.A. Zainal, A.R. Mohamed, M. Mohammadi: *Bioresources Technology*, **144** (2013), 288−295.
16. G. Wang, J. Zhang, J. Shao, Z. Liu, H. Wang, X. Li, P. Zhang, W. Geng, G. Zhang: *Energy*, **114** (2016), 143−154.

17. A. Bhat, J.V.R. Bheemarasetti, T.R. Rao: *Energy Conversion and Management*, **42** (2001), 2061−2069.
18. K. Kirtania, J. Axelsson, L. Matsakas, P. Christakopoulos, K. Umeki, E. Furusjö: *Energy*, **118** (2017), 1055−1065.
19. R-s. Xu, J.-l. Zhang, G-w. Wang, H-b. Zuo, P-c. Zhang, J-g. Shao: *Chemical Engineering Research and Design*, **107** (2016), 34−42.
20. T. Kitsuka, B. Bayarsaikhan, N. Sonoyama, S. Hosokai, C.-Z. Li, K. Norinaga, J.-i. Hayashi: *Energy Fuels*, **21** (2007), 387−394.
21. H-S. Kim, S. Kudo, K. Tahara, Y. Hachiyama, H. Yang, K. Norinaga, J.-i. Hayashi: *Energy Fuels*, **27** (2013), 6617−6631.
22. E. Byambajav, Y. Hachiyama, S. Kudo, K. Norinaga, J.-i. Hayashi: *Energy Fuels*, **30** (2016), 1636−1646.
23. Karnowo, Z.F. Zahara, S. Kudo, K. Norinaga, J-i. Hayashi: *Energy Fuels*, **28** (2014), 6459−6466.
24. C.-Z. Li, C. Sathe, J.R. Kershaw, Y. Pang: *Fuel*, **79** (2000), 427−438.
25. T. Okuno, N. Sonoyama, J.-i. Hayashi, C.-Z. Li, C. Sathe, T. Chiba: *Energy Fuels*, **19** (2005), 2164−2171.
26. B. Bayarsaikhan, J.-i. Hayashi, T. Shimada, C. Sathe, C.-Z. Li, A. Tsutsumi, T. Chiba: *Fuel*, **84** (2005), 1612−1621.
27. G. Bruno, M. Buroni, L. Carvani, G. D. Piero, G. Passoni: *Fuel*, **67** (1988), 67−72.
28. L. Kühn, H. Plogmann: *Fuel*, **62** (1983), 205−208.
29. S. Kudo, Y. Hachiyama, H-S. Kim, K. Norinaga, J.-i. Hayashi: *Energy Fuels*, **28** (2014), 5902−5908.
30. H. Wu, J.-i. Hayashi, T. Chiba, T. Takarada, C.-Z. Li: *Fuel*, **83** (2004), 23–30.
31. H. Yang, S. Kudo, K. Norinaga, J.-i. Hayashi: *Energy Fuels*, **30** (2016), 1616–1627.
32. N. Ellis, M.S. Masnadi, D.G. Roberts, M.A. Kochanek, A.Y. Ilyushechkin: *Chemical Engineering Journal*, **279** (2015), 402−408.
33. Y. Huang, X. Yin, C. Wu, C. Wang, J. Xie, Z. Zhou, L. Ma, H. Li: *Biotechnology Advances*, **27** (2009), 568−572.
34. Y. Zhang, M. Ashizawa, S. Kajitani, K. Miura: *Fuel*, **87** (2008), 475−481.
35. Y. Ohtsuka, K. Asami: *Catalisis Today*, **39** (1997), 111−125.
36. H. Yamashita, S. Yoshida, A. Tomita: *Energy Fuels*, **5** (1991), 52−57.
37. K. Asami, P. Sears, E. Furimsky, Y. Ohtsuka: Fuel Processing Technology, **47** (1996), 139−151.

Chapter 3

Kinetic and Mechanistic Analysis and Modelling of Steam Gasification of Char from Sugarcane Bagasse

3.1 Introduction

Alkali and alkaline earth metallic (AAEM) species such as Na, K, Mg, and Ca have been known for their catalytic contribution in gasification. [1–12] These catalytic species can be found abundantly in lignocellulosic biomass, and due to this characteristic, the gasification of biomass has been receiving attention from academics and industries. [13] Not only AAEM species but also transition metals like Fe have been investigated for their catalytic role in char gasification. [14,15]

Despite its being intensively discussed in many studies, the kinetic study of the gasification of char from biomass (biochar) has followed the prototypical kinetic models. For instance, structural and/or simplified models like the volumetric model (VM), random pore model (RPM), and shrinking core model (SCM) have been applied for biochar gasification regardless of their reoccurring failures and difficulties describing the entire range of the biochar conversion. [5,16,17] Several studies have reported the relatively minor effect of the nature of lignocellulosic fuel on biochar reactivity compared to the effect of the amount of the inherent metallic species. [18–20] For instance, the specific surface area, as it has been considered in RPM, is not an important factor in biochar gasification. [19,20] Wu *et al.* claimed that due to the heterogeneous and highly disordered structure of biochar, simplified kinetic models are inadequate to describe biochar gasification. It is important to consider both carbon structure changes (non-catalytic gasification) and catalysis by metallic species (catalytic gasification) in parallel. [20] Therefore, study of a kinetic model that assumes the non-catalytic and catalytic gasification of biochar should be performed in order to develop a higher-efficiency gasifier.

The so-called parallel kinetic model has been proven in many studies to successfully describe the entire range of char conversion (X) to $X > 0.995$ in steam and CO_2 gasification of lignite or biomass. [2,21–26] Some studies have also quantitatively explained the catalytic contribution of each catalyst as well as its activation and deactivation during the reaction with

CO_2. [24–26] However, there are no clear studies explaining the catalytic behavior of the inherent catalyst in steam.

The present authors have been studying the parallel kinetic model to describe the steam gasification of biochars from Indonesian sugarcane bagasse (SCBs). To understand the effect of the amount of AAEM on steam gasification, the SCBs were treated beforehand to eliminate the catalytic species through acid washing (AW-SCBs) and water washing (WW-SCBs). The results suggest the catalysis of Na, K, Ca, and Fe and their behavior can be drawn from several qualitative analyses. In addition, this study also analyzed the differences between the catalytic behavior in steam and CO_2 gasification.

3.2 Experimental method

3.2.1 Preparation of SCB samples

The samples of SCBs were collected from different sugar mills in Indonesia, and they are distinguished by their IDs (GB, KB, KR, MK, PJ, SR). Each of the samples was pulverized to sizes smaller than 150 mesh and dried to reach a moisture content below 10 wt. %. To remove the acid-soluble AAEM species, the SCBs were washed with 1 N HCl aqueous solution at 60°C for 24 h, followed by exhaustive washing with deionized water. The removal of water-soluble metallic species in SCBs was carried out with deionized water at 60°C for 24 h. The detailed procedures of the acid and water leaching can be seen in the previous report. [25] The acid-washed and water-washed SCBs hereafter will be referred to as AW-SCBs and WW-SCBs, respectively.

3.2.2 Char preparation and quantification of metallic species

The preparation of the chars from SCBs, AW-SCBs, and WW-SCBs was carried out using the same procedures as reported in previous studies. [19,20] A fixed-bed reactor was utilized, and the pyrolysis conditions were as follows: heating rate, 30 °C min^{-1}; peak temperature, 600°C; holding time at the peak temperature, 15 min; pressure, 0.1 MPa; carrier gas, N_2 (purity > 99.9995 vol.%). The resulting chars hereafter are identified as X-WW and X-AW (X= GB, KB, KR, MK, PJ, SR).

The AAEM species were quantified following the procedures in the previous reports. [25,27] The SCB chars were combusted at 600°C at the heating rate of 1 °C min^{-1}. Then the process was continued with a sequence of dissolution of the ash with a mixture of 1M HNO_3

and 1M HF (1:1) at 60°C, followed by evaporation to dryness at 120°C, resulting in a white residue at the bottom of the ampule. This residue was re-dissolved into an aqueous solution of 4M CH_3SO_3H, which then was analyzed by ion chromatography. All of the procedure was carried out in a plastic apparatus to minimize the incorporation of sodium (which usually occurs when using glass apparatus). The Fe, Si, Al, and other minor content in the ash were quantified by X-ray fluorescence spectroscopy (XRF).

3.2.3 Steam gasification procedure

The conversion of the resulting chars from SCBs, WW-SCBs, and AW-SCBs with steam were analyzed in the thermogravimetric analyzer (TGA) SII NanoTechnology EXSTAR TG/DTA 6200, which was equipped with a horizontal dual beam system. The individual char sample was placed in a Pt crucible and then heated in atmospheric N_2 flowing at 700 mL-stp/min up to 850°C. Upon confirming the steady mass of the char, the atmosphere was then switched to 20 vol. % steam/N_2 with the total flow at 700 mL/min. The gasification was terminated after verifying that there were no further changes in the measured weight.

3.3 Results and discussions

3.3.1 The yield and metallic species composition of chars

Yields of char from pyrolysis of original, WW-SCBs, and AW-SCBs are presented in **Figure 3.1**. There are no significant differences in the yields, whose values are common for similar feedstock. **Table 3.1** shows the elemental composition, ash content, and metallic species (Na, K, Mg, Ca, Fe, Al, and Si) of the chars from original SCBs, while those of WW-SCBs and AW-SCBs are presented in **Table A-1** (**Appendix 1**).

3.3.2 Non-catalytic gasification of chars from AW-SCBs

Figure 3.2 shows the non-catalytic gasification profile of the chars from AW-SCBs. The logarithm of $1 - X$ seems to decrease in a roughly linear manner with t, although there is a slight deviation in the initial gasification from the designated line for the first-order kinetics. The non-catalytic gasification can be described as follows:

$$\frac{dX}{dt} = k_{sp}(1 - X) \quad (1)$$

When the k_{sp} are plotted against the char conversion (X) shown in **Figure 3.3**, it can be seen that k_{sp} decreases exponentially. Therefore, k_{sp} can be considered as a function of X, which is determined by the following exponential equation:

$$k_{sp} = k_{sp,0} + \left(k_{sp,f} - k_{sp,0}\right)(1 - e^{-\alpha X}) \quad (2)$$

where $k_{sp,0}$ denotes the initial specific rate ($k_{sp,0}$ at $t = 0$) and $k_{sp,f}$ indicates the fictitious ultimate specific rate. The α here indicates the coefficient for rapidity of change of k_{sp}.

Equation 1 can describe quantitatively the changes of $1 - X$ over the reaction time in the range of X up to 0.995 for all of the chars from AW-SCBs, as shown in **Figure 3.2**. The optimized kinetic parameters from the calculation are summarized in **Table 3.2**. The initial specific rate, $k_{sp,0}$, is in the range of 1.4×10^{-2} – 1.9×10^{-2} min^{-1}, while the fictitious ultimate specific rate, $k_{sp,f}$, is between 0.8×10^{-2} and 1.1×10^{-2} min^{-1}. The coefficient α distributes over a range between 1.6 and 2. The ultimate specific rate constant, $k_{sp,f}$, is smaller than $k_{sp,0}$ for all of the chars from AW-SCBs. This means that the specific rate decreases monotonously with the progress of gasification.

Figure 3.3 presents the optimized k_{sp} as a function of X for all of the chars from the AW-SCBs. It is seen that k_{sp} at $X = 0.99$ was in a range of 0.0117–0.0123 min^{-1},which is narrower than the initial specific rate, $k_{sp,0}$. Thus, it can be concluded that the reactivities of the chars from AW-SCBs are very similar to one another. This result indicates that the carbonaceous structure relevant to intrinsic reactivity toward steam was not influenced by the original type of bagasse within the range of conditions for the present study.

Previous studies have reported on kinetic analysis of non-catalytic gasification of chars from various types of biomasses and lignites. [2,15] They found that all chars underwent gasification following first-order kinetics and that the specific surface area was not the influencing factor for the rate of gasification. The results implied that the steam was able to penetrate the entire portion of chars. Additionally, they have revealed that in some chars, the rate constant (k_{sp}) is not necessarily steady over the whole range of char conversion X. k_{sp} rather decreased slightly with the progress of gasification, showing a distributed reactivity with steam in the char. It would be reasonable if more reactive components were gasified more rapidly than less reactive ones. [2,19]

The decrease of k_{sp} over the conversion may be due to the change in the carbonaceous structure of char along with the conversion and resultant decrease or increase in the reactivity. This is speculative but plausible because steam gasification generates active hydrogen, whose presence leads to rearrangement of aromatic ring systems. Bazardorj *et al.*[22] studied the

steam gasification of lignite in a fluidized bed reactor at 1120–1223 K and found inhibition of char gasification in the presence of nascent volatiles, which played the role of an active hydrogen donor. They also found that the exposure of the char to the nascent volatiles decreased the char's reactivity with steam.

Another possible explanation for the changes of k_{sp}, although still a hypothesis, could be the activity of the acid-insoluble species that remained in the char after acid washing. The study in CO_2 [25] showed the increasing activity of char from AW-SCBs at conversion $X > 0.9$ due to the activity of the remaining metallic species. However, in steam gasification, the surviving catalytic species were activated at the beginning of gasification rather than in the late stage of gasification. The evidence of the possibility of fast activation of catalytic species in steam gasification will be explained later.

3.3.3 The kinetics of catalytic gasification of the chars from SCBs and WW-SCBs

Figure 3.4 shows the measured changes of $1–X$ with time from the gasification of chars from the original and WW-SCBs. These chars were gasified faster than the AW-SCBs due to the presence of inherent catalytic species. The chars from the original SCBs and those of WW-SCBs showed a similar tendency to the chars from AW-SCBs, which followed the first-order kinetics. Thus, at first, the overall rate of gasification of the chars could follow non-catalytic gasification, as explained by Equation 1.

It is also seen in **Figure 3.5** that the specific rate, $(dX/dt)/(1 - X) = r_{sp}$, of chars from SCBs and WW-SCBs decreases through the progress of conversion. Hence, the description of the gasification profile was done by the following kinetic model. The overall rate of steam gasification is described by the progress of non-catalytic and catalytic gasification in parallel.

$$\frac{dX}{dt} = \left(\frac{dX}{dt}\right)_{non-cat.} + \left(\frac{dX}{dt}\right)_{cat.} = k_{sp}(1 - X) + k_{cg} \quad (3)$$

k_{cg} is the rate constant of the catalytic gasification. In this study, the k_{cg} of the chars from the original SCBs and WW-SCBs is calculated by the difference between the overall dX/dt and the non-catalytic one; the results are summarized in **Figure 3.6**. It can be seen that the k_{cg} of the individual chars can be higher or lower than the k_{sp} depending on the type of the char, and the k_{cg} decreases with respect to the char conversion. The decrease of k_{cg} can be described by a simple exponential function assuming a single type of catalyst component, as shown in Equation 4:

$$k_{cg} = k_{cg,0} exp(-k_{loss} t) \quad (4)$$

When the description of k_{cg} by Equation 4 fails, then an assumption of two types of catalysts is needed, and Equation 4 can be modified to

$$k_{cg} = k_{cg1,0}exp(-k_{loss1}t) + k_{cg2,0}exp(-k_{loss2}t) \quad (5)$$

k_{cg} of every char is summarized and shown in **Figure 3.7**, which demonstrates the linear decay of the k_{cg} with char conversion, although some of the chars decrease more rapidly in the early stages of gasification than in the later stages. The profiles are almost identical to one another in the chars from original SCBs and in those from WW-SCBs. When compared with the results from the study [25] on the CO_2 gasification of similar samples, the rate of the catalytic gasification with steam straight-forwardly shows a monotonous decline through the conversion of chars. In CO_2 gasification, [25] the necessity of assumption of a catalyst precursor in the kinetic model was suggested. Catalyst precursor here indicates the potential amount of the metallic species that will transform into active catalytic species as its concentration in char increases. However, the profile shown in **Figure 3.7** indicates the fast transformation of catalyst precursor to the catalyst in the steam gasification. Therefore, unlike with the kinetic model of CO_2 gasification, [25] there is no need to incorporate the catalyst precursor rate into the kinetic model of steam gasification.

The $k_{cg,0}$ and k_{loss} of the individual chars from original SCBs and WW-SCBs were determined by a linear approximation, as shown in **Figure 3.8**. The optimized kinetic parameters of gasification of the chars from original and water-washed SCBs are summarized in **Table 3.3**. The $k_{cg,0}$ and the k_{loss} of chars from WW-SCBs are lower than those of the original ones. The $k_{cg1,0}$ of char from original SCBs ranges from $2.7x10^{-2}$ to $4.04x10^{-2}$ min^{-1}, while k_{loss-1} ranges from $3.9x10^{-2}$ to $5.6x10^{-2}$ min^{-1}. The chars from WW-SCBs have lower ranges of $k_{cg1,0}$ (from $1.29x10^{-2}$ to $1.68x10^{-2}$) and of $k_{cg2,0}$ (from $1.5x10^{-4}$–$4.12x10^{-2}$ min^{-1}), while the k_{loss-1} ranges between 2.82x10-2 and 3.49x10-2 and k_{loss-2} ranges from $1x10^{-5}$ to $2.3x10^{-3}$ min^{-1}.

Figure 3.9 shows the kinetic contributions of the catalytic gasification to the overall rate of gasification. The value of the fraction depends on the type of char, and the profiles clearly suggest that the catalytic gasification was significant along with the progress of gasification. However, compared to that in the study [25] in CO_2 gasification, the catalytic contribution in steam is slightly lower, but there is no evidence of a significant increase of the contribution during gasification. These results and the comparison shown in **Figure 3.7** reassure that there is a quick transformation of the catalyst precursor to the catalyst at the early stage of steam gasification. In CO_2 gasification of the same biochar, this transformation was slower, which caused the increase of the catalyst contribution through the conversion of char.

The very different rate of the transformation of catalyst between steam gasification and CO_2 gasification can be explained by **Figure 3.10**. Firstly, the free energies were calculated according to the possible reactions [25, 28–31] that can occur during steam gasification, and the results are summarized in **Table 3.4**. The indication from this analysis is that the AAEM species react with the steam to form hydroxides (i.e., NaOH, KOH, $Ca(OH)_2$), which have a low melting point. This type of formation is liquid and very mobile in the char matrix. Thus, it very actively contributes to the char conversion. It is still speculation that after involvement in the catalysis, the species form an aggregate or silicates that are inactive, and then it is eliminated from the char matrix.

The elimination of the catalytic species in steam gasification can also occur through volatilization. **Figure 3.11** shows the concentration of catalytic species retained in the char during gasification, especially that of Na, K, Mg, and Ca. It can be seen that the volatilization of Na and K is dominant compared to that of Mg and Ca, which aligns with previous studies. [33,34] On the other hand, since the majority of the reactant was CO_2, the catalytic species in CO_2 gasification formed carbonates (i.e., Na_2CO_3, K_2CO_3, $CaCO_3$) that have a higher melting point than hydroxides. Therefore, the catalyst was less mobile, and the gasification was concentrated around the active catalysts in char. These catalysts then agglomerated and deactivated inside the char matrix. [25]

3.3.4 The correlation of catalytic species with its activity at the beginning of the reaction

The initial activity of chars, k_{cg0}, was believed to correlate with the inherent catalytic species in the char matrix at the beginning of the gasification. Therefore, k_{cg0} could be explained by the concentration of the individual catalytic species or the sum of them. Here, the species considered as catalysts were limited to Na, K, Ca, Mg, and Fe based on previous studies, [2,23–25] and their concentration is defined at $t = 0$ and denoted by $C_{M,0}$ (M = Na, K, Ca, Mg, and/or Fe) in the unit of moles per kilogram of dry char.

It was first assumed that $k_{cg,0}$ is a function of one or more initial catalytic species' conversion (at $t = 0$), for instance, $k_{cg,0} = f(C_{M,0})$. Then, to figure out the catalyst's importance, several functions were scrutinized by considering the linearity of $k_{cg,0}$ and $f(C_{M,0})$ following the step-by-step methodology described in the previous study. [25]

Table 3.5 summarizes the results while illustrating the logical consideration of the correlation with the steps mechanism. In steps 1.1 and 1.2, it was found that the correlation factors (r^2) of individual values for M = Na, Ca, Mg, or Fe with $C_{M,0}$ were clearly lower, and

therefore this consideration didn't continue to the next steps. The correlation of the remaining was improved by modifying $k_{cg,0}$ into $k_{cg,0}/k_{sp}$ in step 1.2, which suggest the significant influence of the intrinsic reactivity of char as well as the catalyst activity on the rate of catalytic gasification.

In step 2.1, the five candidates were modified by multiplying $C_{M,0}$ by ($C_{M,0}/C_{Si,0}$) on the basis of the abundance of SiO_2 causing the loss of the effective concentration of catalytic species. The consideration of $C_{Si,0}$ and $C_{Al,0}$ arose due to the interaction of AAEM species with SiO_2 and Al_2O_3 during the pyrolysis, forming an inactive species. [25] As a result, the correlations with the two candidates ($C_{Na,0} + C_{K,0} + C_{Ca,0} + C_{Fe,0}$) and ($C_{Na,0} + C_{K,0} + C_{Ca,0} + C_{Mg,0} + C_{Fe,0}$) were higher than those with the rest. The correlation factor was similar when the Al concentration was added to the function $\{C_{M,0}/(C_{Si,0} + C_{Al,0})\}$ instead of ($C_{M,0}/C_{Si,0}$).

Finally, the factor of individual species was introduced to the function given that each metallic species has different activity due to the proportions of active and inactive species. Therefore, in step 3.1, $C_{M,0}$ was modified to $C'_{M,0}$, as described in Equation 6:

$$C'_{M,0} = a_1C_{Na,0} + a_2C_{K,0} + a_3C_{Ca,0} + a_4C_{Mg,0} + a_5C_{Fe,0}$$

$$\frac{k_{cg,0}}{k_{sp}} = \alpha\left\{\left(\frac{C'_{M,0}}{C_{Si,0}} + p\right)\right\}C'_{M,0} \quad (6)$$

Every coefficient in Equation 6 was optimized in Microsoft Excel™ with a Solver™, and the results show a higher correlation factor of 0.97 with $a_1 = a_2 = 1.3$, $a_3 = 1$ (fixed), $a_4 = 0$, $a_5 = 0.39$, and $p = 100$ in step 3.1. Meanwhile, in step 3.2, the individual coefficients were optimized at $a_1 = 1$; $a_2 = 1$; $a_3 = 0.94$; $a_4 = 0$; $a_5 = 0.39$, and $p = 2.998$ with a similar correlation factor to that in step 3.1. It can be seen here that both results suggest the factors of Na, K, and Ca were higher than that of Fe. This might imply that Na, K, or Ca actively reacts with chars in steam gasification. On the contrary, the activity of the Na and K in CO_2 gasification was lower than that of Ca and Fe. This has been explained in the previous study: [25] There is an indication of the interaction between each catalytic species, especially that of Na/K with Fe, during the gasification. This interaction causes the increase of the catalytic effect of Fe. In steam gasification, this kind of synergetic effect was suppressed due to the fast transformation of the catalyst. However, it was clearly indicated in the results of the optimization that the catalytic effect of Mg in both steam and CO_2 gasification is negligible, which is in agreement with some previous reports. [12,17,25] The results of correlation in Steps 1.1 to 3.2 are summarized in **Figure 3.12** for M = Na+K+Ca+Fe.

3.3.5 Correlation of catalyst deactivation with its catalyst content

Figure 3.13 shows the correlation of $k_{loss,0}$ with $C_{M,0}$ for M that equals the total concentration of Na, K, Ca, and Fe, considering that the effect of Mg is negligible. It is seen that the correlation cannot be achieved perfectly, but the tendency is quite clear that the catalyst deactivation is higher in a greater catalyst concentration. It is suggested in **Figure 3.14** that the increasing concentration of SiO_2 over inherent catalyst doesn't necessarily increase the rate of catalyst deactivation. This is similar to what was found in previous studies, which concluded that the influence of SiO_2 on catalyst deactivation was insignificant during gasification. [24–26]

Previous studies [25,28–31] suggest the possible reactions of metallic species with SiO_2 in steam gasification as shown in **Table 3.4**. From the calculation of free energies of the possible reactions in steam gasification, it is suggested that the Na/K silicates' formation through their oxide forms is hindered by its metal oxide cycle reaction. However, the silicates' formation through the hydroxide form is possible. Thus, the deactivation of catalyst in steam gasification is affected by the silicates' formation of Na and K through the hydroxides form and by the self-deactivation of the catalytic species itself.

3.3.6 The mechanism of catalyst deactivation in steam gasification

The relationship between the initial activity and the tendency toward deactivation of the inherent catalyst was investigated. **Figure 3.15a** examines the correlation between the rate of catalyst deactivation with the initial activity of chars and that of catalysts at the beginning of gasification. Linearity is achieved for most of the chars, suggesting high correlation of catalyst deactivation with the rate of gasification. Then in **Figure 3.15b**, the initial catalytic activity of chars is plotted against the catalyst deactivation. Here, it can be seen that the high correlation is achieved in the form of the slope-intercept linear equation.

Figure 3.15 suggests the clear difference between the catalyst deactivation rate of steam gasification and that of CO_2 gasification shown in **Figure 3.15c** and **Figure 3.15d**. In steam gasification, the effect of the removal of water-soluble species on deactivation rate is normal. On the contrary, the water-washing's impact on the catalyst causes a very high contrast between the rates of char from SCBs and from SCBs-WW. It has been proposed in the CO_2 gasification study [25] that the water-soluble species' removal suppressed the interaction between Na/K and Fe, thus accelerating Fe deactivation while lowering that of Na and K.

An optimization was further applied to improve the correlation. A coefficient of B shown in Equation 7 was introduced to all chars. This coefficient measures the importance of each component of catalytic species to the deactivation rates of the chars.

$$B = \frac{b_{\mathrm{Na}}C_{\mathrm{Na},0} + b_{\mathrm{K}}C_{\mathrm{K},0} + b_{\mathrm{Ca}}C_{\mathrm{Ca},0} + b_{\mathrm{Fe}}C_{\mathrm{Fe},0}}{C_{\mathrm{Na},0} + C_{\mathrm{K},0} + C_{\mathrm{Ca},0} + C_{\mathrm{Fe},0}} \tag{7}$$

The coefficient of b_{M}, where M is the catalytic species, indicates the significance of the individual catalytic species. As written in Equation 7, this constant considered four types of catalysts shown to be important in gasification. The values of b_{M} were determined by a numerical method with a different assumption in each case described as follows:

Case I

$b_{\mathrm{Na}} = b_{\mathrm{K}} = b_{\mathrm{Ca}} = 1$, $b_{\mathrm{Fe}} \neq 1$

Case II

$b_{\mathrm{Na}} = b_{\mathrm{K}} = b_{\mathrm{Ca}} \neq 1$, $b_{\mathrm{Fe}} \neq 1$

Case III

$b_{\mathrm{Na}} = b_{\mathrm{K}} \neq 1$, $b_{\mathrm{Ca}} \neq 1$, $b_{\mathrm{Fe}} \neq 1$

The optimization for each case was carried out by Microsoft Excel™ with Solver™ until maximum correlation was reached. The final coefficients of b_{M} for the correlation between $(k_{\mathrm{cg},0} + k_{\mathrm{sp},0})\cdot B$ and k_{loss} are as follows:

Case I

$b_{\mathrm{Na}} = b_{\mathrm{K}} = b_{\mathrm{Ca}} = 1$, $b_{\mathrm{Fe}} = 0.9265$

Case II

$b_{\mathrm{Na}} = b_{\mathrm{K}} = b_{\mathrm{Ca}} = 1.0135$, $b_{\mathrm{Fe}} = 0.9389$

Case III

$b_{\mathrm{Na}} = b_{\mathrm{K}} = 0.8991$, $b_{\mathrm{Ca}} = 1.3064$, $b_{\mathrm{Fe}} = 0.8979$

The optimized correlation of $(k_{\mathrm{cg},0} + k_{\mathrm{sp},0})\cdot B$ and k_{loss} of the three cases was plotted in **Figure 3.16**. It can be seen that the factor can be improved to 0.9816, 0.9816, and 0.9858 for case I, case II, and case III respectively. The coefficient of catalytic species suggests that the importance of Na, K, and Ca is similar. Although it is slightly lower, Fe also has a significant contribution to the deactivation.

Figure 3.17 examines the consideration of the optimization of $(k_{\mathrm{cg},0}/k_{\mathrm{sp},0})\cdot B$ versus k_{loss}. With the slope-intercept type of function, the optimized correlation of the three cases can reach up to 0.9292, 0.9479, and 0.9558 for case I, case II, and case III, respectively, when the final coefficients of b_{M} are as follows:

Case I

$b_{Na} = b_K = b_{Ca} = 1$, $b_{Fe} = 0.7745$

Case II

$b_{Na} = b_K = b_{Ca} = 1.121$, $b_{Fe} = 0.3888$

Case III

$b_{Na} = b_K = 0.9304$, $b_{Ca} = 1.6188$, $b_{Fe} = 0.3426$

Compared to the correlation of $(k_{cg,0} + k_{sp,0})\cdot B$ versus k_{loss}, the results here suggest a small contribution of Fe to the deactivation of the catalyst compared to those of Na, K, and Ca. However, both analyses suggest the importance of the intrinsic deactivation or the decrease in activity of the parent char (that from AW-SBs) due to the activity of the remaining acid-insoluble species. It was also proposed that the decreased reactivity of char with steam may be due to the exposure of the char to the nascent volatiles. [22]

Therefore, the mechanism of the catalyst during gasification can be estimated as follows: (a) The interaction or synergetic catalytic effect between Na/K/Ca and Fe was limited, while Na, K, and Ca had equal contributions higher than that of Fe. The lack of Na/K/Ca interaction with Fe caused the acceleration of the deactivation rate of Fe. A previous study [35] suggested that Fe as a single catalyst tended to undergo phase transformation and aggregated, causing its inactivity and loss of mobility as the reaction progressed. (b) The decreased interaction of catalytic species may enhance the activity of Na and K in steam gasification and lower its deactivation rates. (c) Loss of catalytic species of K and Na due to volatilization have less effect on its activity and its deactivation during gasification.

3.4 Conclusions

This study has investigated the kinetic model for describing steam gasification of 18 chars from six different types of SCBs. The following conclusions can be drawn:

1. Both non-catalytic and catalytic gasification of the SCB chars in steam obeys first-order kinetics with respect to the residual mass of char.
2. The gasification catalyzed by inherent metallic species is the major contributor to the overall rate of gasification, dX/dt over the entire range of X.
3. By considering the progress of non-catalytic and catalytic gasification in parallel, the proposed kinetic model with the assumption of the presence of one to two catalytic species can describe the gasification profile over an entire range of conversion.

4. The catalytic activity, k_{cg}, is affected by the concentration of the inherent metallic species. Na, K, and Ca play important roles in the catalyst activity, and each species behaves as a single catalyst during the gasification.
5. The more active catalyst undergoes more rapid deactivation. The rate of catalyst deactivation is roughly proportional to the initial catalyst activity, and it is also affected by the intrinsic reactivity of the char.
6. The comparison between the results from steam gasification and CO_2 gasification indicates the different catalyst behavior in char, which is affected by the interaction of the gasifying agent with catalytic species.

Table 3.1. Elemental composition, ash contents, and those of AAEM species of chars from SCBs.

District	ID	C	H	N	ash	Na	K	Mg	Ca	Fe	Al	Si
		wt%-daf			wt%-dry	mol/kg-char						
Gondang Baru	GB	76.7	1.96	0.61	3.68	0.071	0.21	0.057	0.13	0.059	0.1	1.9
Krebet Baru	KB	78.1	1.83	0.6	3.26	0.065	0.19	0.05	0.079	0.038	0.077	1.8
Kremboong	KR	78.2	1.74	0.57	2.57	0.061	0.17	0.059	0.086	0.026	0.069	1.8
Madukismo	MK	74.8	2.04	0.52	3.87	0.058	0.089	0.026	0.055	0.064	0.19	2
Panji	PJ	73.8	1.95	0.39	6.16	0.08	0.12	0.011	0.051	0.12	0.23	3.5
Sragi	SR	76.7	2.04	0.53	2.95	0.062	0.21	0.06	0.11	0.022	0.049	1.8

Table 3.2. $k_{sp,0}$, $k_{sp,f}$, and α for chars from AW-SCBs.

ID	$10^{-2}\cdot k_{sp,0}$,min^{-1}	$10^{-2}\cdot k_{sp,f}$,min^{-1}	α, -
GB-AW	1.7	0.8	2.0
KB-AW	1.8	1.0	1.6
KR-AW	1.4	0.8	2.0
MK-AW	1.9	0.8	2.0
PJ-AW	1.6	1.1	2.0
SR-AW	1.8	1.0	1.6

Table 3.3. Optimized kinetic parameters for catalytic gasification.

ID	$k_{cg1,0}$, min^{-1}	$k_{cg2,0}$, min^{-1}	k_{loss-1}, min^{-1}	k_{loss-2}, min^{-1}
GB	4.04E-02		5.30E-02	
KB	3.90E-02		5.20E-02	
KR	4.02E-02		5.60E-02	
MK	2.70E-02		4.00E-02	
PJ	2.65E-02		3.90E-02	
SR	2.71E-02		4.40E-02	
GB-WW	1.68E-02	3.28E-04	3.23E-02	2.30E-03
KB-WW	1.59E-02	2.82E-04	3.49E-02	1.00E-04
KR-WW	1.65E-02		3.00E-02	
MK-WW	1.43E-02	4.12E-04	2.96E-02	1.00E-03
PJ-WW	1.56E-02	1.50E-04	2.82E-02	4.00E-04
SR-WW	1.29E-02	1.92E-04	3.08E-02	1.00E-05

Table 3.4. The list of possible reactions which occurs during steam gasification.

Reactions	**ΔG_r, kJ/mol at 850°C**
The metal-oxides cycle	
$2Na + H_2O \leftrightarrow Na_2O + H_2$	–80.34
$Na_2O + C \rightarrow CO + 2Na$	+61.09
$2K + H_2O \leftrightarrow K_2O + H_2$	–12.06
$K_2O + C \rightarrow CO + 2K$	–7.19
$Ca + H_2O \leftrightarrow CaO + H_2$	–328.9
$CaO + C \rightarrow CO + Ca$	+309.65
$Fe + H_2O \leftrightarrow FeO + H_2$	–3.10
$FeO + C \rightarrow CO + Fe$	–16.15
The silicates formation from oxides	
$Na_2O + SiO_2 = Na_2SiO_3$	–195.33
$K_2O + SiO_2 = K_2SiO_3$	–291.33
$2FeO + SiO_2 = Fe_2SiO_3$	–20.95 [25]
$CaO + MgO + 2SiO_2 = CaMgSi_2O_6$	–133.83
$CaO + SiO_2 = CaSiO_3$	–88.57
The silicates formation from hydroxides	
$2Na + 2H_2O = 2NaOH + H_2$	–111.16
$2K + 2H_2O = 2KOH + H_2$	–116.02
$Ca + 2H_2O = Ca(OH)_2 + H_2$	–272.72
$2NaOH + SiO_2 = Na_2SiO_3 + H_2O$	–164.52
$2KOH + SiO_2 = K_2SiO_3 + H_2O$	–187.37
$2Ca(OH)_2 + SiO_2 = 2CaSiO_3 + 2H_2O$	–289.51
Oxide-carbonate cycles	
$Na_2O + CO_2 = Na_2CO_3$	–149.64
$Na_2CO_3 + C = 2CO + Na_2O$	+123.56
$K_2O + CO_2 = K_2CO_3$	–227.73
$K_2CO_3 + C = 2CO + K_2O$	+201.64
$CaO + CO_2 = CaCO_3$	+3.38
$CaCO_3 + C = 2CO + CaO$	–29.47
$FeO + CO_2 = FeCO_3$	+128.01
$FeCO_3 + C = 2CO + FeO$	–154.10

The silicates formation from carbonates	
$Na_2CO_3 + SiO_2 = Na_2SiO_3 + CO_2$	–45.67
$K_2CO_3 + SiO_2 = K_2CO_3$	–63.59
$CaCO_3 + SiO_2 = CaSiO_3 + CO_2$	–91.95
The silicates formation from salts	
$NaCl + H_2O + SiO_2 = Na_2SiO_3 + 2HCl$	+153.49
$KCl + H_2O + SiO_2 = K_2SiO_3 + 2HCl$	+135.73
Water-Gas Shift reactions	
$CO + H_2O = CO_2 + H_2$	+6.84

Table 3.5. Correlation factors (r^2) for functions ($y = ax + b$ or $y = ax$) employed in the process for numerical expression of initial catalytic activity.

Step ID	1.1	1.2	2.1	2.2	3.1	3.2
Parameter for catalytic activity (y)	$k_{cg,0}$, min^{-1}	$k_{cg,0}/k_{sp,0}$, -	$k_{cg,0}/k_{sp,0}$, -	$k_{cg,0}/k_{sp,0}$, -	$k_{cg,0}/k_{sp,0}$, -	$k_{cg,0}/k_{sp,0}$, -
Parameter for composition of metallic species (x)	$C_{A,0}$	$C_{A,0}$	$(C_{A,0})(C_{A,0}/C_{Si,0})$	$(C_{A,0})\{C_{A,0}/(C_{Si,0}+C_{Al,0})\}$	$(C'_{A,0})(C'_{A,0}/C_{Si,0}+p)$	$(C'_{A,0})(C'_{A,0}/C_{Si,0}+p)$
Fe	0.062	0.0223	*eliminated*	*eliminated*	*eliminated*	*eliminated*
Na	0.4657	0.4798	*eliminated*	*eliminated*	*eliminated*	*eliminated*
Mg	0.863	0.8101	*eliminated*	*eliminated*	*eliminated*	*eliminated*
Ca	0.6198	0.6364	*eliminated*	*eliminated*	*eliminated*	*eliminated*
K	0.9063	0.9238	0.8508	0.8451	*eliminated*	*eliminated*
Na+K+Ca	0.9313	0.9522	0.8571	0.8521	*eliminated*	*eliminated*
Na+K+Ca+Mg	0.9417	0.9498	0.8522	0.847	*eliminated*	*eliminated*
Na+K+Ca+Fe	0.8225	0.9043	0.9014	0.8997	0.9723	0.9694
Na+K+Ca+Mg+Fe	0.8808	0.9427	0.8978	0.8948	0.9714	0.967
Type of function for correlation	$y = ax + b$	$y = ax + b$	$y = ax + b$	$y = ax + b$	$y = ax$	$y = ax$

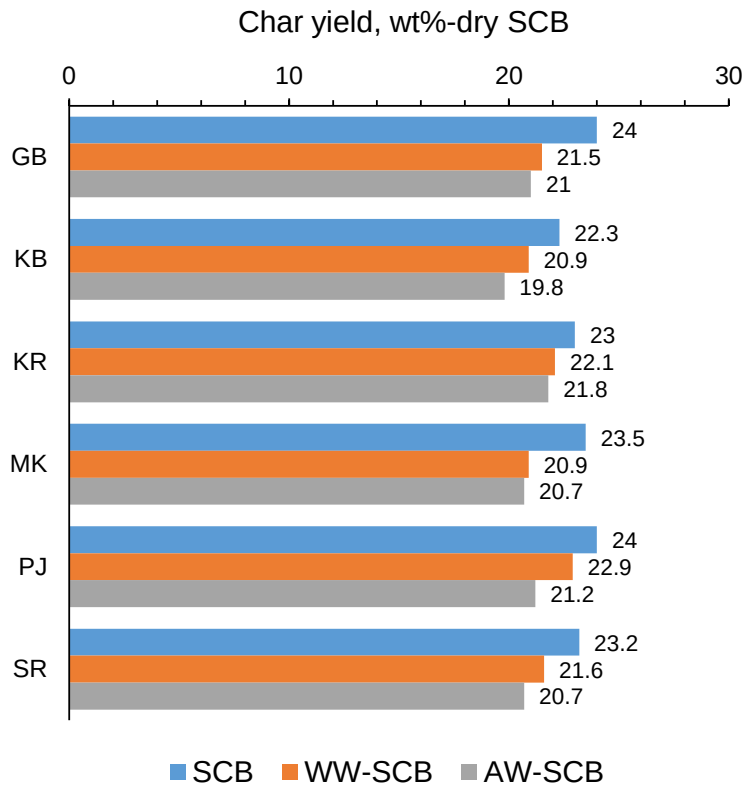

Figure 3.1. Char yields from original SCBs, WW-SCBs and AW-SCBs.

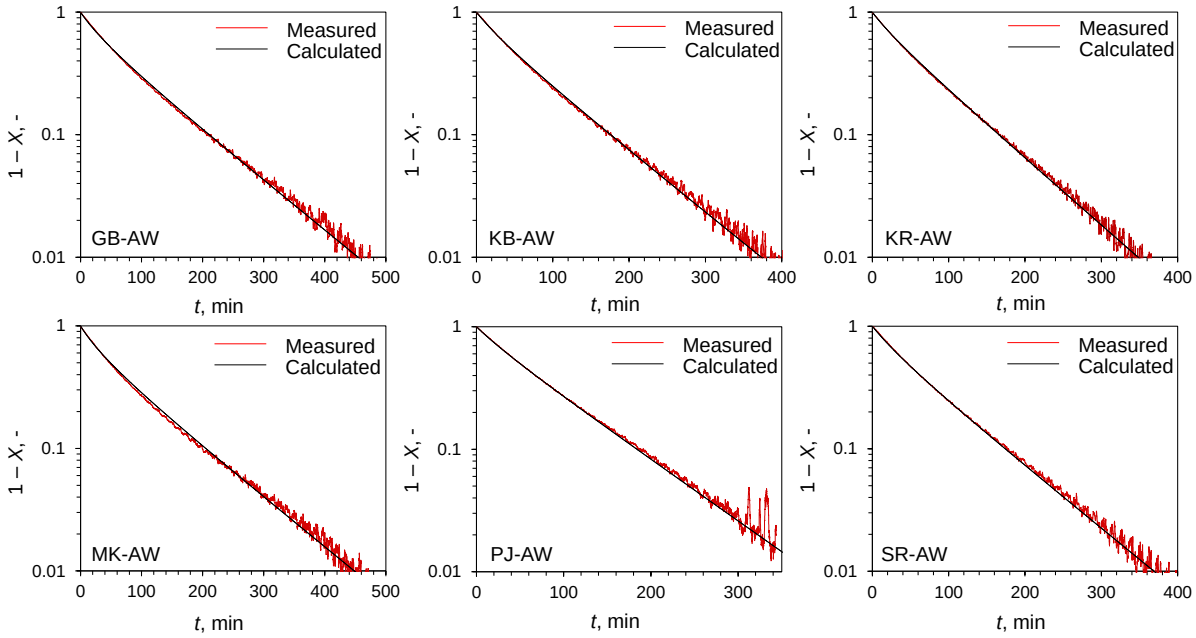

Figure 3.2. 1–*X* vs *t* profiles for gasification of chars from AW-SCBs. The profiles showing decrease in 1–*X* in a linear manner with *t*, which are indicative of first-order kinetics with respect to 1–*X*.

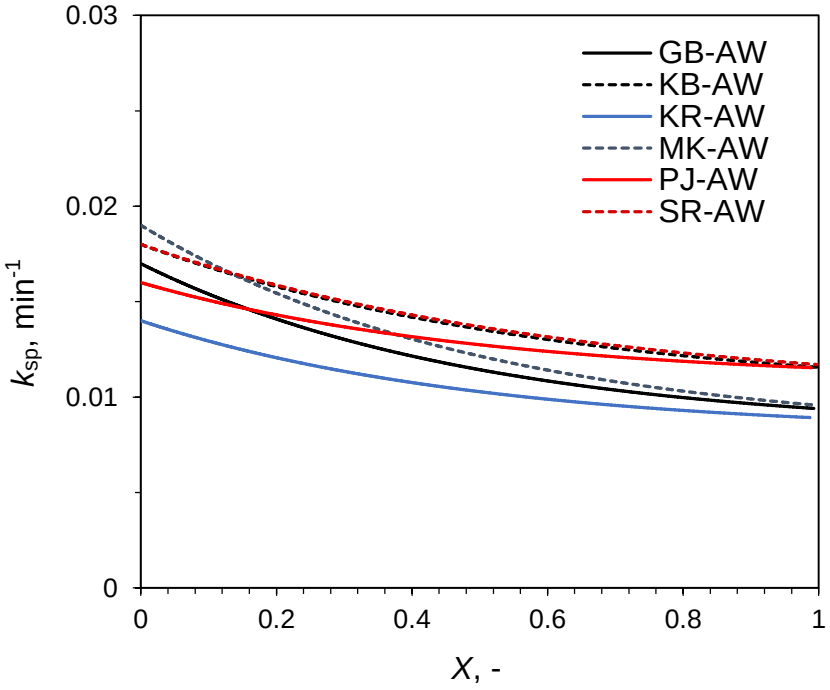

Figure 3.3. The k_{sp} of chars from AW-SCBs.

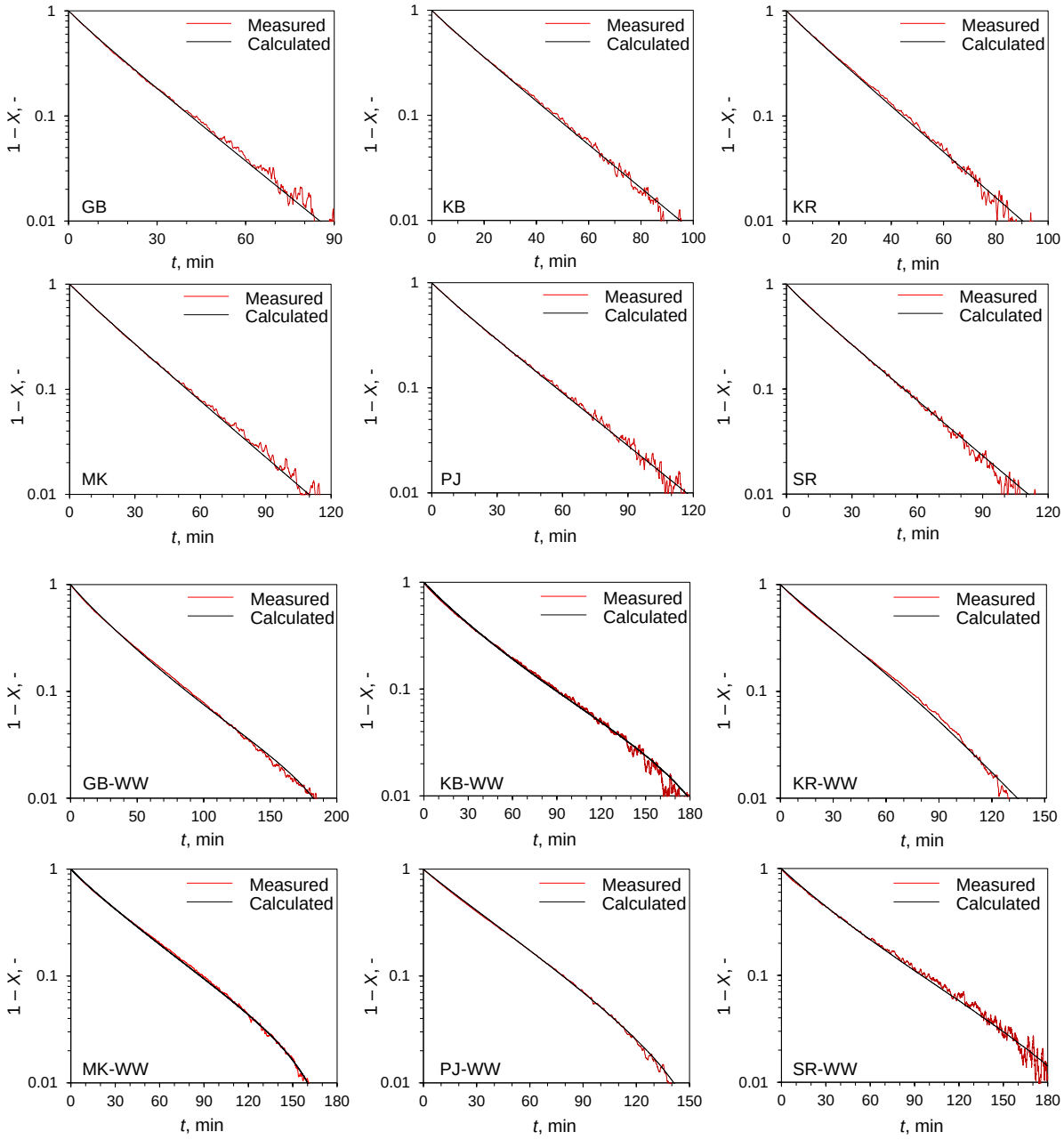

Figure 3.4. Measured and calculated 1–*X* vs *t* profiles for the gasification of chars from the original SCBs and those from WW-SCBs.

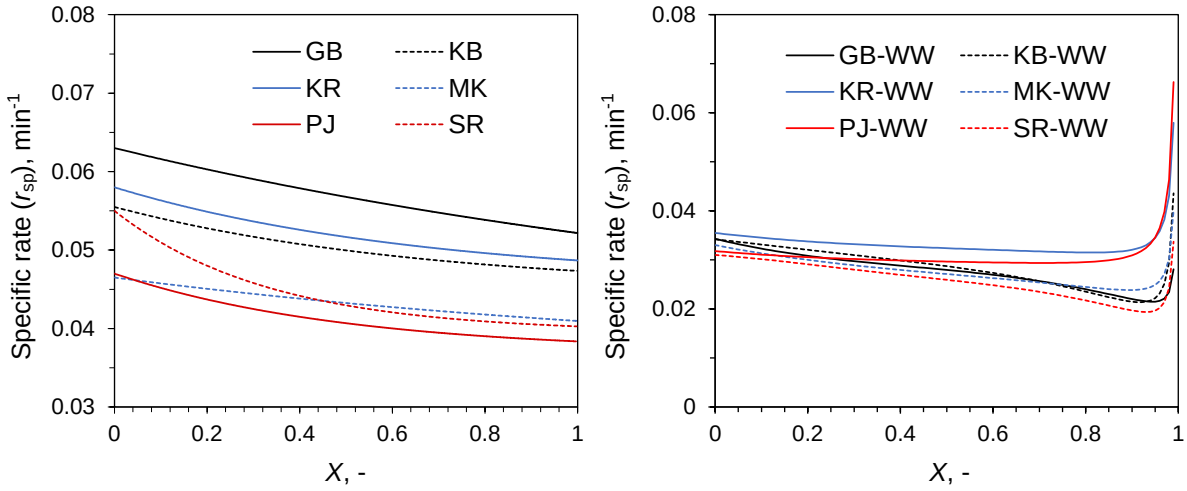

Figure 3.5. The specific rate of the steam gasification of chars from SCBs (left) and WW-SCBs (right).

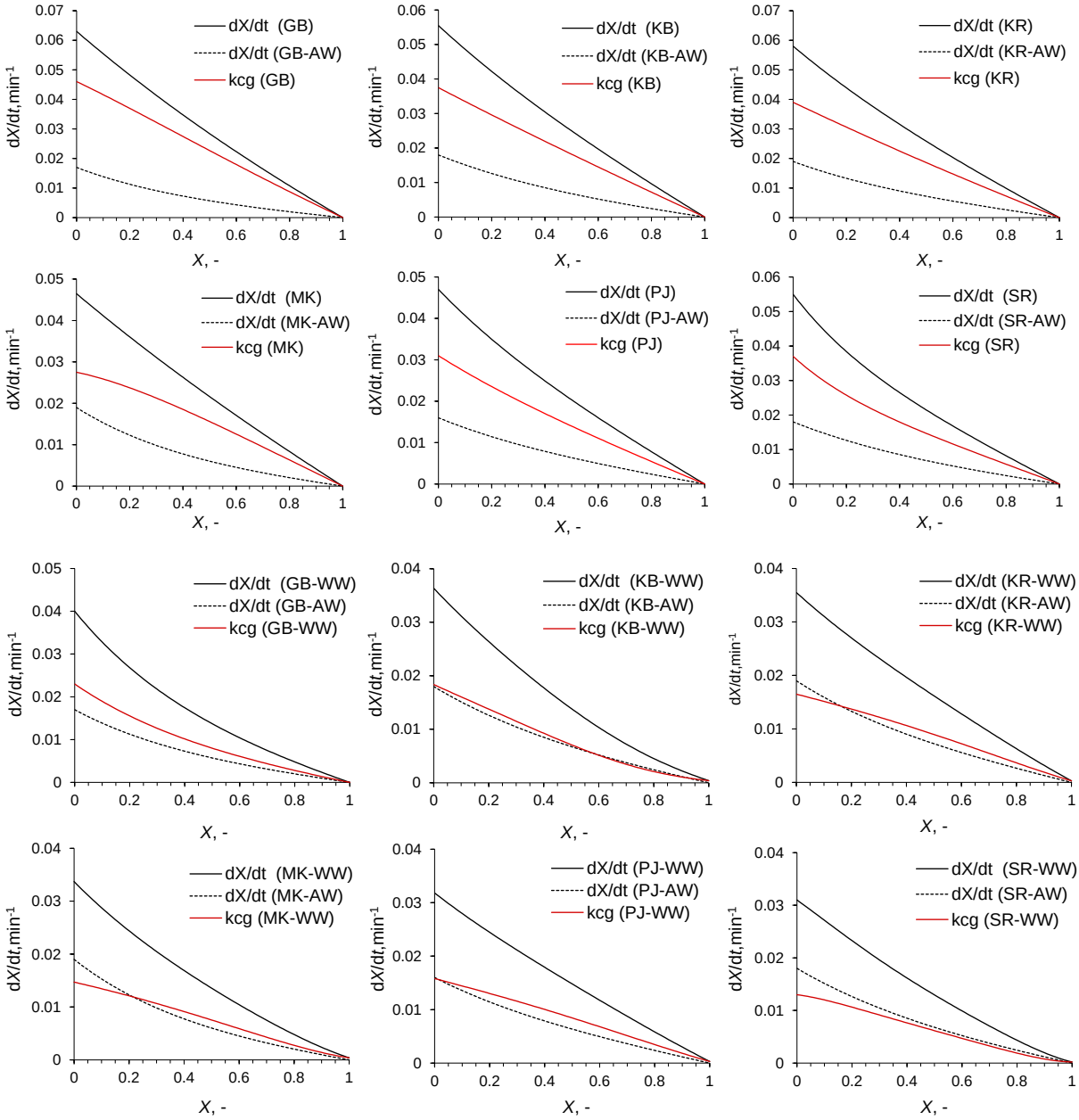

Figure 3.6. Measured and calculated changes in dX/dt with X for the gasification of chars from the original SCBs and those from WW-SCBs. The red-line indicates the k_{cg} derived from the calculation.

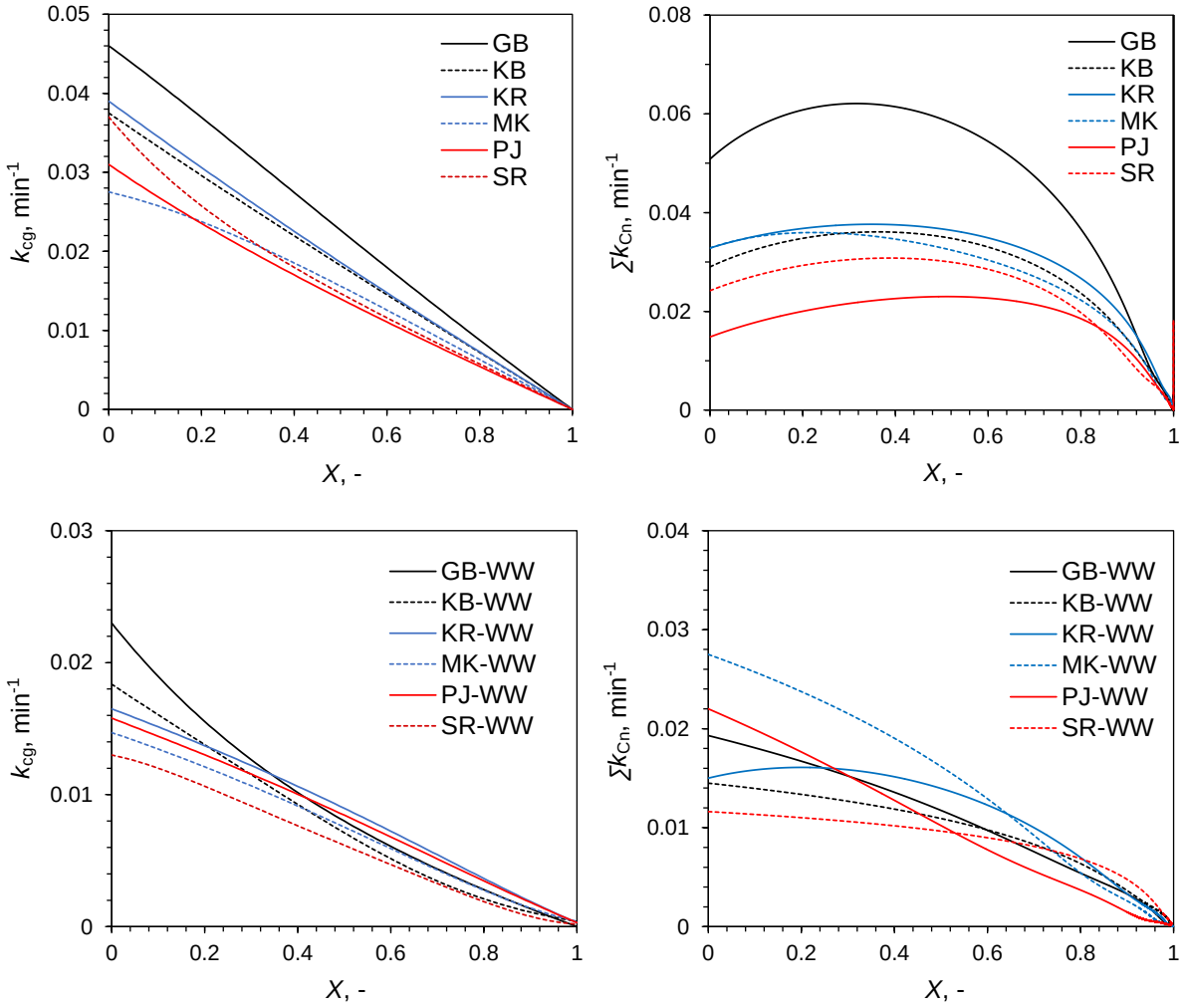

Figure 3.7. Comparison between the catalytic gasification rate of steam gasification (left) and CO_2 gasification (right). [25] The upper figures are the profiles from chars from original SCBs, while the lower profiles are results from WW-SCBs k_{cg} of chars from original SCBs (left) and WW-SCBs (right).

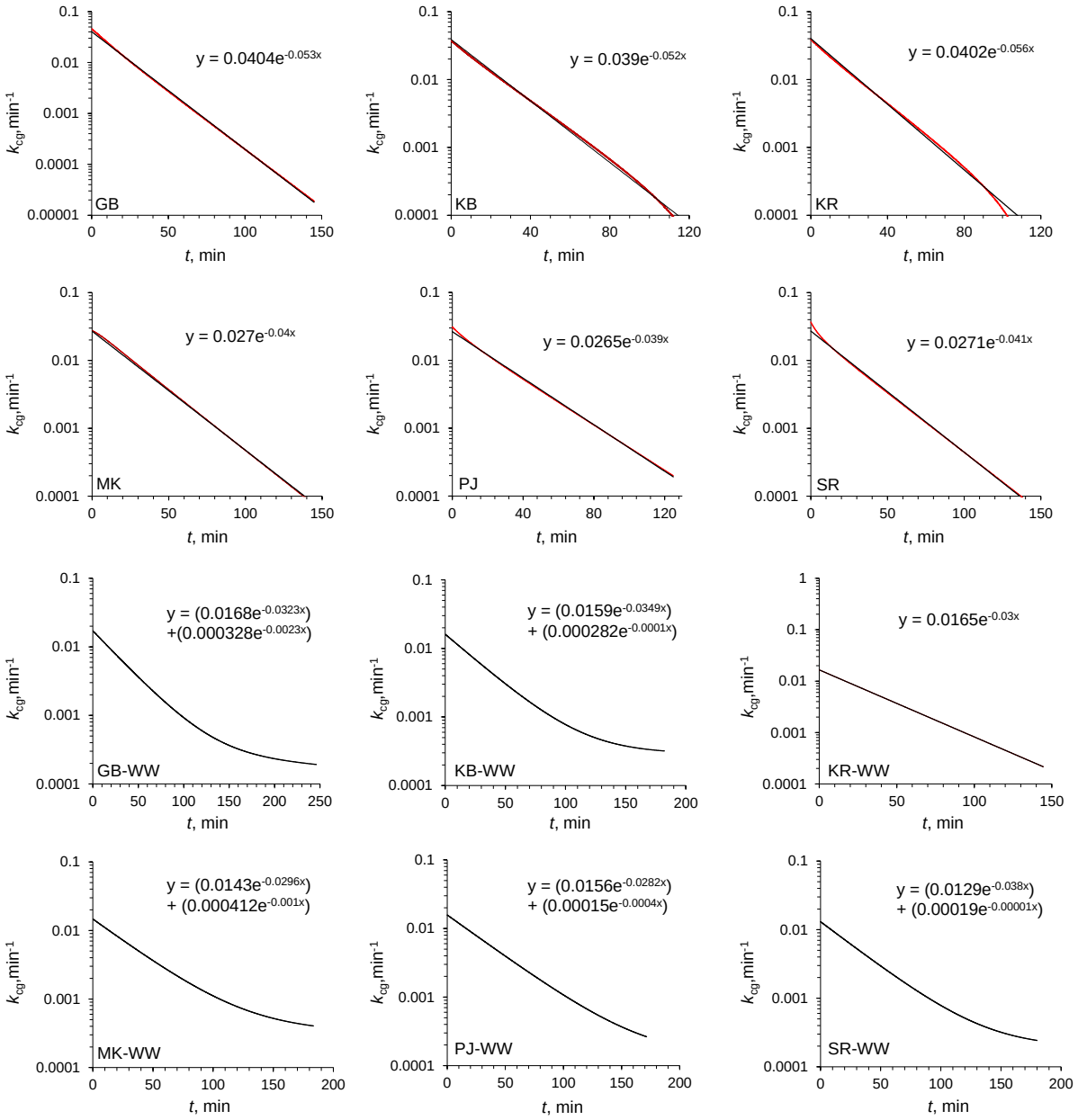

Figure 3.8. The linear approximation for determining the k_{cg} of chars from original SCBs and WW-SCBs.

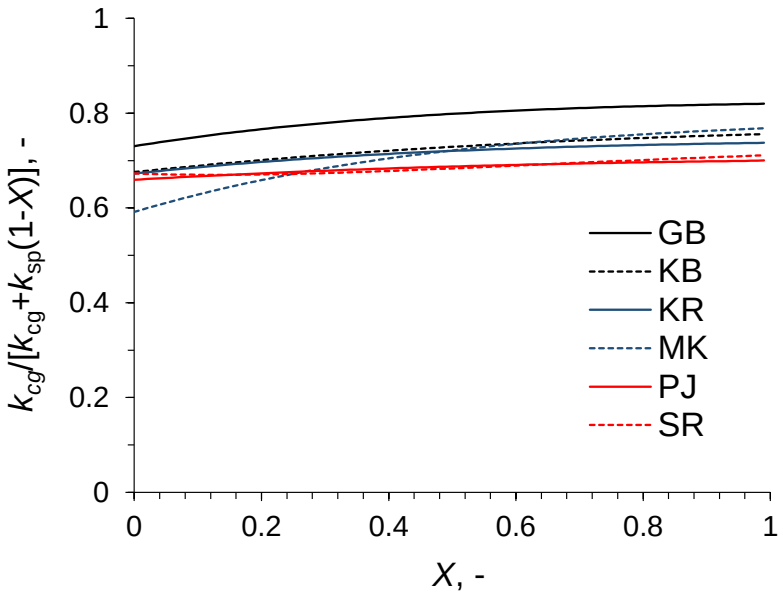

Figure 3.9. The contribution of catalytic gasification to the overall rate of gasification (dX/dt) as a function of X for the chars from the original SCBs. The meaning of the vertical axis is (rate of catalytic gasification)/(overall rate of gasification).

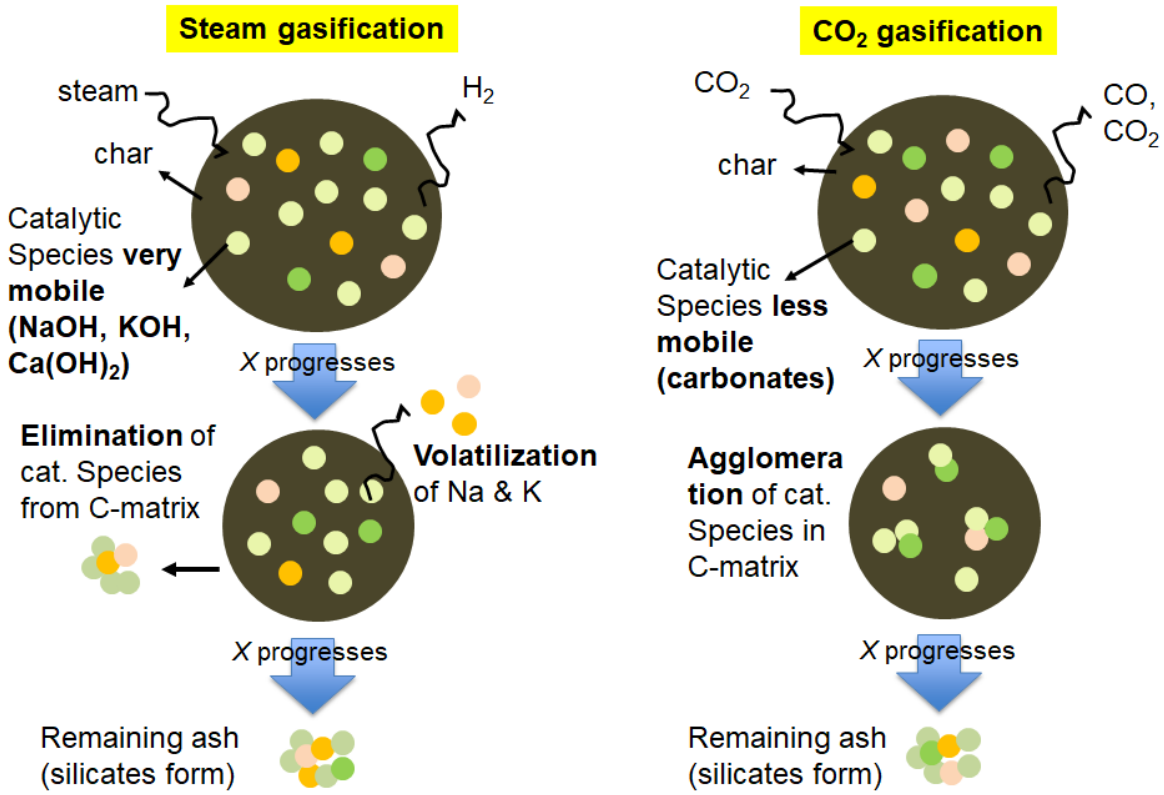

Figure 3.10. The proposed mechanism of catalyst behavior in biochar, suggesting the differences between steam and CO_2 gasification.

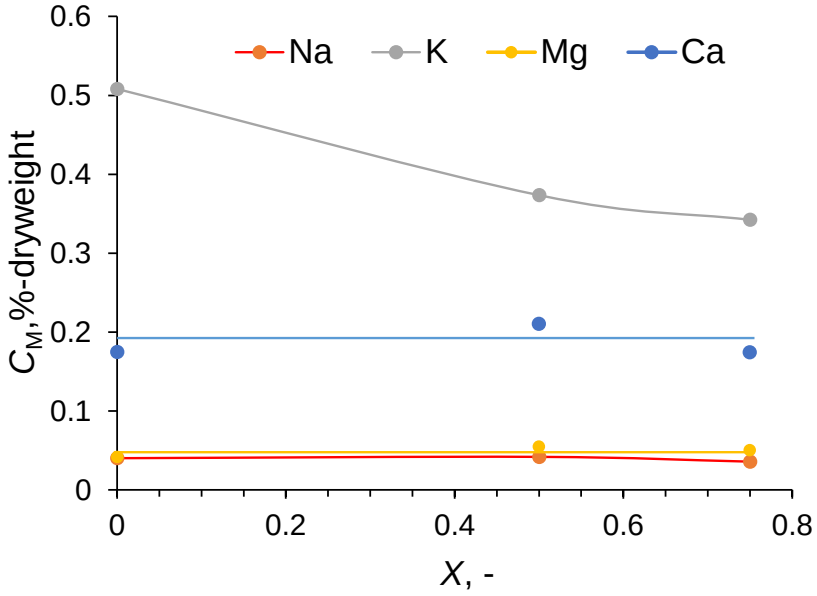

Figure 3.11. The retention of AAEM species during steam gasification.

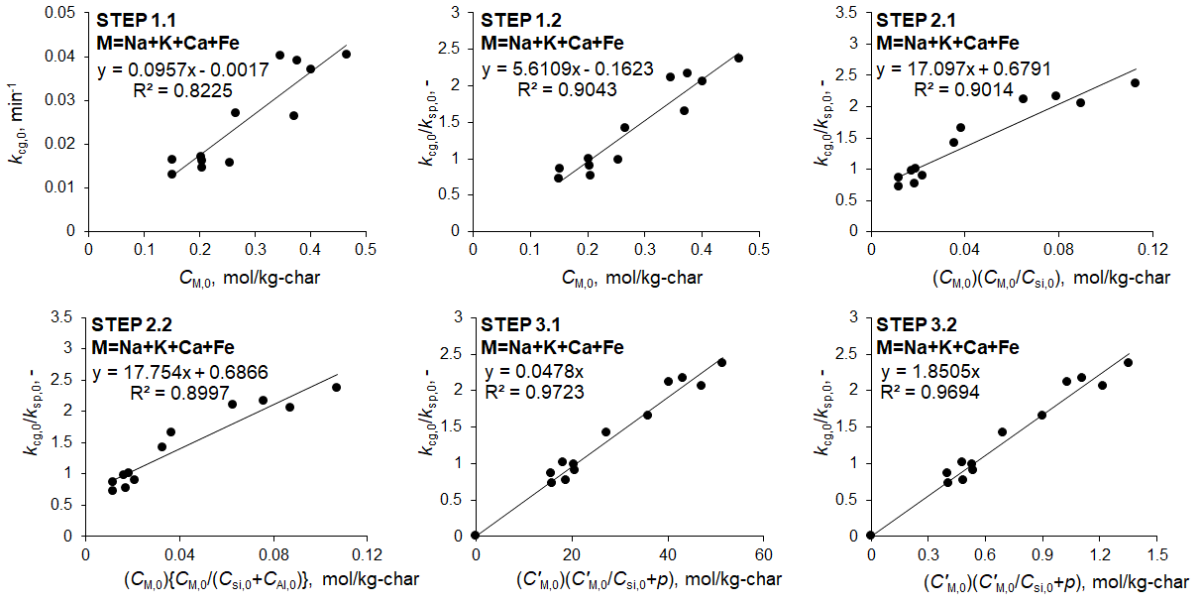

Figure 3.12. Correlation of $k_{cg,0}/k_{nc}$ with the total concentration of Na, K, Ca, and Fe.

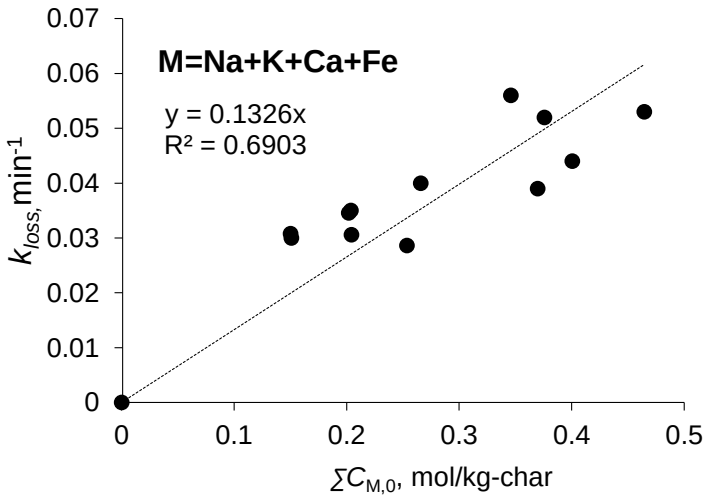

Figure 3.13. Correlation of k_{loss} with the total concentration of Na, K, Ca, and Fe ($\sum C_{M,0}$).

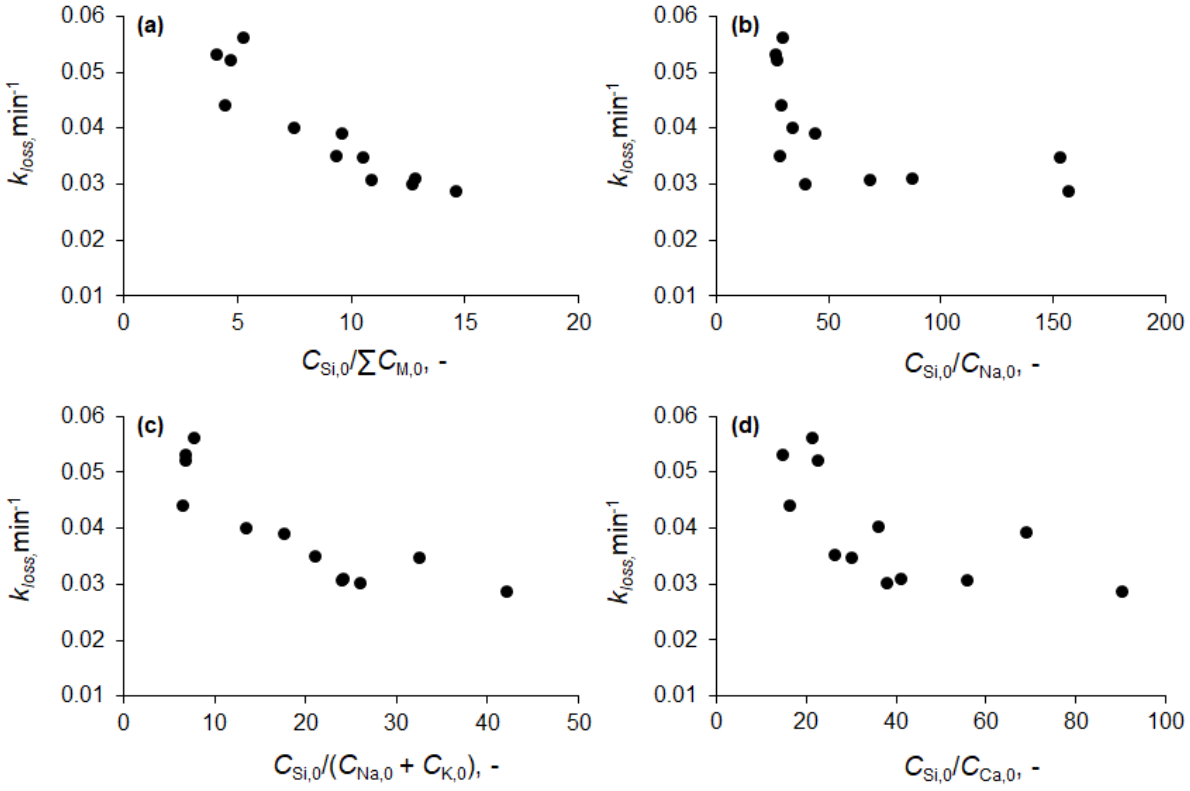

Figure 3.14. Correlation of k_{loss} with (a) $C_{Si,0}/\sum C_{M,0}$, (b) $C_{Si,0}/C_{Na,0}$, (c) $C_{Si,0}/(C_{Na,0}+ C_{K,0})$, (d) $C_{Si,0}/C_{Ca,0}$.

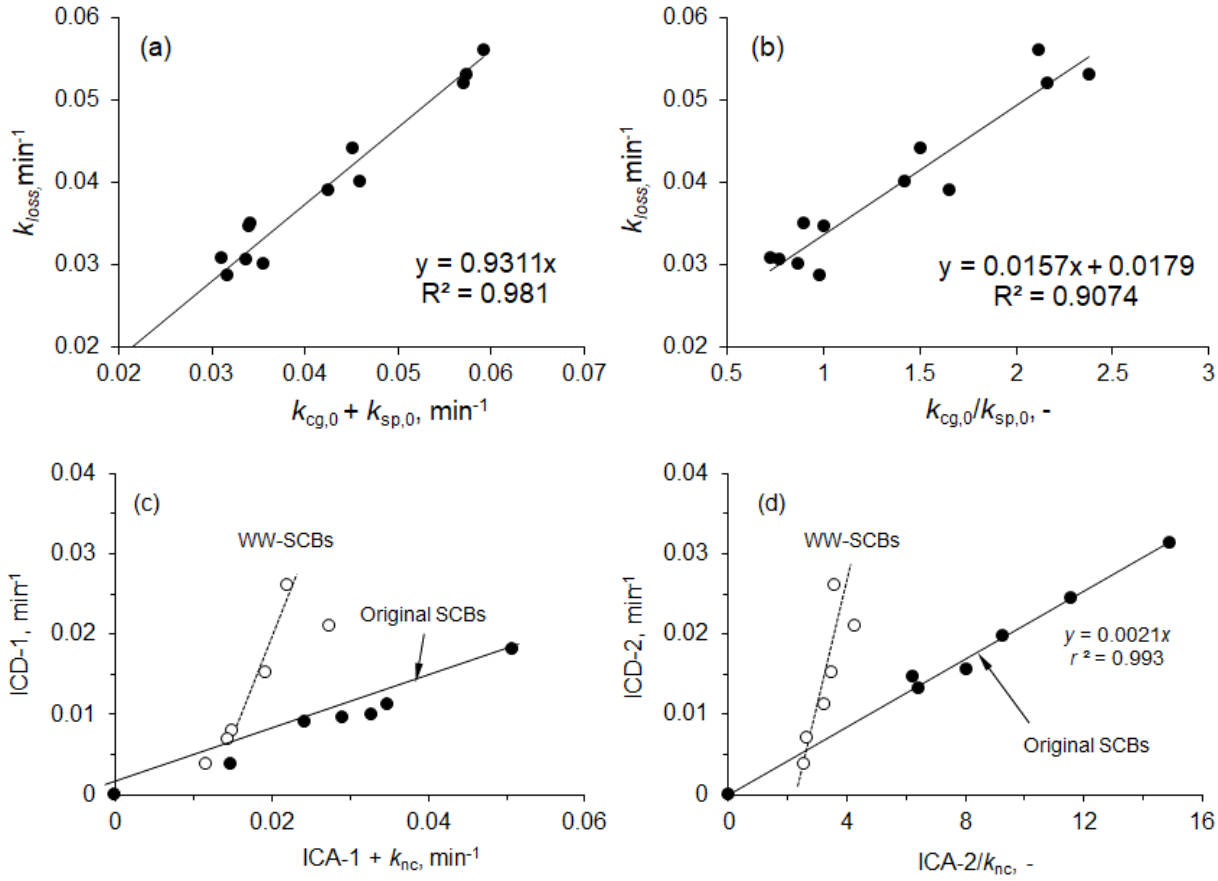

Figure 3.15. Correlation of k_{loss} with (a) $k_{cg,0} + k_{sp,0}$, which represents dX/dt at t = 0, and (b) $k_{cg,0}/k_{sp,0}$ compared to the results [25] of the correlation of initial catalyst deactivation, ICD-1 or ICD-2 with (c) ICA-1+k_{nc}, and (d) ICA-2/k_{nc}.

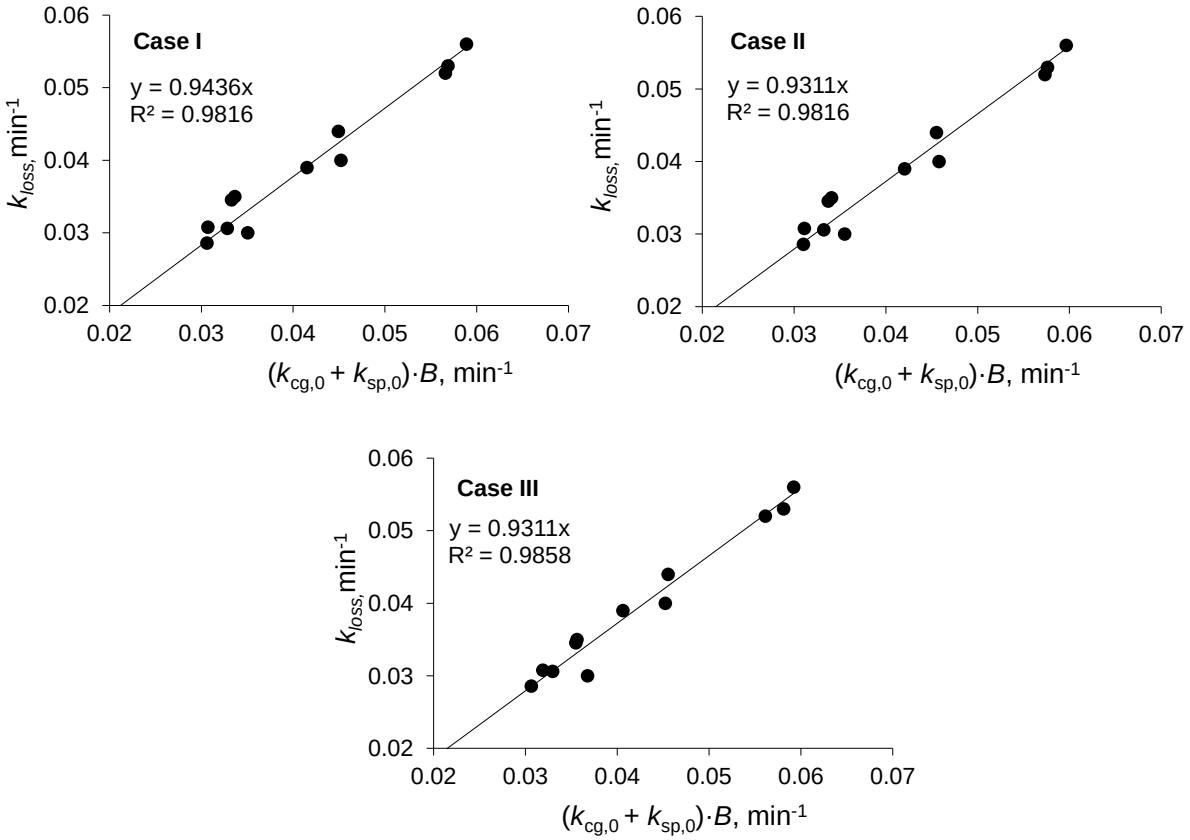

Figure 3.16. Optimized correlation of k_{loss} with $(k_{cg,0}+k_{nc})\cdot B$.

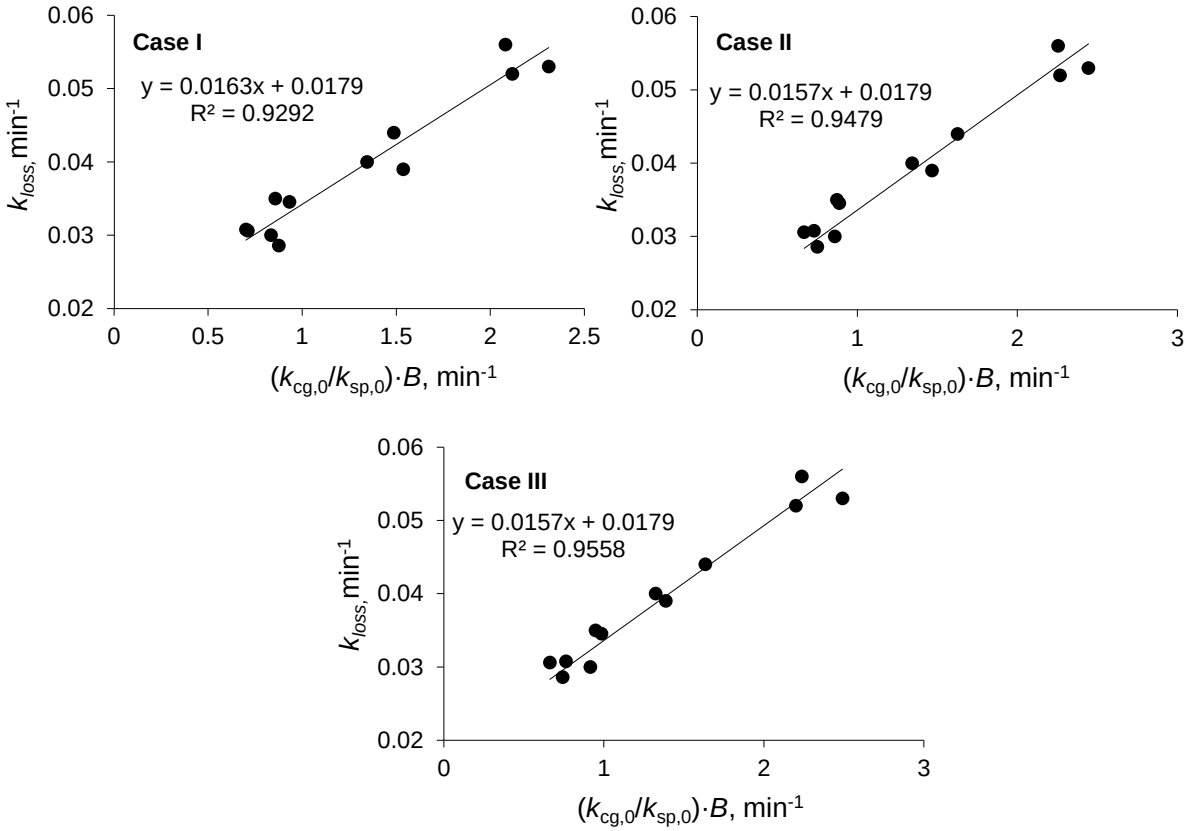

Figure 3.17. Optimized correlation of $k_{\mathrm{loss},0}$ with $(k_{\mathrm{cg},0}/k_{\mathrm{nc}})\cdot B$.

3.5 References

1. M. Perander, N. DeMartini, A. Brink, J. Kramb, O. Karlström, J. Hemming, A. Moilanen, J. Konttinen, M. Hupa: *Fuel*, **150** (2015), 464–472.
2. M. Kajita, T. Kimura, K. Norinaga, C.-Z. Li, J.-i. Hayashi: *Energy Fuels*, **24** (2010), 108–116.
3. D. Feng, Y. Zhao, Y. Zhang, H. Xu, L. Zhang, S. Sun: *Fuel*, **212** (2018), 523–532.
4. R.P.W.J. Struis, C. von Scala, S. Stucki, R. Prins: *Chemical Engineering Sciences*, **57** (2002) 3593–3602.
5. N. Sadhwani, S. Adhikari, M.R. Eden, Z. Wang, R. Baker: *Fuel Processing Technology*, **150** (2016), 64–70.
6. C. Dupont, S. Jacob, K.O. Marrakchy, C. Hognon, M. Grateau, F. Labalette, D.D.S. Perez: *Energy*, **109** (2016), 430–435.
7. C. Dupont, T. Nocquet, J.A.D. Costa Jr., C. Verne-Tournon: *Bioresouce Technology*, **102** (2011), 9743–9748.
8. K. Yip, F. Tian, J.-i. Hayashi, H. Wu: *Energy Fuels*, **24** (2010), 173–181.
9. J. Kramb, N. DeMartini, M. Perander, A. Moilanen, J. Konttinen: *Fuel Processing Technology*, **148** (2016), 50−59.
10. K. Mitsuoka, S. Hayashi, H. Amano, K. Kayahara, E. Sasaoka, Md.A. Uddin: *Fuel Processing Technology*, **92** (2011), 26−31.
11. T. Suzuki, H. Nakajima, N.-o. Ikenaga, H. Oda, T. Miyake: *Biomass Conversion and Biorefinery*, **1** (2011), 17–28.
12. P. Lahijani, Z.A. Zainal, A.R. Mohamed, M. Mohammadi: *Bioresources Technology*, **144** (2013), 288−295.
13. Li, C.-Z: Process Safety and Environmental Protection, **84** (2006), 407–408.
14. H. Yamashita, S. Yoshida, A. Tomita: *Energy Fuels*, **5** (1991), 52–57.
15. K. Asami, Y. Ohtsuka: *Industrial and Engineering Chemistry Research*, **32** (1993), 1631–1635.
16. L.D. Mafu, H.W.J.P. Neomagus, R.C. Everson, G.N. Okolo, C.A. Strydom, J.R. Bunt: *Bioresources Technology*, **258** (2018), 70–78.
17. G. Wang, J. Zhang, J. Shao, Z. Liu, H. Wang, X. Li, P. Zhang, W. Geng, G. Zhang: *Energy*, **114** (2016), 143–154.
18. C. Di Blasi: Progress in Energy and Combustion Science, **35** (2009), 121–140.

19. S. Kudo, Y. Hachiyama, H-S. Kim, K. Norinaga, J.-i. Hayashi: *Energy Fuels*, **28**, **9** (2014), 5902−5908.
20. H. Wu, K. Yip, F. Tian, Z. Xie, C.-Z. Li: *Industrial and Engineering Chemistry Research*, **48** (2009), 10431–10438.
21. T. Kitsuka, B. Bayarsaikhan, N. Sonoyama, S. Hosokai, C.-Z. Li, K. Norinaga, J.-i Hayashi: *Energy Fuels* **21** (2007), 387−394.
22. B. Bayarsaikhan, J.-i. Hayashi, T. Shimada, C. Sathe, C.-Z. Li, A. Tsutsumi, T. Chiba: *Fuel*, **84** (2005), 1612−1621.
23. H.-S. Kim, S. Kudo, K. Tahara, Y. Hachiyama, H. Yang, K. Norinaga, J.-i. Hayashi: *Energy Fuels*, **27** (2013), 6617−6631.
24. E. Byambajav, Y. Hachiyama, S. Kudo, K. Norinaga, J-i. Hayashi: *Energy Fuels*, **30** (2016), 1636−1646.
25. Z.F. Zahara, S. Kudo, Daniyanto, U.P.M. Ashik, K. Norinaga, A. Budiman, J.-i. Hayashi: *Energy Fuels*, **32,4** (2018) 4255–4268.
26. C. Choi, U.P.M. Ashik, S. Kudo, K. Uebo, K. Norinaga, J.-i. Hayashi: *to be published*.
27. Karnowo, Z.F. Zahara, S. Kudo, K. Norinaga, J.-i. Hayashi: *Energy Fuels*, **28** (2014), 6459−6466.
28. L. Kühn, H. Plogmann: *Fuel*, **62** (1985), 205–208.
29. J. Werkelin, B.-J. Skifvars, M. Zevenhoven, B. Holmbom, M. Hupa: *Fuel*, **89** (2010), 481–493.
30. C.A. Jordan, G. Akay: *Fuel*, **91** (2012), 253–263.
31. T. Yang, F. Liu, R. Li, X. Kai, K. Jia, Y. Sun: *Energy Fuels*, **29** (2015), 4298–4304.
32. S. Shiomi, N. Sano, Y. Matsushita: *Tetsu-to-Hagané*, **2** (1975), 177–181.
33. H. Wu, D.M. Quyn, C.-Z. Li: *Fuel*, **81** (2002), 1033–1039.
34. X. Li, H. Wu, J.-i. Hayashi, C.-Z. Li: *Fuel*, **83** (2004), 1273–1279.
35. K. Asami, P. Sears, E. Furimsky, Y. Ohtsuka: *Fuel Processing Technology*, **47** (1996), 139–151.

Chapter 4

Characteristic of Hydrothermal Treatment with Recycling of Process Water and Characteristic of Hydrothermally Upgraded Biomass

4.1 Introduction

Heat treatment of biomass in hot-compressed water at 150–350 °C is normally termed hydrothermal treatment (HT). HT has been studied by a number of researchers,[1–8] who putting main focal points of characteristics such as (i) conversion of carbohydrates (i.e., cellulose and hemicellulose) into sugar monomers/oligomers, furans and/or lower acids,[4–6] and/or (ii) removal of oxygen from the biomass that results in production of solid fuel with increased calorific value as high as coal.

The upgrading of biomass into coal-equivalent solid fuel may be, unfortunately, economically infeasible in the fuel industry in consideration of expensiveness of HT as a high-pressure multi-phase process together with inexpensiveness of solid fuel. The present authors propose application of hydrothermally upgraded biomass to production of value-added carbon based material taking most advantage of particular properties of HUB. During HT, the water becomes acidic due to formation of acids (acetic and other lower acids), given an ability of leaching of the inherent metallic species that are represented by AAEM species. The absence of AAEM species enables production of clean activated carbon and other materials.

The previous authors [9] reported that acid-washed (i.e., near AAEM-free) chars from the pyrolysis of biomass are excellent starting materials of high surface area active carbon. The absence of AAEM species allowed steam gasification to develop micro-/meso-porous structures of char to its specific surface area even over 2500 m^2 g^{-1}. HT, if operated at temperature around 240–260 °C, eliminates a substantial portion of the carbohydrate, transform its another portion into organic-solvent-soluble aromatic solid, while partially depolymerize the lignin. The chemical composition of thus upgraded biomass is expected to be an excellent raw material of metallurgical coke, which is produced through a sequence of hot briquetting to form high-density coke precursor and its carbonization.

The present study investigated characteristics of HT of woody biomass at 250 °C in terms of the yield, chemical composition (including contents of AAEM species) and

thermochemical properties (in gasification and carbonization), and formation of water-soluble products. Investigation was also made on the effects of the repeated use of water (i.e., HT with recycling of water), which avoids or minimizes the wastewater, on the performance of HT. It was also expected that accumulation of acids, if occurred, promoted acid-catalyzed hydrolytic decomposition of the carbohydrate lowering the temperature for HT.

4.2 Material and methods

4.2.1 Hydrothermal treatment (HT)

The first run of HT (HT1) was performed with a mixture of cedar (cryptomeria japonica, particle size; 40 – 850 μm, 15 g-dry) and deionized water (105 ml) that was charged in an autoclave together with 1.0 MPa N_2. The autoclave was immersed in a bath of fluidizing sand at 250 °C for 60 min, and then quenched in iced water. The resulting slurry was taken out of the autoclave and subjected to filtration at ambient temperature. The filtrate (LIQ-1) was recovered and used for the next run while the solid was washed with 20 g deionize water under ultrasonication, and then filtered while the filtrate (washing) was recovered as LIQ-2. The solid (upgraded cedar) was dried at 50 °C under vacuum until its mass became constant. In the second run (HT2), a 75 ml portion of LIQ-1, 15 g-dry of the fresh cedar and 30 ml makeup water were charged in the autoclave. The procedures of HT and the post treatments were the same as the HT1. HT runs were repeated up to HT4, simulating the recycling of product water by that of LIQ-1's. Analyses determined elemental and chemical compositions of the upgraded cedar, the concentrations of organic carbon (TOC) and lower acids and furans in LIQ-1 and LIQ-2. Details of the analyses are reported elsewhere.[10]

4.2.2 Steam gasification

The original cedar and upgraded one from HT1 (cedar-HT1) were pyrolyzed upon heating at 10 °C min-1 to 900 °C in an atmospheric flow of N_2 (purity > 99.9996 vol%). The resulting char samples, hereafter referred to as Char-I and Char-II, respectively, were subjected to steam gasification. Other char samples were also prepared. Another char sample, Char-IIa, was prepared through washing of the cedar-HT1 with 3N HCl and the subsequent pyrolysis in the same way as above. Char-IIa was loaded with K_2CO_3 at 0.95 or 4.6 wt%-K/dry for preparation of K-catalyst-loaded chars (Char-IIa-K1 or Char-IIa-K, respectively). These L-

loaded chars were prepared for investigating the effect of AAEM species on the pore development of char during the gasification.

A thermogravimetric analyzer was used for measuring the kinetics of steam gasification of the char samples at 850 °C and steam concentration of 20 vol%. More details of the procedure of the steam gasification are found elsewhere.[11]

4.2.3 Preparation of coke

Experimental examination was made on the production of metallurgical coke from the original cedar and cedar-HT1. These solids (after pulverized to sizes smaller than 100 μm) were briquetted upon heating at 200 °C and at a mechanical pressure of 114 MPa. The briquettes, which were in a form of disk (diameter; ca., 14 mm, thickness; ca. 5 mm) were carbonized to coke by heating at a rate of 3 °C min^{-1} up to 900 °C (briquettes from the cedar-HT1) or 1000 °C (those from the original cedar). The tensile strengths of the coke samples were measured at ambient temperature. Details of the experimental procedures, which have been developed originally by the present authors, are reported elsewhere.[12,13]

4.3 Results and discussion

4.3.1 Characteristics of HT

Figure 4.1 shows changes in the product yields with the run number (n) of HT, i.e., with the progress of recycling of water. The yield is defined on a carbon basis by the following equation.

$$\text{Yied at } n\text{-th run} = \frac{\text{Amount of product from } n\text{-th run}}{\text{Amount of cedar fed in } n\text{-th run}} \quad (1)$$

The yield of the cedar-HT seems to become steady at ca. 85% even at n = 2. This steady yield is higher by 12% than the yield at n = 1. The increase in the yield of upgraded biomass is explained by conversion of the water-soluble matter (WS) into a part of cedar-HT. Though not shown in the figure, an assumption of steady conversion, around 57%, of the recycled WS explains well the observed trend of the WS and predicts a steady yield of 35%.

Figure 4.2 presents the change in the chemical composition of the cedar within the range of run number up to 4 where the cedar-HT yield is already stable. There are three clear trends. First, HT removes more than 85% of the original carbohydrates. Second, HT hardly changes the net fraction of lignin. Third, HT forms substantial amount of material that is

extractable with benzene/ethanol (2/1 in vol.). It is reasonably concluded from these trends that HT converts the carbohydrates into water-soluble matter and the benzene/ethanol extract.

It is known that the primary products from the hydrolysis of carbohydrates are sugar monomers and oligomers, and these are further converted to furans, acid and gas. It is believed that the benzene-ethanol extract originates from the carbohydrates via sugars and/or furans under catalysis of the *in-situ* formed acids.[10] The analysis of LIQ-1 and LIQ-2 demonstrated formation of glycolic, succinic, acetic and formic acids as well as that of sugars and furans (furfural and 5-hydroxymethyl furfural). The recycling of water increased the concentration of those four major acids until the third run, and stabilized later. The concentration of the acid catalysts seemed to be high enough to cause the substantial formation of the benzene/ethanol extractable.

As seen in **Table 4.1**, pH of water after each run was between 3.0 and 3.1 regardless of the run number. The acidification of the water was undoubtedly due to the formation of lower organic acids. It was then expected that leaching of the inherent AAEM species occurred extensively during HT. The removal rates are in a range of 90–96%. **Table 4.1** shows the removal rates of K, Mg and Ca from the cedar for the first to fourth runs. Measurement of Na removal rates was not successful due to elution (leaching) of Na from glass bottles used in the analytical process. It was, however, believed that the removal rate of Na was as high as that of K, according to the present authors' recent investigation on the leaching of AAEM species from biomass. [14] **Table 4.1** also shows that the leaching ability of the water is maintained at least until the fourth run. The ability will be lost eventually after many runs of HT, but it is expected from the result that the recycling of water is rather durable.

The results of from HT with repeated use of the water thus demonstrated its effectiveness in simultaneous maximization of the yield of upgraded cedar (cedar-HT), elimination of a major portion of the carbohydrates, their chemical transformation into a portion of the upgraded cedar, and then removal of AAEM species.

4.3.1 Coke production from upgraded biomass

Coke samples were prepared from the original cedar and cedar-HT's from the first and fourth runs. **Table 4.2** summarizes the result. The mass yield of coke from the original cedar is only 27.5 wt%-briquette. Such a low yield arises from high volatility of the carbohydrates, in particular, cellulose. Substantial release of volatiles during the pyrolysis and carbonization makes the resulting coke more macro-porous and thereby lowering its mechanical strength.

The tensile strength of the coke from the original cedar is slightly higher than average strength of commercially available blast furnace coke. However, this does not directly mean feasibility of the coke to the use in blast furnace. Its reactivity with CO_2 at elevated temperature, which is often represented by a particular measure, CRI (coke reactivity index), is extraordinary high due to the catalysis of the inherent AAEM species. Such a high CRI will make the operation of blast furnace difficult.

HT greatly improves the yield and properties of the coke. The coke yields near 50 wt% is attributed to the elimination of the highly volatile carbohydrates. It was found in the present authors' recent study [10] that the benzene/ethanol soluble material of the hydrothermally upgraded biomass contributed to the coke (in terms of its mass) near-equally to the lignin. The presence and/or abundance of this material also enhance the plasticization of the upgraded biomass and its densification during the hot briquetting. The cokes from the cedar-HT's have much higher bulk densities than that from the original cedar. The micrographs of **Figure 4.3** show that the dense matrix formed at the briquetting has been maintained in the carbonization. Pores are seen on the fractured surface but their sizes are well below 10 μm.

The bulk density as high as 1.2 g cm^{-3} gives tensile strengths as high as 40 MPa, which is even higher than those of cokes from lignites that were prepared by the same procedure as in the present study.[12,13] Another importance with the cokes from the cedar-HT's is that HT has removed the major portion of AAEM species. Though not reported here in detail, the reactivity with CO_2 of the cokes from the cedar-HT was slightly higher but similar to that of a commercially used blast furnace coke.

4.3.1 Steam gasification of char from upgraded biomass

Figure 4.4 compares the kinetics of steam gasification of Char-I, Char-II and Char-IIa. Char-I from the original cedar undergoes very fast gasification, which was catalyzed by the inherent AAEM species. The gasification obeys zero-th order kinetics, which occurs when the catalyst are highly dispersed in the gasifying carbonaceous matrix of char. The change in the rate of conversion around 15 min is due to transformation of the catalyst at which its concentration reaches a loading saturation level (LSL).[11] HT not only slows down the char conversion but also alter the mechanism by the elimination of AAEM species. The kinetic analysis revealed that the gasification of Char-II followed first-order kinetics over the entire range of char conversion, which was typical to non-catalytic gasification. In fact, the gasification of Char-IIa, in other words, the char from the HCl aq.-washed cedar-HT, takes

place tracing a profile near-identical to that for Char-II. Thus, HT did not fully removed AAEM species, but eliminated the catalytic AAEM species completely.

Investigation of partially gasified Char-II revealed a value of upgraded cedar. **Figure 4.5** illustrates the change in the specific surface area (SSA) of Char-II with the progress of gasification in terms of conversion. SSA increases monotonically with the char conversion beyond 2,000 $m^2 g^{-1}$. Though not shown here, the gasification of K-loaded Char-II (i.e., Char-II-K1 and Char-II-K2) caused the development of SSA, but much less extensively than those of Char-II and Char-IIa. The maximum SSA was 1,200 – 1,400 $m^2 g^{-1}$. The substantial increase in SSA was thus attributed to the absence of AAEM species. [9] The upgraded cedar is an excellent raw material of clean and high-surface-area carbon material, and also applicable to co-production of such material and syngas.

4.4 Conclusion

The present study has demonstrated that HT with recycling of water maximizes the yield of upgraded cedar that is free from catalytic AAEM species. The upgraded cedar is an excellent raw material of high-strength metallurgical coke and also that of high-surface-area carbon materials.

Table 4.1. Removal rates of AAEM species from the solid for HT1–HT4.

n	pH of water (after run)	removal rate, %		
		K	Mg	Ca
1	3.05	95.8	94.4	90.9
2	3.09	94.9	81.2	92.1
3	3.12	94.0	90.7	89.6
4	3.10	95.8	94.0	89.1

The removal rate is defined as the fractional amount of metallic species leached out of the cedar to that contained initially.

Table 4.2. Yield and properties of coke samples.

Precursor of coke	yield, wt%-briquette	tensile strength, MPa	bulk density, g cm^{-3}
Cedar	27.5	8.6	0.87
Cedar-HT1	48.6	39.6	1.21
Cedar-HT4	48.8	36.6	1.22
Reference[a)]	-	5 - 6	-

a) commercially available blast furnace coke.

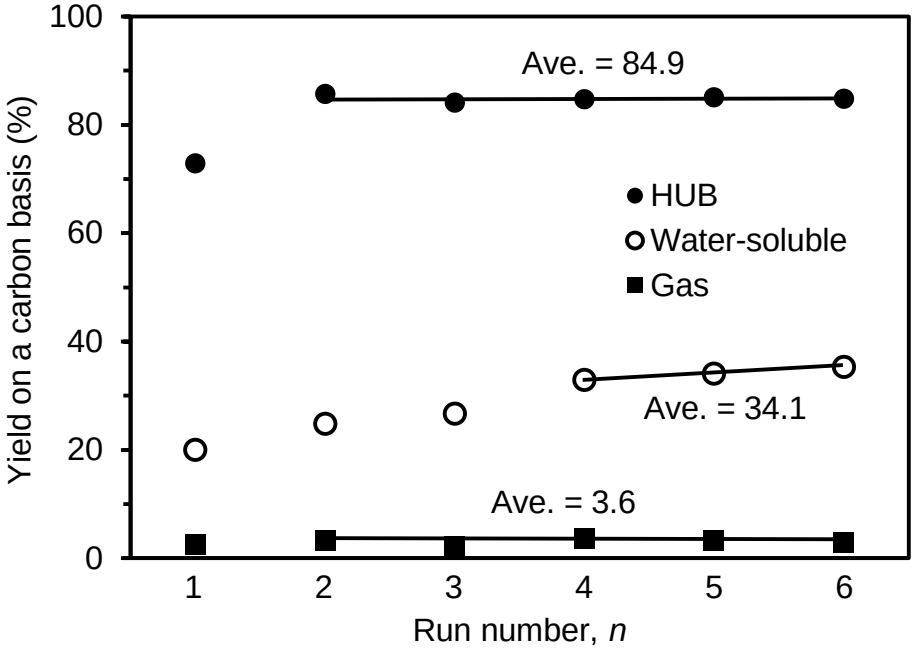

Figure 4.1. Yields of solid (cedar-HT*n*), gas and liquid as a function of run number *n*. The yields are defined for each run based on carbon of cedar charged in autoclave.

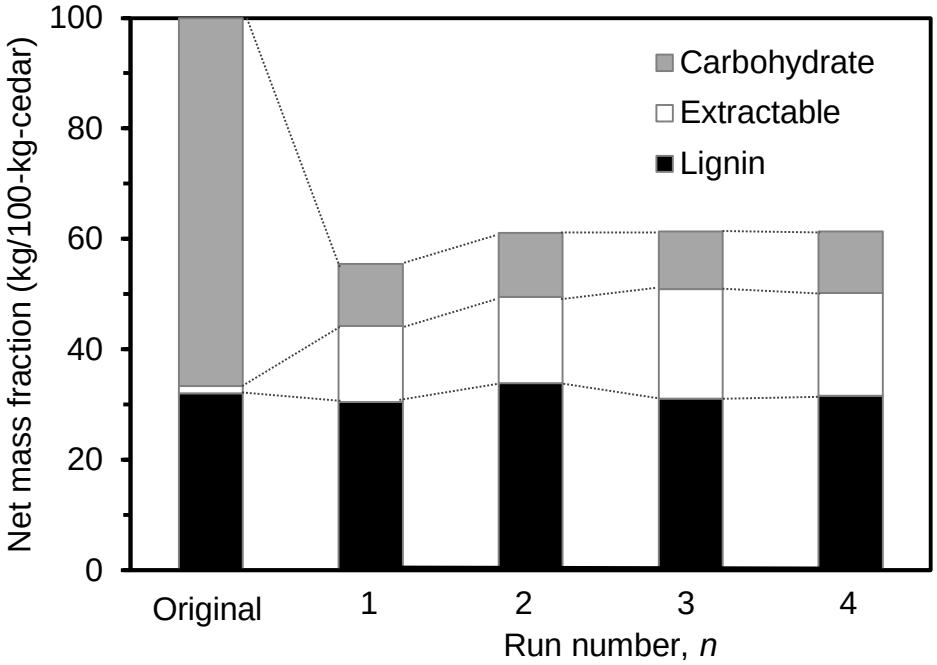

Figure 4.2. Net mass fractions of carbohydrate (cellulose and hemicellulose), lignin and benzene/ethanol extractable matter in the original cedar and cedar-HT at different run number (*n*).

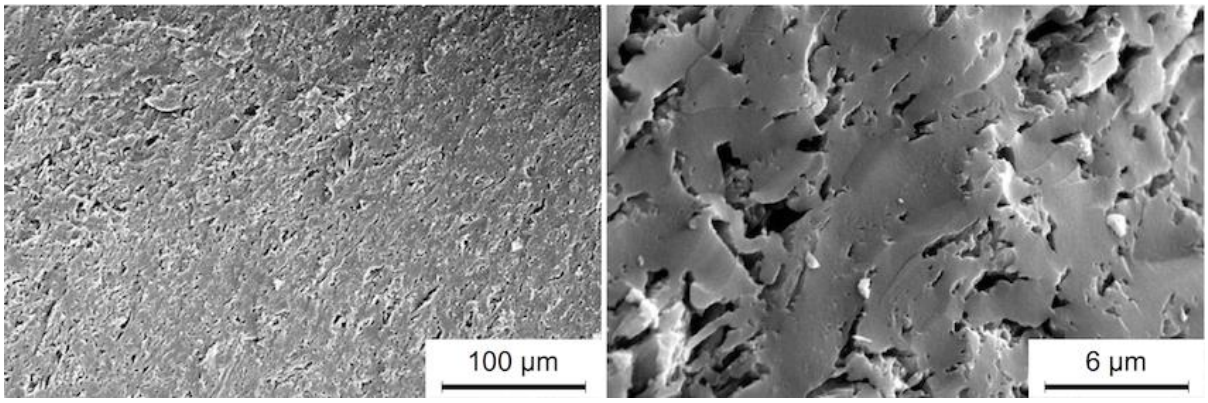

Figure 4.3. Scanning electron micrographs of fracture surfaces of a coke sample from cedar HT1.

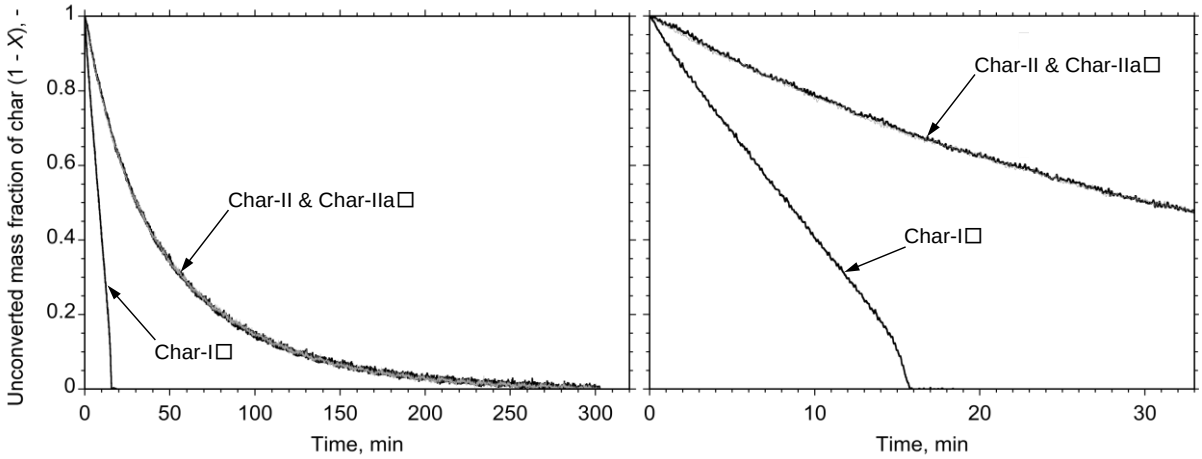

Figure 4.4. Time profiles for steam gasification of Char-I, Char-II and Char-IIa. The left and right graphs are drawn with different time scales.

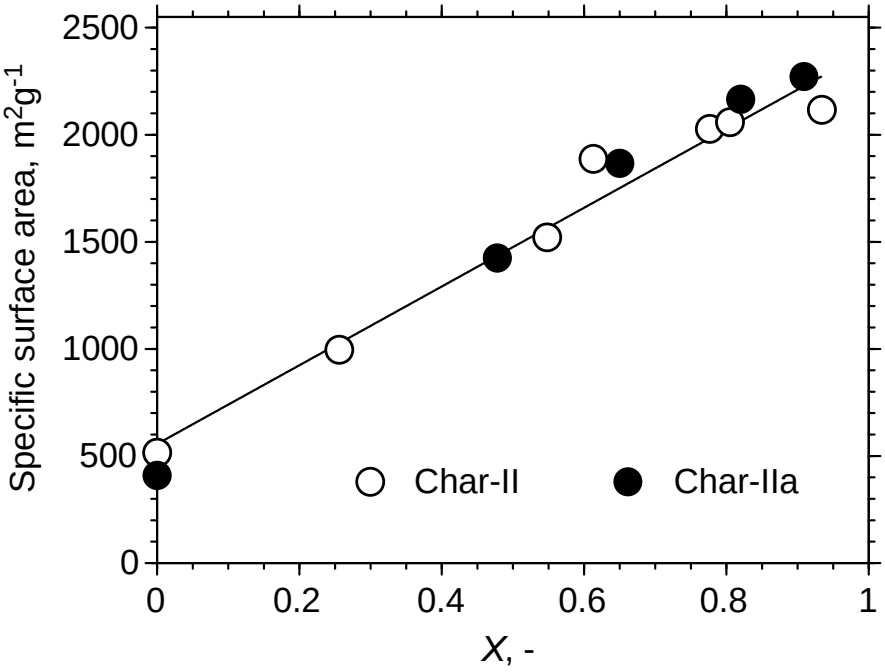

Figure 4.5. Specific surface areas of Char-II and Char-IIa as a function of conversion.

4.4 References

1. N. Mosier, C. Wyman, B. Dale, R. Elander, Y.Y. Lee, M. Holtzapple, M. Ladisch: *Bioresource Technology*, **96** (2005), 673–686.
2. A.T.M.W. Hendriks, G. Zeeman: *Bioresource Technology*, **100** (2009), 10–18.
3. S.S. Toor: *Energy*, **36** (2011), 2328–2342.
4. N. Phaiboonsilpa, K. Yamauchi, X. Lu, S. Saka: *Wood Science*, **56** (2010), 331–338.
5. H. Wu, K. Yip, F. Tian, Z. Xie, C-Z. Li: *Industrial and Engineering Chemistry Research*, **48** (2009), 10431–10438.
6. M. Sasaki, B. Kabyemela, R. Malaluan, S. Hirose, N. Takeda, T. Adschiri, K. Arai: *The Journal of Supercritical Fluid*, **13** (1998), 261–268.
7. L. Kong, G. Li, H. Wang, W. He, F. Ling: *Journal of Chemical Technology and Biotechnology*, **83** (2008), 383–388.
8. F. Jin, Z. Zhou, T. Moriya, H. Kishida, H. Higashijima, H. Enomoto: *Environmental Science and Technology*, **39** (2005), 1893–1902.
9. S. Kudo, Y. Hachiyama, H-S. Kim, K. Norinaga, J.-i. Hayashi: *Energy Fuels*, **28** (2014), 5902−5908.
10. S. Kudo, A. Mori, R. Soejima, F. Murayama, Karnowo, S. Nomura, Y. Dohi, K. Norinaga,J.-i. Hayashi: *ISIJ International*, **54**, 11 (2014), 2461–2469.
11. H-S. Kim, S. Kudo, K. Tahara, Y. Hachiyama, H. Yang, K. Norinaga, J.-i. Hayashi: *Energy Fuels*, **27** (2013), 6617−6631.
12. A. Mori, S. Kubo, S. Kudo, K. Norinaga, T. Kanai, H. Aoki, J-i. Hayashi: *Energy Fuels*, **26** (2012), 296–301.
13. A. Mori, M. D. Yuniati, A. T. Mursito, S. Kudo, K. Norinaga, M. Nonaka, T. Hirajima, H-S. Kim, J-i. Hayashi: *Energy Fuels*, **27**, 27 (2013), 6607−6616.

Chapter 5

General Conclusions

Biomass is the prospective feedstock in gasification due to its inherent catalytic species such as Na, K, Ca, and Fe which could accelerate the reaction of the carbonaceous matter with the oxidizing agent. These catalytic species should have been considered in the formulation of the kinetic model in order to improve the efficiency of gasifier. The present thesis studied the influence of the inherent catalytic species and successfully proved the application of the modified parallel kinetic model to describe the entire range of biochar conversion in steam and CO_2. This thesis also considered the leaching of Alkali and Alkaline Metallic (AAEM) species by hydrothermal pretreatment, and it was proven here that it could upgrade biomass to solid fuel and high-surface-area carbon materials. The general conclusion of these works was summarized.

In CO_2 gasification, the first order kinetics were seen in the non-catalytic gasification, while catalytic gasification followed the zero-th order kinetics. Then, the parallel kinetic model was described in this study with the consideration and assumption of catalyst precursor (C_{1prec}) and 1–4 types of catalytic species were able to explain the entire range of conversion. It was suggested in this study that the catalyst precursors were mainly from the water-soluble species. It is, therefore, the assumption of the catalyst precursor was inapplicable to the char from WW-SCBs, except for KR-WW even though the value was very low. In CO_2 gasification, the interaction of Na/K with Fe accelerated the deactivation of Na, K, and Ca while decelerated Fe deactivation. While as a result of the insufficient number of Na/K due to the water washing, Fe was deactivated very quickly.

Aside from the intrinsic reactivity of the biochar, it is shown that the presence of Na, K, and Ca contributed to the acceleration of rate gasification of biochar in steam. The non-catalytic and catalytic gasification were following the first order kinetics over an entire range of conversion (X) suggesting the fast activation and deactivation of catalytic species from the early stage of gasification. The profile can be successfully described by the parallel kinetic model with an assumption of one or two types of catalysts. The optimization of the correlation between initial activities with catalytic species suggested that each kind played as single

catalysts which then quickly deactivated during the conversion. The less interaction between catalytic species also affected to lower the activity of Fe in steam gasification.

The organic acids (mainly consists of glycolic, succinic, acetic, and formic acids) occurred during hydrothermal pretreatment of biomass at 250°C could remove more than 90% content of AAEM species in the biomass. This treated biomass, or so-called as upgraded biomass, had a very low concentration of AAEM species which was suitable for coke production with a very high tensile strength that could reach up to 39.6 MPa. The absence of the catalytic species also was an advantage to produce activated carbon with a high surface area (>2000 m^2/g). The recycling process of the treatment could maintain the removal rate of AAEM species while increasing the yield of upgraded biomass in the form of benzene/ethanol-soluble solid.

The studies that were carried out here are only considering the effect of the multi-catalytic species on the gasification of biochar, and the investigation of the impact of the concentration of catalytic species was only limited to the removal of water-soluble species. Future study on the gasification of biochar should consider the single catalytic effect on the conversion rates. Aside from the catalyst precursor, the variable C1-C4 assumed in this kinetic model should correlate to a certain amount or a particular kind of catalytic species. In order words, by adding a single catalyst, (*i.e.*, K_2CO_3, Na_2CO_3, Ca_2CO_3) the catalysis behavior of each type of species can be investigated. Another possibility to measure C1-C4 is through leaching of soluble species in different leaching agent. In biochar, some of the inherent metallic species are soluble in ammonium acetate as organically associated minerals. These AAEM-CH_3COONH_4 soluble species may give a different perspective on the catalyst behavior in gasification.

APPENDIX 1

Specific rate of CO_2 gasification of chars from acid-washed lignite, polymer resin and AW-SCBs.

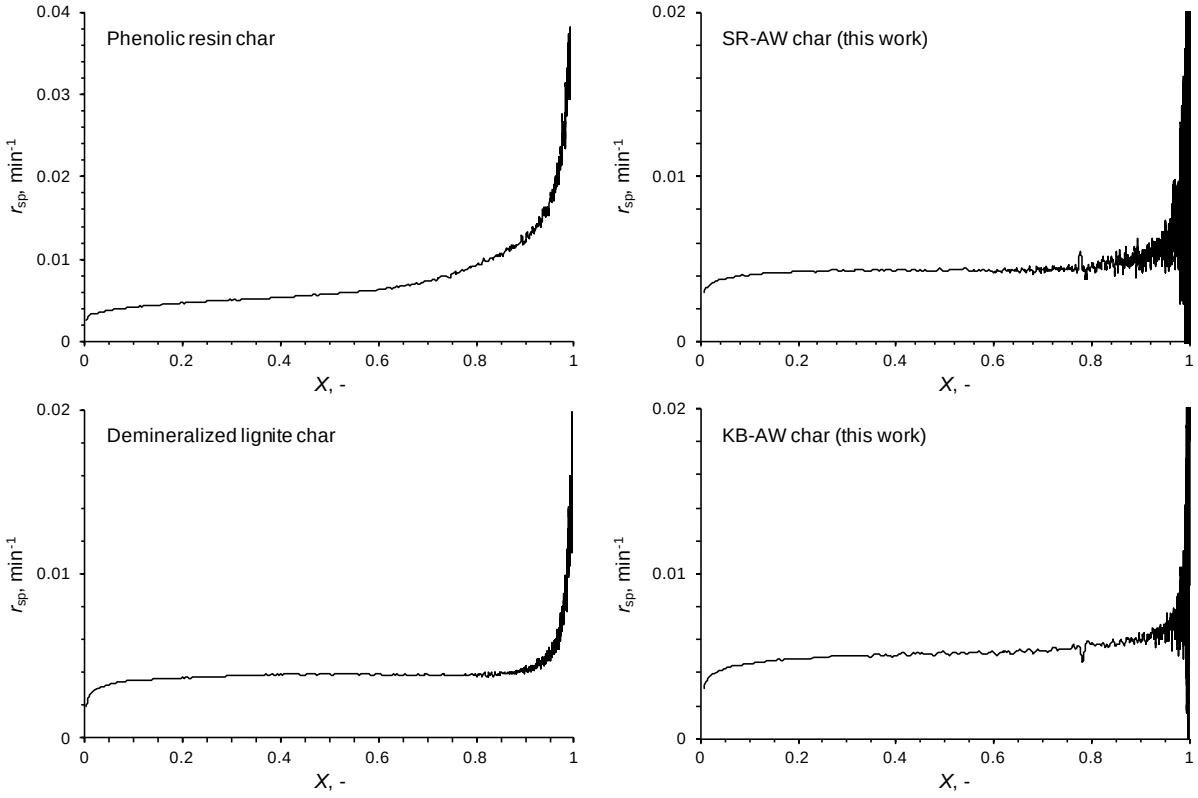

Figure A-1. Specific rate of CO_2 gasification as a function of char conversion. The char from the phenolic resin contained no metallic species, but r_{sp} increases quickly in the late stage conversion. Though not shown here, r_{sp} for chars from demineralized bituminous and sub-bituminous coals changed in manners very similar to that for the phenolic resin char. Such increase cannot be described by well-known kinetic models such as the original random pore model (Bhatia, S.K. and Perlmutter, D.D. AIChE J.1980, 26, 379) shrinking core models. r_{sp} for the gasification of a char from a demineralized lignite is steady at X = 0–0.9, and then increases remarkably later.

APPENDIX 2

Composition of metallic species contained in the chars from the original SCBs, WW-SCBs and AW-SCBs.

Table A-1. Concentration of metallic species in char at $t = 0$.

Char ID	Concentration, mol/kg-char						
	Mg	Na	K	Ca	Fe	Al	Si
GB	0.057	0.071	0.205	0.129	0.059	0.101	1.912
KB	0.050	0.065	0.193	0.079	0.038	0.077	1.789
KR	0.059	0.061	0.172	0.086	0.026	0.069	1.839
MK	0.026	0.058	0.089	0.055	0.064	0.190	1.990
PJ	0.011	0.080	0.119	0.051	0.119	0.228	3.546
SR	0.060	0.062	0.208	0.109	0.022	0.049	1.791
GB-WW	0.021	0.014	0.052	0.070	0.066	0.113	2.135
KB-WW	0.012	0.066	0.024	0.072	0.041	0.082	1.909
KR-WW	0.006	0.048	0.025	0.050	0.027	0.071	1.914
MK-WW	0.011	0.033	0.060	0.040	0.072	0.214	2.238
PJ-WW	0.010	0.024	0.065	0.041	0.124	0.239	3.717
SR-WW	0.013	0.022	0.058	0.047	0.024	0.053	1.924
GB-AW	0.010	0.020	0.010	0.020	N/A	N/A	N/A
KB-AW	0.010	0.010	0.000	0.010	N/A	N/A	N/A
KR-AW	0.020	0.020	0.010	0.020	N/A	N/A	N/A
MK-AW	0.010	0.020	0.010	0.040	N/A	N/A	N/A
PJ-AW	0.000	0.030	0.020	0.030	N/A	N/A	N/A
SR-AW	0.010	0.010	0.000	0.000	N/A	N/A	N/A

APPENDIX 3

Profiles of char conversion for the gasification of chars from AW-SCBs.

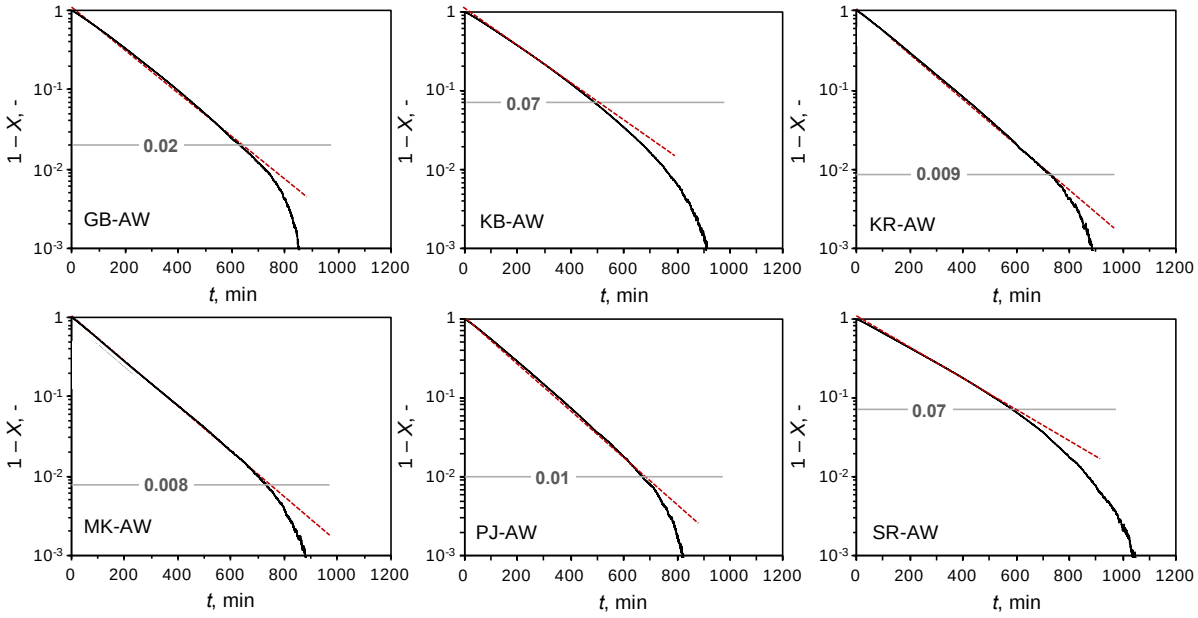

Figure A-2. 1–*X* vs t profiles for gasification of chars from AW-SCBs. Each red-colored broken line is drawn for showing decrease in 1–*X* in a linear manner with *t*, which are indicative of first-order kinetics with respect to 1–*X*.

APPENDIX 4

Detailed discussion on the validity of the assumption: The non-catalytic gasification obeys the first-order kinetics over the entire range of X.

Possible claim on uncertainty in prediction of the rate of non-catalytic gasification at the late stage (X > 0.9). For the two chars from KB-AW and SR-AW, the first-order kinetics can apply within limited ranges up to ca. 0.93. If the equation; $dX/dt = k_{nc}(1–X)$ is applied in the kinetic analysis, estimation of the rate of catalytic gasification will be associated with more or less errors.

Comment to the claim. If the increase in r_{sp} was fully or mainly due to the catalysis of metallic species that had been left by the acid-washing, it is reasonable to define k_{nc} directly from the slope of the line in **Figure 3.2** within the range where the linearity between $(1–X)$ and time is guaranteed. It is difficult to completely deny the catalysis of the remaining metallic species in the earlier stage, but, if any, errors arisen from this event is not significant.[19] On the other hand, if the increase in r_{sp} in the late stage is intrinsic (in other words, if the increase occurs even without catalysis), it should be considered more carefully. **Figure A-3** shows an example of $1–X$ *vs* t profile for the char from SR-AW.

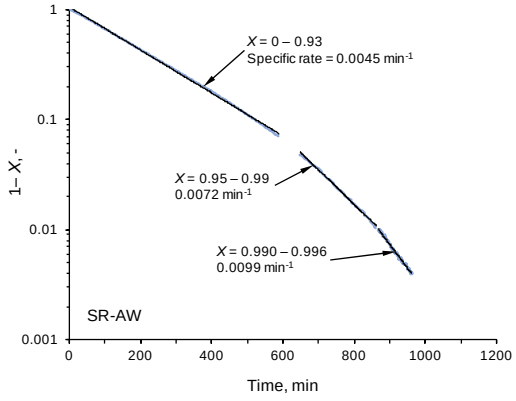

Figure A-3. Detailed kinetic analysis of gasification of SR-AW. The slopes of the $1–X$ *vs* t curve were determined at three different intervals of $1–X$ = 0–0.93, 0.95–0.99 and 0.990–0.996. The first interval was employed for defining k_{nc}.

Explanation of Figure A-3. r_{sp} for the SR-AW char, 0.0045 min^{-1}, was determined from the slope over a range of X up to 0.93. The slope for the later stage gasification is clearly greater than that at $X \leq 0.93$. For example, r_{sp} at X = 0.990–0.996 is as high as 0.099, and also greater

than that at $X \leq 0.93$ by a factor of 2.2. Such increase in r_{sp} was in fact observed commonly among chars from demineralized (HCl/HF aq.-washed) lignites and synthesized polymers (such as phenolic resins). It is therefore difficult to attribute the specific rate increase at the late stage gasification fully to the presence of small amount of catalytic species. There have so far been no studies with a particular focus on the r_{sp} increase in the late stage gasification. The present authors have been investigating the mechanism that causes this phenomenon. Although not mentioned in detail here, in the kinetic analysis of the gasification of chars from the original and WW-SCBs, the major part of the rate of gasification at the late stage was contributed by the catalytic gasification, where, more or less change in k_{nc} had little effects on the evaluation of the kinetic parameters for the catalytic gasification.

APPENDIX 5

Effective amount of C1 catalyst precursor.

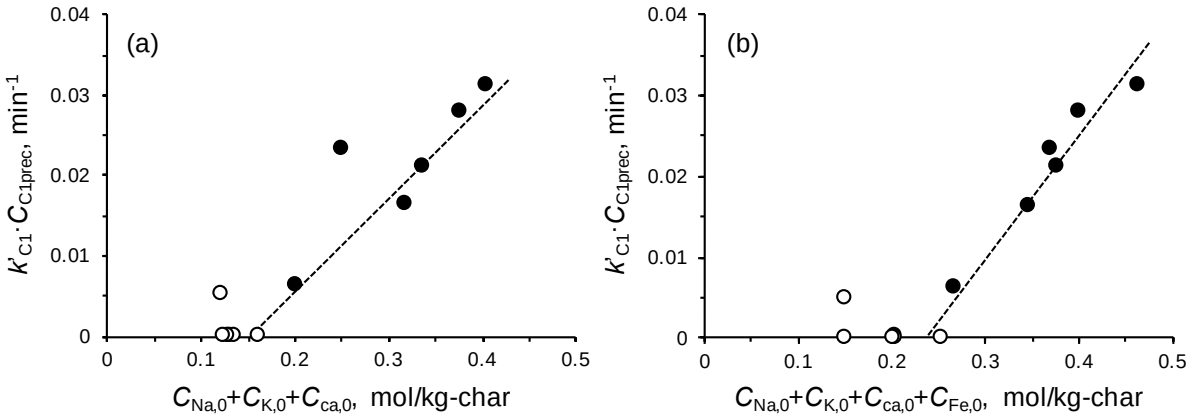

Figure A-4. Plot of $k'_C C_{C1prec}$ against (a) the total concentration of Na, K and Ca in the char at $t = 0$ and (b) the total concentration of Na, K, Ca and Fe in the char at $t = 0$. Symbols: solid; chars from the original SCBs, open: those from WW-SCBs.

APPENDIX 6

Correlation of ICD-2 with contents of individual metallic species.

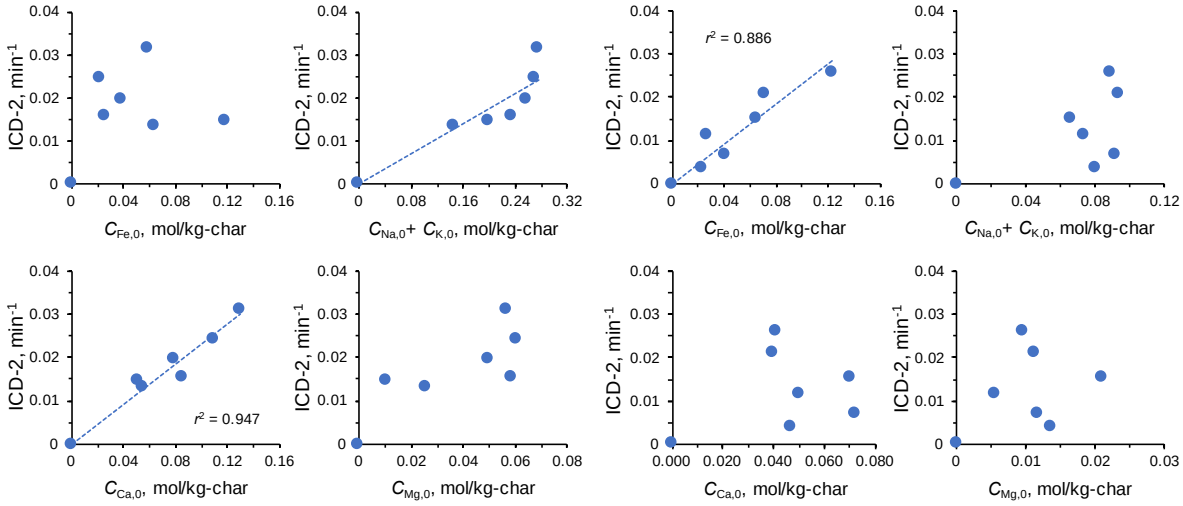

Chars from original SCBs *Chars from WW-SCBs*

Figure A-5. Correlation of ICD with concentration of specific metallic species. This figure is to be involved in SI, or otherwise, some graphs will be presented if these are useful in discussing importance of Fe catalyst for the overall catalyst deactivation for the chars from WW-SCBs, while Ca and Na/K are important for those from the original SCBs.

APPENDIX 7

Examination of the relationship between the rate constant for catalyst deactivation and overall initial catalytic activity for C1–C3 components.

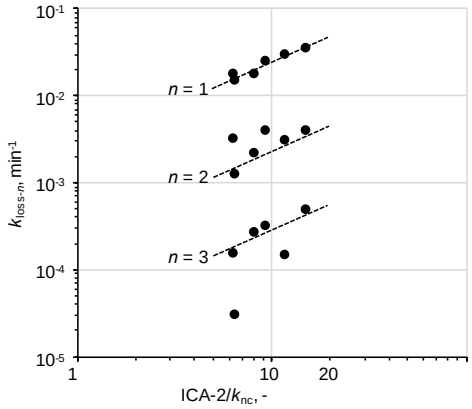

Figure A-6. Relationship between $k_{loss\text{-}n}$ and k'_C/k_{nc} (n = 1–3) for the chars from original SCBs. The slopes of the dashed lines are unity (i.e., $y = ax$).

APPENDIX 8

Relationship between the initial activity and rate of catalysis loss for the individual catalytic components.

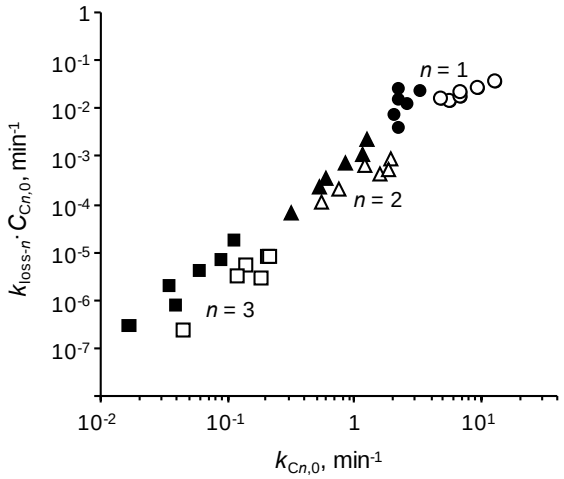

Figure A-7. Overview of relationship between $k_{cn,0}$ and $k_{loss\text{-}n}\cdot C_{Cn,0}$. The initial rate of deactivation distributes over a wide range from 10^{-6} to 10^{-1} min^{-1}. It is also clear that more active catalyst undergoes more rapid deactivation. The initial activity and deactivation rate of the catalysts may have *continuous* distribution over very wide ranges. The present kinetic model expresses such continuous distribution by *discrete* ones.

APPENDIX 9

Examination of a mechanism of catalyst deactivation by its reaction with SiO_2.

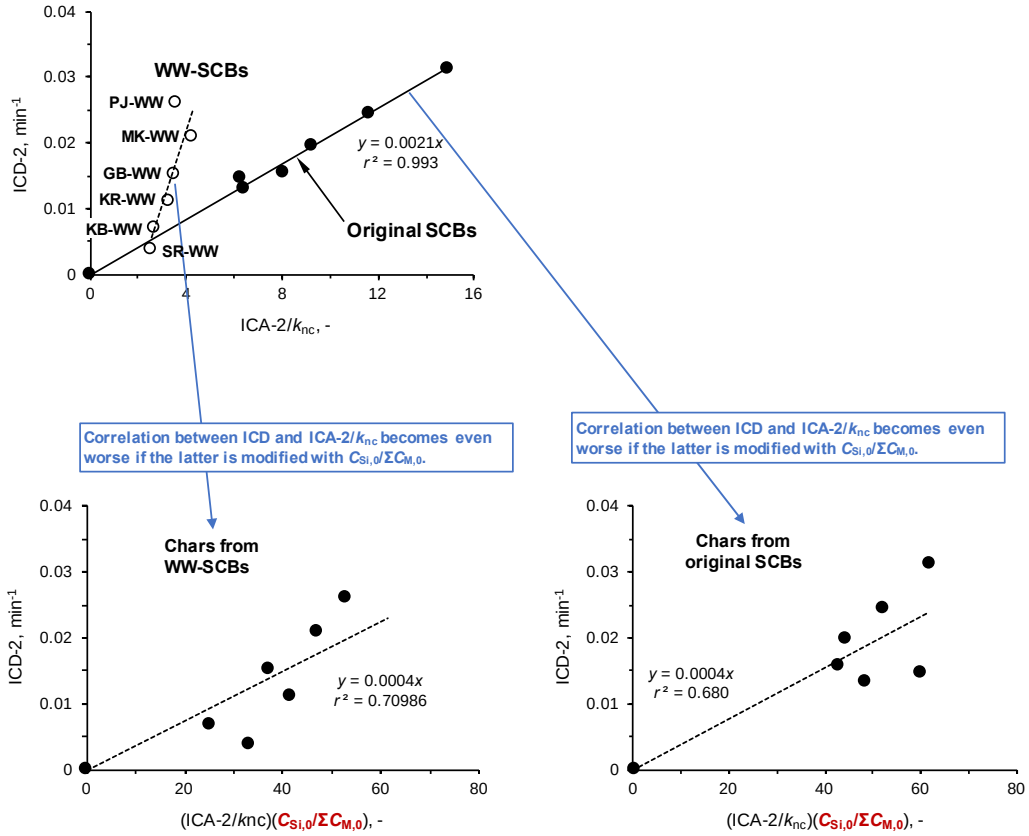

Figure A-8. Correlation of ICD-2 with ICA-2/k_{cn} with its modification by $C_{Si,0}$. The decreases in the correlation factors (r^2) for both chars from the original SCBs and WW-SCBs indicate that the deactivation due to reactions between catalysts and SiO_2 was, if any, not important during the gasification.

APPENDIX 10

Thermodynamic consideration of reactions of K, Na and Ca oxides with SiO_2 as a function of temperature relevant to pyrolysis and gasification.

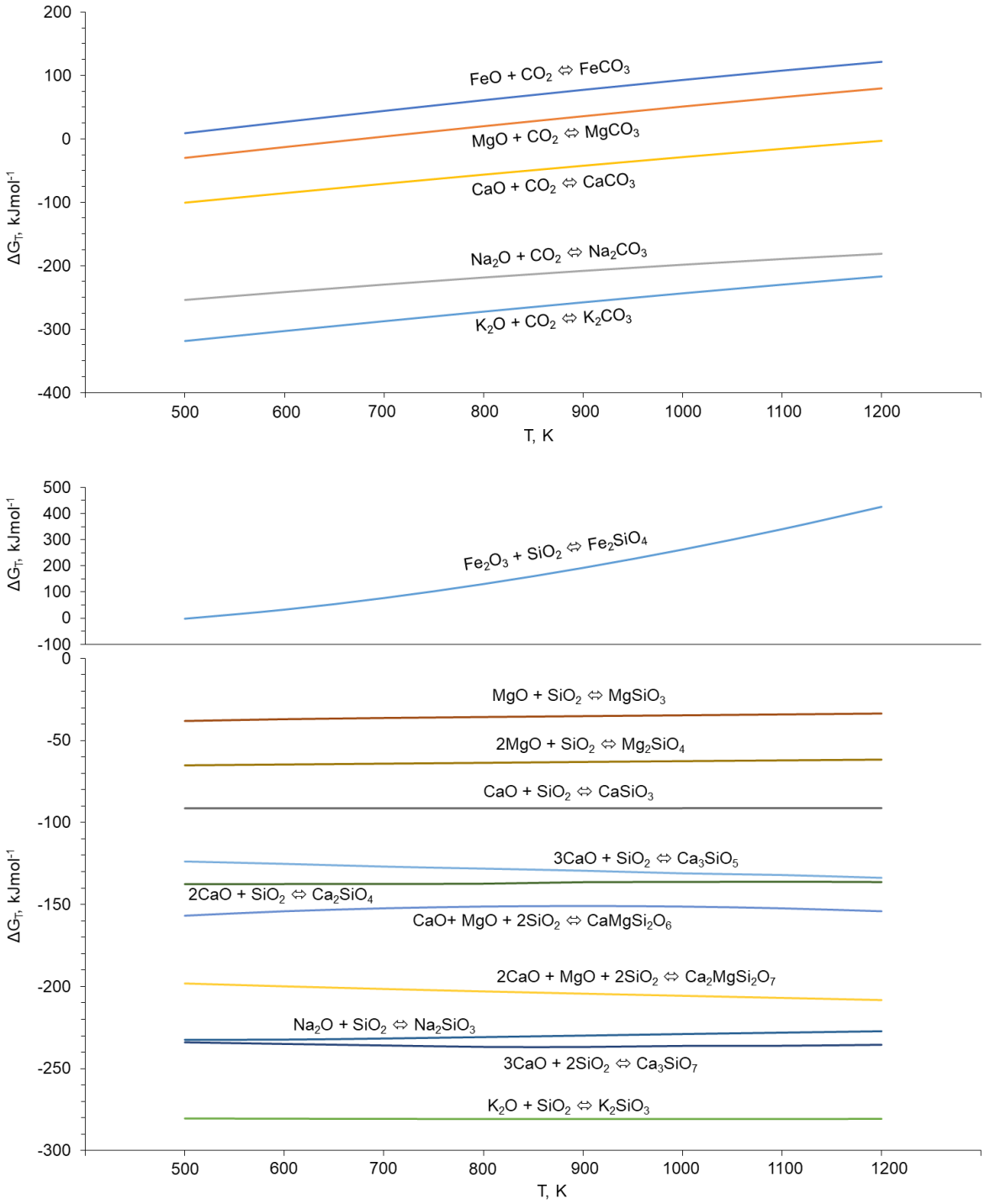

Figure A-9. The Gibbs free energy for reactions of Na, K, Ca and Fe oxides with SiO_2 or CO_2.

APPENDIX 11

The comparison between the char gasified in CO_2 at 900°C and 850°C following the temperature that was used in this study.

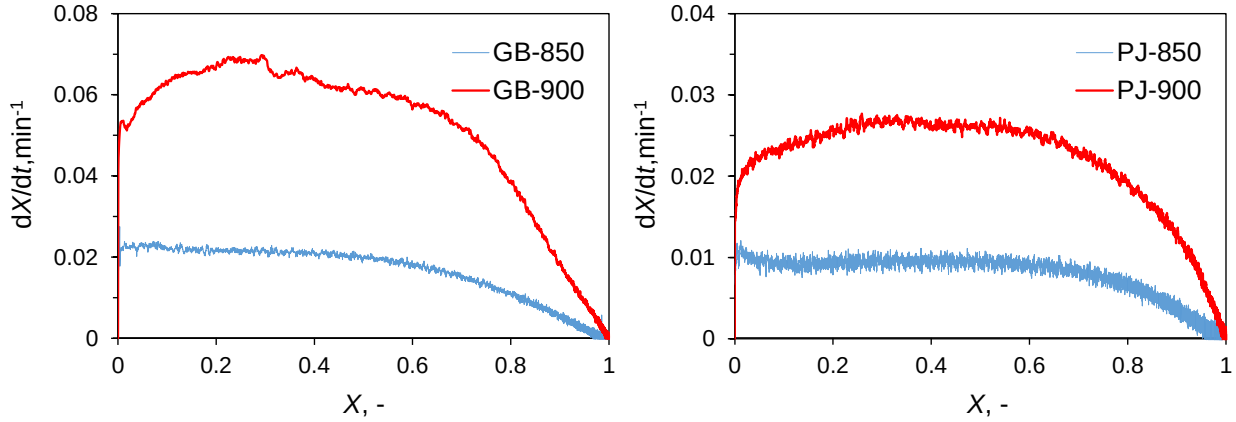

Figure A-10. The overall rate of CO_2 gasification profiles of GB (left) and PJ (right) were plotted against the char conversion, *X*. The red lines were drawn from the measured data at 900°C, while the blue lines were obtained from the results at 850°C. These profiles were constructed to show that if the gasification was carried out at the same temperature condition as the one applied in this study, the catalyst behavior is more or less similar to the one gasified at a higher temperature.